Quantitating the Energetics and Binding of Syt1 C2 Domain to Lipid Bilayers

Anusa Thapa
Kathmandu, Nepal

B.S. Chemistry, Converse College, SC 2009

A Dissertation presented to the Graduate Faculty
of the University of Virginia in Candidacy for the Degree of Doctor of Philosophy

Department of Chemistry
University of Virginia, Dec 2014

ABSTRACT

Signaling in the central nervous system is mediated by the fusion of synaptic vesicles to the presynaptic membrane of the neuron. This fusion event is driven by membrane-anchored SNAREs (Soluble NSF Attachment Protein Receptors), but requires a number of additional proteins including munc18, complexin and Synaptotagmin 1 (Syt 1). Synaptotagmin 1 functions as the Ca^{2+} sensor in neuronal fusion, and it may act by bridging bilayers and assisting SNARE-mediated fusion. We have determined the role of electrostatics and electrostatic screening in determining the membrane association of a tandem fragment of Syt1 containing its two C2 domains. Charge neutralization of two highly conserved arginine residues opposite the Ca^{2+} binding sites (R398Q/R399Q) did not alter the binding of C2AB to membranes composed of mixtures of PS and PIP_2; however, neutralization of charge in the conserved polybasic face (K326A/K327A) dramatically reduced binding. The polybasic face also demonstrated specificity for PIP_2 both with and without Ca^{2+} through a mechanism that is likely driven by electrostatics. ATP is known to modulate the interactions of Syt1 (Park et al. (2012), NSMB 19, 991) and ATP dramatically alters the membrane binding of C2AB. 2D HSQC NMR experiments were used to determine the sites of interaction of ATP and of the PIP_2 headgroup, IP_3. At levels that are physiologically relevant, both ATP and IP_3 modulate chemical shifts in the polybasic face of C2B, suggesting that these electrolytes reversibly associate at these sites in Syt1. Polyelectrolytes are also seen to interact with

the membrane binding loops of both C2A and C2B. EPR power saturation depth measurements indicate that the binding mode of C2AB is different in PCPS vesicles versus PCPIP$_2$ vesicles. It was found that the Ca^{2+}-binding loops do not insert into bilayers where PIP$_2$ is the only anionic lipid present. This was in contrast to PCPS suggesting that the mechanism of Syt1 binding is significantly different in PIP$_2$ bilayers. The results suggested that certain regions in C2B domain are specific to either PS or PIP$_2$. These interactions are likely to play an important role in controlling the membrane interactions of Syt1 in vivo.

TABLE OF CONTENTS

LIST OF FIGURES

ACKNOWLEDGEMENT

My research in graduate school has taken me on a long and challenging journey, but, along the way, several individuals have provided support and guidance for my work. Many of them have contributed much more than they may have realized. First, I would like to thank my advisor, Prof. David Cafiso, for allowing me the opportunity to learn from his expertise in biophysics. Thank you for always taking time to answer my questions and for trusting in my ability and my work.

I would like to acknowledge Dr. Jeff Ellena for his NMR and computing expertise. Thank you for patiently advising me and helping me to troubleshoot and understand my experimental results. I appreciate your guidance, without which I would have much been behind.

I would like to acknowledge my collaborator, Dr. Angel Perez, from Prof. Reinhard's lab in Max Planck Institute, Gottïngen. His research insights and ideas have allowed us to advance further into our understanding of the Ca^{2+} triggered exocytosis phenomenon. Therefore, I would like to thank him and Prof. Jahn for their suggestions and fruitful discussions. I would also like to thank Prof. Tamm and his lab for being our neighboring lab as we exchanged scientific ideas and samples. The PPG collaboration has allowed me to meet amazing young scientists and share scientific outcomes and goals.

Next, I would like to thank my past lab members who have been inspirational and instrumental to my development as a research student. I would

like to thank Alex Lai who mentored me in the beginning and passed on his knowledge to me. I would like to thank my three beautiful seniors, Audrey, Weiwei and Dawn, who were great role models in everyway. I would like to thank Jessica Sarver, who is capable of making anyone's day in lab, for her support and scientific help. I would also like to thank the present lab members for their friendship, enthusiasm for scientific knowledge and their help in troubleshooting problems in lab.

I would like to thank my undergraduate advisor, Prof. Jerry Howe, for influencing my path into chemistry and research. Your strict endeavor for your chemistry majors has helped me transition well and progress. I would also like to thank Prof. Edna Steele, my biology professor and host-mom, for being an excellent example of a great professor and mom! You and your family have encouraged me to do well.

I would like to thank my parents for striving to make my and my siblings education possible. Your courageous efforts have motivated me to work harder. I would like to thank my sister, Puspa, for always being there for me, as my only family member in the country. I would like to thank all my friends that I met in college and graduate school. They have been integral in helping me balance my workload with personal life.

Finally, I would like to thank my yoga guru, John Bultman. For the last two years, you have challenged me to go so far that I never could have seen myself attempt it. I have been blessed to know a true yogi devout who helps others and inspires me to keep going farther.

CHAPTER

1. Introduction

Neuronal Exocytosis and Membrane fusion

Cell secretion is highly organized and efficient, and the discovery of the protein mediated pathway for secretion won the 2013 Nobel Prize in medicine. This breakthrough led to several important advances in the field of the life sciences. Calcium triggered exocytosis is a process characteristic of many eukaryotic cells.

While membrane fusion in the synapse has been the best studied, the same signaling mechanism also governs granule exocytosis in mast cells, hormonal release in endocrine cells and lysosome exocytosis in fibroblasts[1]. The neuronal membrane fusion is a highly coordinated event, which is mediated by the tight control of several proteins such as the soluble NSF- ethylamine binding receptors (SNAREs), Synaptotagmin 1, Complexin and Munc13. This allows for synchronous neurotransmitter release on an extraordinarily fast sub-millisecond timescale upon Ca^{2+} influx – making this the fastest possible membrane fusion event known in the cell[2].

Schekman and Rothman demonstrated the importance of these fusion proteins through genetic manipulation of homologous yeast secretory proteins[3, 4; 5]. Their influential work established that all eukaryotes have similar protein secretion pathways[6]. The fast nature of this important

biological event suggests that an efficient mechanism is required to initiate fusion[7].

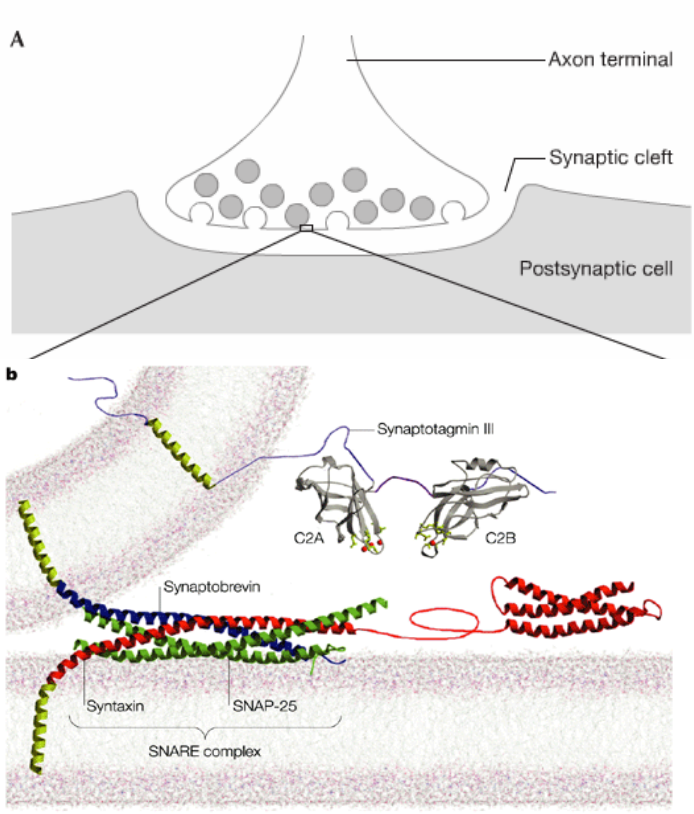

Figure 1. Neuronal exocytosis: SNAREs and Synaptotagmin prior to vesicle fusion (adapted from Carr 2007 and chapman, 2002)

Several interactions underlie the membrane fusion event, and protein-lipid interactions are critical to the fusion phenomenon. This event underlies the vesicle-based secretory pathway in most cells[4]. Bernhard Katz first quantized neurotransmitter release in 1951 and later discovered that Ca^{2+} propagates this synaptic response [8, 9, 10].

The SNARE proteins, figure 1, have been found to make up the core of the fusion machinery and are required to fuse the synaptic vesicle into the plasma membrane of the presynaptic nerve terminal[11,12]. In the neuronal systems, the SNAREs include Synaptobrevin, which has a helical membrane anchor in the synaptic vesicle, Syntaxin, which has a helical anchor in the plasma membrane and SNAP-25, which is palmitoylated and has two SNARE forming helices. Together these three proteins assemble into a four-helix bundle to make-up a highly stable core SNARE complex.

Synaptotagmins, like the SNARE family are highly conserved in the cell secretory pathways[13]. Some of the other regulatory protein/components that have been found to influence membrane fusion in neuronal exocytosis include Complexin, Munc 13, Munc 18, and RIM. The exactly molecular role of these critical protein components is not understood, but they are necessary to coordinate appropriate molecular assembly of the SNARE complex and bring about fast neuronal exocytosis.

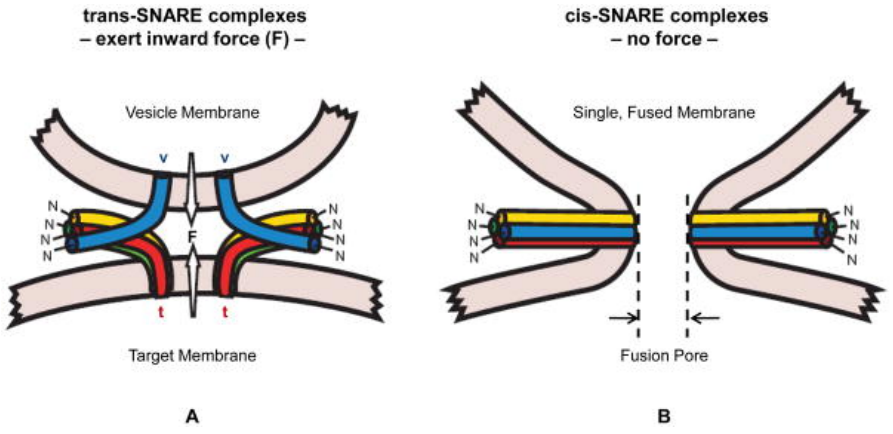

Figure 2. Zipper model of SNAREs in membrane fusion and force exerted for pore opening (taken from Sudhof 2009)

It is important to elaborate on the energy barrier in membrane fusion to understand the process by which fusion takes place. Membrane fusion in neuronal exocytosis has to overcome a high-energy barrier due to a number of unfavorable processes[5]. The first is the coloumbic repulsion of like charges in opposing membrane bilayer from the synaptic vesicle and plasma membrane. The second is the desolvation penalty to remove a water molecule from the surface of protein and the hydrophobic membrane when merging charged membranes together[14]. The third is the energy required to bend the membrane during hemi-fusion state, which is the process where the outer leaflet deforms to merge with the opposing membrane to form a stalk-like structure[15]. Further energy is required to open the fusion pore as shown in figure 2B[15]. The fusion of the vesicle to the presynaptic membrane is hence believed to be energetically unfavorable and several factors may contribute to the energy of disrupting and merging membrane bilayers in the cell.

Cohen and Melikyan reported that the physical deformation and fusing of the outer leaflets in the membrane bilayer to reach hemifusion requires 40-50 k_BT (k_B = Boltzman constant, T = temperature in Kelvin, 1 k_BT = 0.593 kcal/mol)[16]. Surface force experiments determined that the energy provided by assembling a SNARE complex is 35 k_BT [17]. Martens and McMahan estimated the energy release from the buckling of membrane leaflets to stalk formation mediated by Synaptotagmin – SNARE activation is 20 k_BT[18]. It is postulated that the SNARE stabilization energy together with the latter energy release due to membrane perturbation reduces and overcomes the energy barrier between negatively charged lipids in membranes.

With recent work elucidating the importance of several other proteins in this SNARE-mediated fusion, a clear structural mechanism for exocytosis is still lacking. The SNARE complex alone does not regulate the sub-millisecond membrane fusion event, and this is a role that accessory proteins and phospholipids play in this process.

The SNARE Paradigm

The SNARE family of proteins is ubiquitous in the cell secretory pathway[19]. Schekman's discovery of the yeast, S. cerevisiae, sec22 family, in 1979, paved the way to identify the family of proteins essential for secretion and integral to membrane trafficking in the secretory pathway[20]. The cell secretory pathway involves vesicle or membrane trafficking from the ER to the Golgi and to other cellular compartments. Neuronal exocytosis is part of this protein transport mechanism that can be triggered electrically or chemically[21]. When an action potential reaches the nerve terminus, the neuronal exocytosis occurs quickly to facilitate neurotransmitter release for cell communication and signaling.

Neuronal exocytosis involves two types of events, asynchronous and synchronous release. The slower asynchronous release occurs in few hundred milliseconds and is more sporadic and spontaneous. It is not believed to be important in neurotransmission since it gets outcompeted by the far more efficient synchronous release[1]. However the asynchronous release is thought to have a physiological importance in shaping neural function[1]. Synchronous release is only triggered by a Ca^{2+} signal and results in the complete fusion of hundreds of vesicles within sub-millisecond timing. Determining how synchronous release occurs in sub-millisecond timescale has been the subject of an intense research effort[22]. In 1993, Rothman and colleagues discovered the SNARE complex as the protein specific to vesicle trafficking and fusion[23; 24]. How

do the SNAREs accomplish this energetically unfavorable activity? The answer lies in the biochemical and biophysical properties of the SNARE proteins and their structure.

The importance of SNAREs was highlighted when it was found that the SNAREs were targets of clostridial neurotoxin (CNT) light chain proteases such as Botulinum and Tetanus[25]. The cleaving or proteolysis of the neurotoxins on Synaptobrevin resulted in inability of SNARE complex formation and consequently, the inhibition of vesicle fusion in neuronal exocytosis.

The SNARE proteins are evolutionary conserved and homologous, with different isoforms being involved in various exocytosis processes in the cell secretory pathway. Exocytosis in endocrine cells is mediated by this same fusion machinery (SNAREs) as well as the SM-proteins and synaptotagmin, which were discovered in the synapse[26]. SNAREs are also involved in insulin secretion in endocrine cells though the timescale is reported to be slower at a few hundred milliseconds[27, 28].

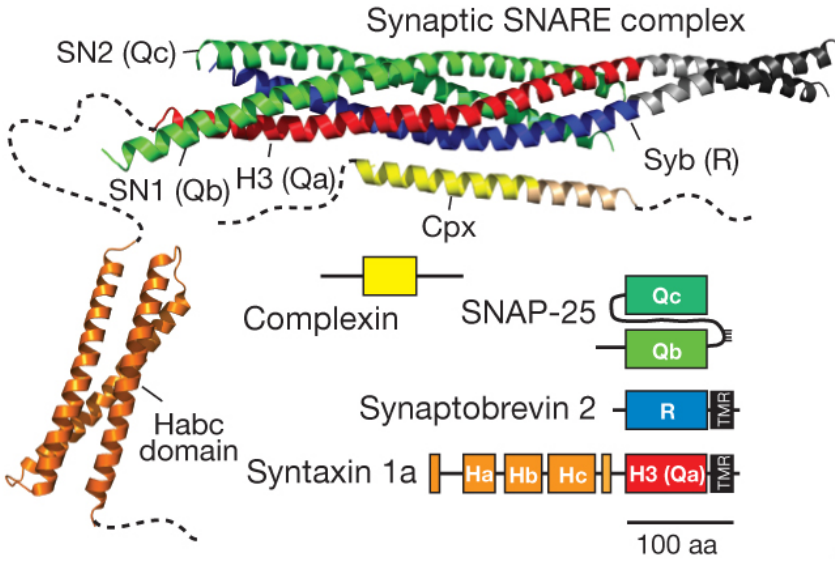

Figure 3. Crystal structure of individual SNARE protein domains and core complex with complexin (taken from Jahn and Fasshauer, 2012)

The individual SNARE proteins include of Synaptobrevin, Syntaxin and SNAP-25. Synaptobrevin (Syb), shown as blue in Figure 3, is a synaptic vesicle - bound protein and also known as VAMP (vesicle-associated membrane protein)[20]. It has a transmembrane region (TMR) and a highly conserved motif that shares the SNARE core domain. As illustrated in figure 3, it falls in the subtype R-SNARE since it contributes arginine in its middle ionic layer in the SNARE core motif[29]. Syntaxin also has a transmembrane region that spans into the plasma membrane of the presynaptic cell. It has two characteristic motifs, one of which is the highly conserved SNARE motif, H3, and is connected by a flexible linker to the other: the Habc domain[29]. The H3 domain, Qa, is in red in figure 3 while the Habc domain is in orange. The SNARE motif of Syntaxin, the H3 domain, has the subtype Qa since it contributes one of the three glutamine residues in the SNARE ionic layer. SNAP-25 (synaptosome-associated protein

of 25 kDa) unlike the other two SNARE proteins is a cytosolic protein lacking the TMR. However, it resides on the plasma membrane postulated to be anchored by cysteine-palmitoylation[20]. SNAP-25 is a double helical protein in which both its helices make up the SNARE core motif, Qb and Qc, shown in green in figure 3. Hence the SNARE core made up of four helices from the three proteins is known as the ternary SNARE complex.

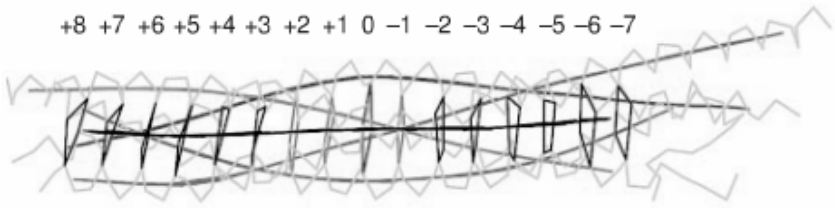

Figure 4. Q- and R- SNARE core complex with the conserved central ionic layer (taken from Sutton,1998)

The importance of Synaptobrevin and SNAP-25 was confirmed when double knockout mice of Synaptobrevin and its homolog, Cellubrevin, were found to completely hinder Ca^{2+}- triggered exocytosis[30, 31]. The assembly of the SNARE protein into the core complex by its zippering mechanism was established when a 2.4 Å crystal structure of the neuronal SNARE complex was determined[32]. The SNARE complex is a parallel four-helix bundle and it is the assembly of this bundle that appears to drive fusion. The ternary SNARE complex, as shown in figure 4 consists of sixteen hydrophobic layers, which are formed by interacting side-chains from each of the helices. As mentioned earlier and as shown figure 4, each of the four helices contribute a residue to the central ionic layer, arginine and three glutamines, classifying the SNARE proteins to their characteristic subtypes R, Qa, Qb and Qc. The feature of these hydrophobic and ionic layers is evolutionarily conserved in the SNARE family[32] and mutating the ionic layer

decreases the stability of the SNARE complex resulting in inefficient membrane trafficking[32,33]. The endosomal SNARE core complex has also been found to adopt a very similar structure to the post-fusion coiled-coil helical bundle in neuronal SNAREs, emphasizing the structural conservation of the SNAREs[34]. The formation of the ternary SNARE complex from individual proteins that are disordered is postulated to be represent a free energy change of $\Delta G = -38$ kcal/mol[20; 35]. This shows that there is a highly favorable interaction between the SNARE proteins. The neuronal SNARE complex has also been found to be extremely stable thermally and chemically, with resistance to boiling and denaturation by strong detergents[20].

While the SNAREs have been found to be critical in neuronal exocytosis, the exact mechanism of action or the biophysical basis of how they are able to induce pore opening is uncharacterized. One of the generally accepted models for SNARE function is that the zippering or complex formation of the SNAREs creates a mechanical force on the opposing membranes that induces fusion[34]. The “zipper” model, figure 2, hypothesizes the SNARE core complex assembles or zippers from the membrane-distal amino termini to the membrane-proximal carboxyl termini[36]. This ‘zippering’ to form a highly stable complex physically enables the merger of lipid membranes by straining and deforming the hydrophilic-hydrophobic boundary[34]. The number of SNARE complexes required for the fusion event is another question of current interest. Different groups have shown in vitro experiments with liposomes showing SNAREs alone can induce

fusion events, which ranged from 1 to 15 SNAREs as being sufficient for membrane fusion[37; 38, 38, 39].

The relationship of the juxta-membrane linker region, between the transmembrane region and the SNARE motif, of Synaptobrevin with the ability of the SNARE complex to drive fusion was also delineated[40]. Since the SNARE complex relies heavily on its respective membrane anchor on the opposing vesicle and plasma membrane for its role, the function of the flexible linker that connects the SNARE motif to the membrane was investigated. Experiments using high-resolution membrane capacitance measurements and amperometry showed that increasing the length of the juxtamembrane linker in Synaptobrevin reduced the primed stage of chromaffin granules in mice[40]. It was concluded that the shorter inter-membrane distance created by the linker was essential for generating the necessary mechanical strain on the bilayers. The juxtamembrane linker regions of both Synaptobrevin and Syntaxin also contain clusters of basic residues that promote membrane association of the linker through electrostatic interactions[41, 42].

SNAREs may also play a role in the docking and priming of the vesicle to the presynaptic plasma membrane. The physiological process in neuronal signaling involves many events that ultimately lead to synchronous release following the Ca^{2+} trigger. The docking and priming steps that place vesicles at the active-zone of fusion are important in accounting for the rapid timescale of the fusion

process. Just like the complexity of this neuronal fusion event, we can also look at the simpler version where the role of the SNAREs is to set the hundred of vesicles in a release ready (on-the-go) to prompt fusion to occur upon influx of Ca^{2+} in the event of an action potential. Several proteins like the Rab, GTPase, Calmodulin, RIM and Doc proteins have been implicated in vesicle tethering and docking, which brings the vesicle within 50nm of target membrane[43]. The role of the SNAREs in priming vesicles is to set the hundreds of vesicles in a release ready (on-the-go) to prompt fusion to occur upon influx of Ca^{2+} in the event of an action potential. This priming involves setting the vesicle within 20nm of the target membrane, and preparing the systems for the final exocytosis step[43, 44]. In vitro experiments show that fusion is possible with the SNAREs alone, however, the SNAREs may not necessarily go through normal docking and priming states and Synaptotagmin, which triggers rapid fusion, is not present.

C2 domains and Synaptotagmin

There are a number of Ca^{2+} sensor proteins with differing roles in the calcium signaling pathways. Calmodulin, Doc2, Synaptotagmin (Syt) and the neuronal calcium sensor (NCS) protein family have been found to be involved in a wide range of Ca^{2+} signaling events in the neurons[45, 46]. Matthew et al. first identified Synaptotagmin in 1981, as being localized in synaptic vesicles and LDCVs[47]. Almost a decade later, Sudhof determined the primary structure of Syt 1, and elucidated the role of the Ca^{2+} sensor in triggering synchronous exocytosis[48]. While there are 16 isoforms in the synaptotagmin family, Syt 1 is the fast Ca^{2+}

sensor, has been the most extensively studied.

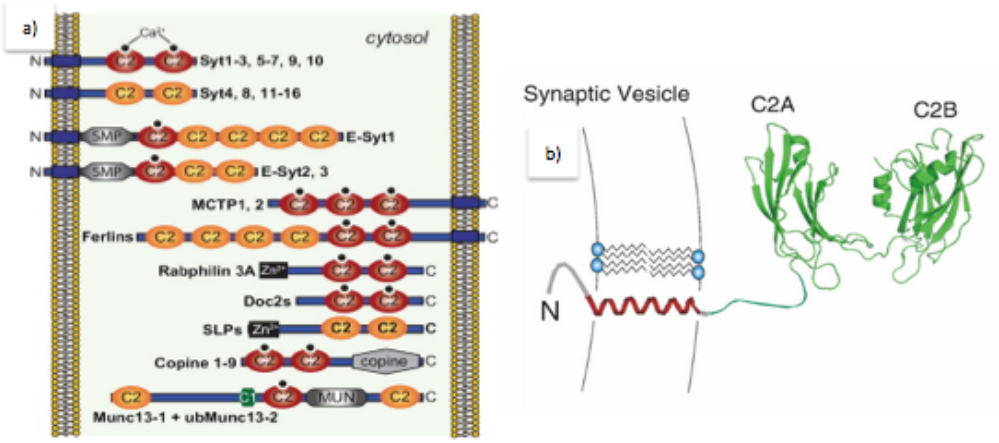

Figure 5. Synaptotagmin family and structure b) N-terminal TMR connected to a flexible linker and C2 domains (images taken from Kaeser 2014 and Herrick 2009).

As shown in figure 5, synaptotagmin is a membrane protein which has a N-terminal intravesicular sequence, transmembrane region (TMR) connected by a linker sequence to two of its cytoplasmic C2 domains, C2A and C2B, which are Ca^{2+}-binding modules[49, 50]. The C2 domain is named after the second conserved domain in PKC, and it is sometimes functions as a Ca^{2+} binding and phospholipid-binding module[23]. However not all C2 domains or C2 domains in Synaptotagmin isoforms have affinity for Ca^{2+}. Three isoforms of Synaptotagmin, Syt1, Syt2 and Syt9, have been found to be involved in Ca^{2+} binding at the synapse, however each plays a distinct roles in exocytosis[1].

The crystal structure of Syt 3 and the NMR structures of the C2A and C2B domains revealed that the secondary structure of the domains consist of eight stranded β-sandwich each having flexible loops for Ca^{2+} binding[51, 52].

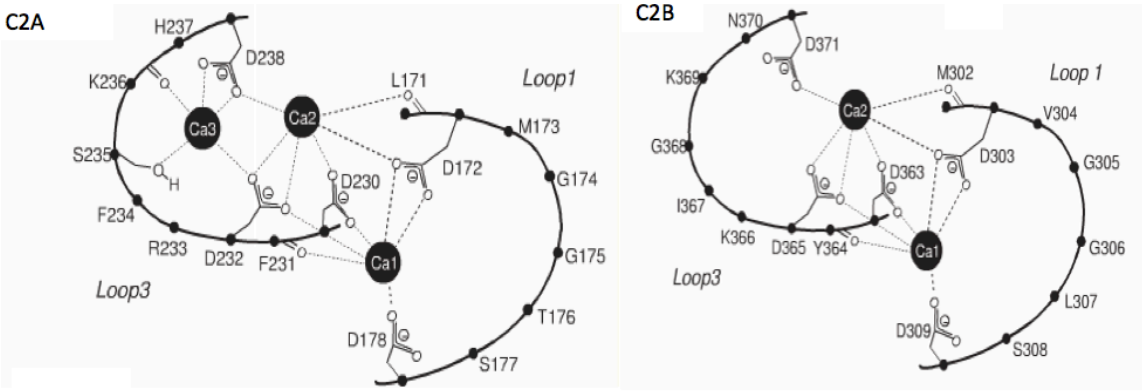

Figure 6. Residues involved in Ca^{2+} - coordination in binding loops of C2A and C2B domain (taken from Zhang 1998 and Ubach 2001).

As shown in figure 6, the C2A domain binds three Ca^{2+} ions and the C2B domain binds two Ca^{2+} ions[52, 53]. In each domain, five acidic aspartate side chains coordinate with Ca^{2+}. In the C2A domain, residues D172, D178, D230, D232, and D238 mediate binding. While residues D303, D309, D363, D365, and D371 are involved in Ca^{2+} binding in the C2B domain. Mutating these residues has been found to impair the Ca^{2+} sensitivity of Synaptotagmin and cause defects in synchronous release[54]. Further proof that Synaptotagmin was the Ca^{2+} sensor in synaptic transmission was obtained from experiments that genetically rescued evoked release[54].

The basal level of intracellular Ca^{2+} is in the range of 40-100 nM. Changes to this local concentration of Ca^{2+} in neurons stimulates neuronal exocytosis[45]. Syt1 on its own has a low mM affinity for Ca^{2+} and it is believed to have an incomplete coordination sphere (figure 6) for the divalent cation. In the presence of negatively charged phospholipid headgroups, the coordination sites are complete; increasing the Ca^{2+} affinity by up to 1000-fold[54]. Hence, the uptake of

the Ca^{2+} by Syt1 triggers an interaction that has been implicated to be electrostatic in nature and driven by hydrophobic interaction of the loops to the lipid membrane.

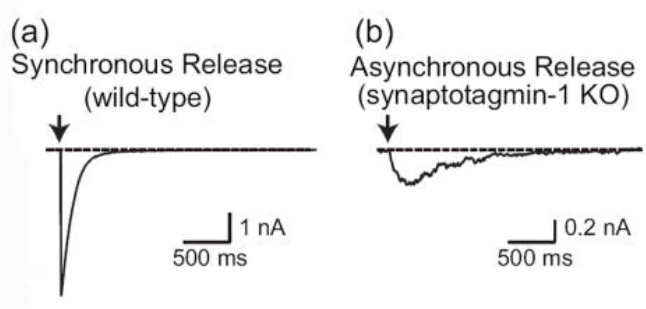

Figure 7. Synchronous and asynchronous release detected by whole-cell patch clamp recordings (taken from Pang 2010)

Studies have shown that Syt1 knockouts affect the rapid synchronous release in excitatory hippocampal neurons as shown in figure 7[55]. This was done by amperometry and whole cell patch clamp studies where a dramatic increase in the current occurs following Ca^{2+} triggered fast release. Syt1 was shown to be critical to the size of the vesicle fusion event[23,56]. While many different fusion process occur by a similar process as that of neurotransmitter release, processes such as hormonal release from endocrine cells occurs on a much slower time scale. This is thought to be due to less efficient mechanism of priming the vesicles near the release sites hence not being tightly coupled to the Ca^{2+} channels[1].

Synaptotagmin is also hypothesized to be responsible for switching the asynchronous release into the synchronous component, by inhibiting fusion until the influx Ca^{2+} [1]. Members of the C2 domain protein family and Synaptotagmin

have also been proposed to facilitate membrane fusion by inducing membrane curvature[46].

The C2B domain has been found to be more critical to Synaptotagmin's role in neurotransmission than C2A. Unlike C2B, electrophysiological studies showed that alteration of the C2A Ca^{2+} binding motif by mutagenesis did not disrupt synchronous release in vivo demonstrating that it has a less severe consequence[57]. It has been postulated that C2B domain maybe involved in communicating with the SNAREs or have a deeper interaction with other negatively charged lipids like phosphatidylinositol 4,5-bisphosphate (PIP_2), which are available in the plasma membrane[57].

Key regulators: Complexin, Munc13 and Munc18

The importance of complexin was revealed when experiments using complexin knockouts showed that Ca^{2+} could not stimulate exocytosis, a response equivalent to Synaptotagmin null mice[58]. Till now, its exact role has not been determined and it does not have a Ca^{2+} binding site that is directly related to the Ca^{2+} signal. It has been given an inhibitory as well as a stimulatory role in the membrane fusion event. Complexin is a 15 kDa soluble protein and it has been crystalized interacting with the SNAREs[59, 60]. The X-ray crystal structure suggests that complexin binds to SNARE complex as if to stabilize it and has been postulated by several groups to function as a clamp[61, 62]. In this clamping model complexin is believed to block synaptic fusion by clamping or inhibiting the

complete assembly of the SNAREs until the Ca^{2+} signal arrives. In this manner it acts as a regulator for the synchronous fusion event.

Giraudo et al. published their finding that there is an intimate interaction between SNARE and complexin which is essential for its regulatory role. The accessory helix of Complexin is thought to bind to the membrane-proximal portion of the t-SNARE (target SNARE – Syntaxin) impeding the zippering with the v-SNARE (vesicle SNARE - Synaptobrevin) hence having an inhibitory role until the signal for fast fusion arrives[63, 26]. It is believed this 'clamping' function of Complexin is also necessary for activating the full zippering of the SNAREs and completing the fusion steps.

The Sec1/Munc18 (SM) protein was first found to be of interest when it was purified bound to Syntaxin[26]. Identifying Munc18 in mice was a revelation since it is homologous to the Sec1 protein in yeast. A series of genetic screening and deletions of the synaptic Munc18 impaired neurotransmission even more strongly than Synaptobrevin knockouts[64]. This shows that the Sec1/Munc18 family of proteins are intricately involved in the cell secretory pathway.

Munc13 contains several domains such as the regulatory alpha helical MUN domain and the Ca^{2+} binding domain, C2B[65, 66]. Electrophysiological experiments on Munc13 knock outs in hippocampal neurons established that MUN domain could rescue function, highlighting its importance in exocytosis[65]. Another group

reported that Munc13 affects the function of Syntaxin by directly regulating its open conformation for fusion[67]. Interestingly, it was found that C2B was the only C2 domain in Munc13 to bind Ca^{2+} and it interacted with phospholipids with an affinity for negatively charged phosphatidylinositol phosphates like PIP and PIP_2 [66].

SNARE and Synaptotagmin mechanism of action

While there are different models for how these fusion proteins regulate synchronous release, the general consensus is that the SNAREs and Synaptotagmin form a minimal machinery for Ca^{2+} dependent fast release. There is no model that accurately provides the structural information for the coupling of the SNARE complex and Synaptotagmin. The exact role of Synaptotagmin especially has been hard to pin down since it has been found to interact with the SNAREs as well as lipid membranes separately. The prevalent model for membrane fusion and release will be discussed in this section.

Tucker et al. were able to study the fusion event mediated by SNAREs reconstituted into vesicles and Synaptotagmin in the presence of Ca^{2+} [68]. Disruption of the SNARE formation by cleaving Synaptobrevin impaired the fusion. Similarly, removing the Ca^{2+} binding capability in Synaptotagmin mutants abolished fusion. The confounding question of what the molecular mechanism of the SNAREs and Synaptotagmin is and how they coordinate fusion has been of great interest. Do they interact with each other when Ca^{2+} signal arrives? The

binding affinity, K_d between SNARE and Synaptotagmin was reported to be in the weak micromolar range[68]. While a 1D NMR experiment done by Zhou et al. reported a much higher apparent K_d of 2uM which was claimed not to be under saturating conditions[69]. While the membrane binding affinity of Synaptotagmin has been reported to be in the low micromolar range suggesting a tighter interaction[70]. The hypothesis that the SNAREs and Synaptotagmin interact is well liked because of the intricate level of synchronization required between the two for the fusion to be exact and accomplished so precisely.

Brunger's group published a model based on their single molecule FRET studies that portrayed Synaptotagmin interacting in a specific manner to the SNAREs [71].

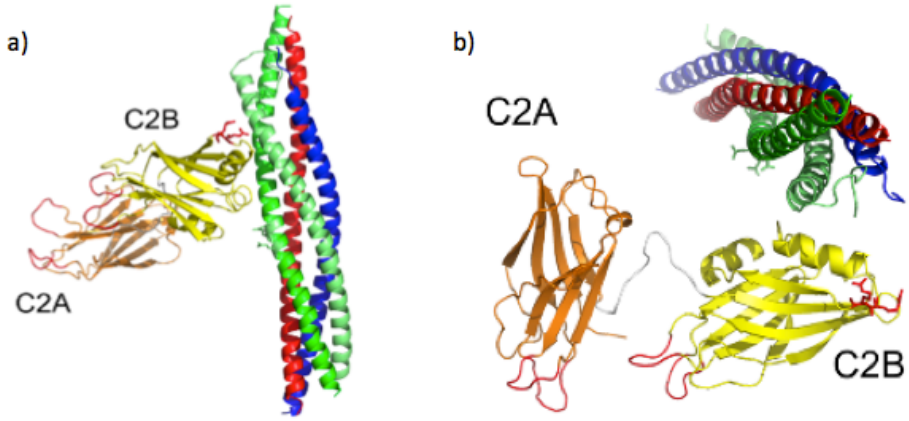

Figure 8. smFRET derived model of Syt1-SNARE interaction in different view angle (taken from Choi 2010)

As shown in figure 8, the membrane reconstituted SNARE complex and the cytoplasmic synaptotagmin domain were fluorescently labeled at various positions and the largest populated FRET signals between the two were used to

generate the model[71]. It shows that the 'bottom' face of C2B domain where the two highly conserved arginine residues (in red sticks, opposite the Ca^{2+} loops), interact with SNAP25 in the SNARE complex. The model also portrays both the Ca^{2+} binding loops in C2A and C2B domain are pointing away from the SNARE complex – as if to facilitate its primary function which is to bind membranes in Ca^{2+} presence[71]. However there was no mention of the polybasic face of Synaptotagmin which has been shown to interact with the SNAREs through NMR and EPR (Electron Paramagnetic Resonance) experiments [69, 72,73]. The experiment was also conducted in membranes containing only phosphatidylcholine (PC). The Ca^{2+} binding function of Synaptotagmin requires negatively charged lipid, phosphatidylserine (PS)[54].

Another model proposed by Rizo's group, showed that Synaptotagmin in the presence of Ca^{2+} binds to phospholipids and SNARE complex simultaneously forming a quaternary SNARE-synaptotagmin-Ca^{2+}-phospholipid complex [72]. The model generated from those data portrayed the polybasic face of synaptotagmin interacting with the SNAREs while the C2 domains inserted into the bilayer in a Ca^{2+} dependent manner. However the NMR data on synaptotagmin showing perturbations, or chemical shift changes, in the presence of the SNARE complex was done in the absence of Ca^{2+} due to experimental artifacts. Since neither of the models from Brunger's and Rizo's group was done in physiological conditions for synaptotagmin's function, it is hard to judge the merits of the proposed models. On the other hand, EPR studies done by Lai et al. reported that the

interaction made by the SNAREs and Synaptotagmin is instead weak and forms a complex that is structurally heterogeneous[74].

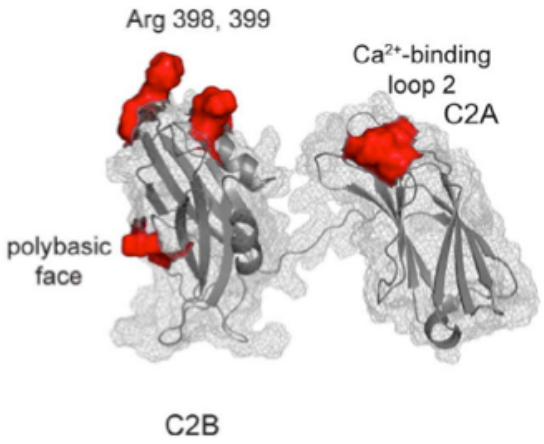

Figure 9. EPR studies on Syt1 C2AB qualitatively indicate several sites showing SNARE interaction (taken from Lai 2011)

Synaptotagmin, C2AB, was spin labeled with a methanethiosulfonothioate spin label (MTSL) at various positions and the SNARE complex was added in excess. EPR experiments based on CW lineshapes and pulsed DEER measurements were used to analyze the structure of the synaptotagmin/SNARE complex. While the arginine apex or the 'bottom' face of C2B domain did experience contact with the SNARE complex just like the smFRET model indicated, it was also shown that other regions (colored in red) in Synaptotagmin experienced SNARE contact. A definite docking model between the two could not be generated that included all the interactions observed.

A recent paper by Sudhof 's group proposed that increasing the number of SNAREs increased the Ca^{2+} sensitivity and speed of the exocytosis process[7].

They used paired patch clamp recordings of the axon terminals and were able to monitor release at a microsecond time resolution[7]. It was postulated that the increase in SNARE complex also affected the Ca^{2+} affinity of release due to recruitment of more Ca^{2+} sensors to the active zone. In his proposed mechanistic model for fusion, he ruled out the opening of the regulatory motif H_{abc} domain in Syntaxin, which has been implicated in an inhibitory role for SNARE formation once the Ca^{2+} signal arrives, due to the impracticality of the complex steps to execute within the hundreds of microsecond time limit. As has been the popular view of the priming stage, he proposed that partial assembly of the SNAREs is necessary before the Ca^{2+} signal.

While there is more to the complex field of membrane fusion and the cell secretory pathway, a great deal of work has focused on elucidation of the key functions of proteins like synaptotagmin. Synaptotagmin acts as the calcium sensor in neuronal exocytosis and one well-defined function of synaptotagmin is to bind membranes containing negatively charged lipids, PS, in the presence of Ca^{2+}. This interaction alone may result in the exocytosis of hundreds of vesicles in a coordinated fashion.

Biochemistry of the cell membrane

The type and amount of charged lipids in the vesicle and cell membrane are important in influencing synaptotagmin and other effector proteins in their function.

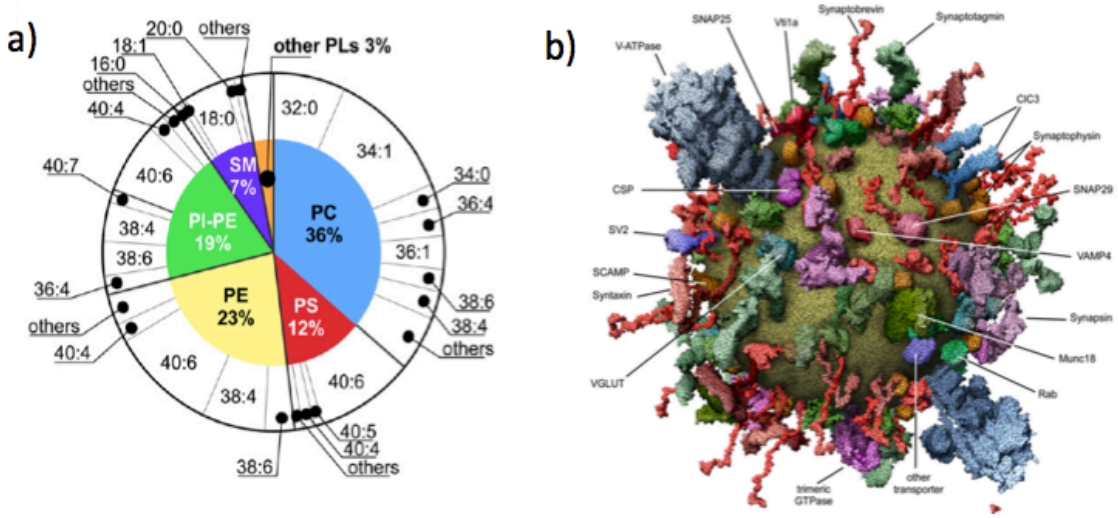

Figure 10. Molecular analysis of a purified synaptic vesicle (taken from Takamori 2006)

In figure 10b, the vesicle is heavily covered by a large number of integral membrane proteins[75]. A major and thorough experimental analysis of the protein and lipid components in purified synaptic vesicles (SVs) from rat brain was performed by Takamori and colleagues[75]. Through mass spectrometry, they were able to accurately quantitate the size and mass of the synaptic vesicle and account for the proteins and lipid composition in the trafficking organelle. It was found that an average synaptic vesicle had a diameter of 41.6 nm with a mass of 17.8 MDa[75]. The protein stoichiometry yielded a surprisingly high surface density of Synaptobrevin compared to the 80 other proteins identified. About 70 copies of Synaptobrevin, 15 copies of Synaptotagmin, 6 of Syntaxin 1 and 2 of SNAP-25 were found to reside per synaptic vesicle[75]. The low number of Syntaxin and SNAP 25 is not surprising since they are ubiquitously found in intracellular membrane compartments, especially on the plasma membrane of the presynaptic cell. As for the lipid composition, it was found that

phosphatidylcholine, a zwitterionic phospholipid, accounted for majority of the lipid in the vesicle while negatively charged phosphatidylserine (PS) accounted for 12% and highly negatively charged phophatidylinositols (PI variants) for less than 2%[75]. It is important to note that the precursors of signal transduction, phosphorylated inositol lipids, are found in the plasma membrane in the presynaptic terminal[76]. For example, phosphatidylinositol 4,5-bisphosphate (PIP_2) has been found to localize in the plasma membrane and hence be involved in membrane targeting since it is specific to several C2 domain containing proteins like PKCα and Synaptotagmin [77, 78; 79, 78, 76].

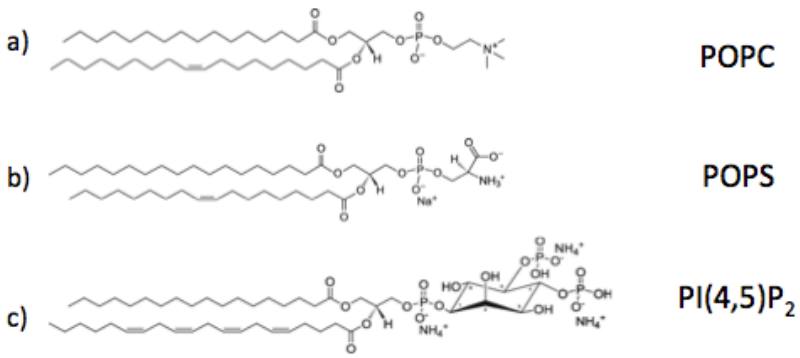

Figure 11. Chemical structure of prevalent phospholipids; POPC, POPS and PIP_2 (taken from Avanti Polar Lipids)

Phosphatidylinositols

Signaling role of phosphatidylinositides in generating second messengers was recognized in the 1980s [80; 81]. It was found that phospholipase C-mediated hydrolysis of PIP_2 yields a byproduct $PI(1,4,5)P_3$ which regulates Ca^{2+} signaling and important phosphorylation mechanisms[81]. The wide range of signaling roles of phosphoinositides, some of which are to activate enzymes, include regulating cytoskeletal assembly, membrane budding and fusion events[80, 82]. They were

later recognized as important cofactors for some peripheral membrane binding proteins aside from their second messenger role. Some of the earlier well-studied proteins that bind to PIP_2 are MARCKS and pleckstrin homology (PH) domains[82]. PIP_2 as seen in figure 11 has three phosphorylated positions on its head group that gives rise to a high negative charge of -3, -4, -5 depending on the local pH[82].

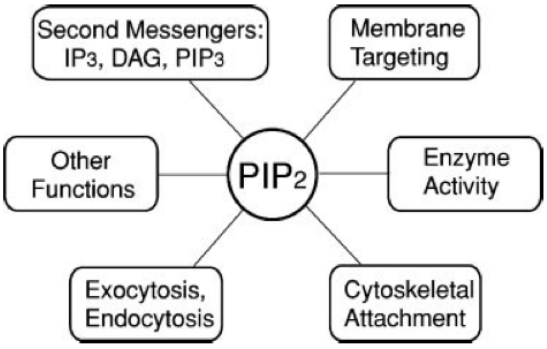

Figure 12. Multiple functions of phosphatidylinositol 4,5 –bisphosphate (PIP_2) (taken from McLauglin 2002)

PIP_2 makes up only 1% of the phospholipid in plasma membrane of a cell, however, it is the most abundant polyphosphoinositide in the cell[82]. The specificity of Synaptotagmin to phosphatidylinositides was first shown by Fukuda in 1994[83]. In particular the C2B domain was found to have a 1:1 stoichiometric binding to PIP_2 and PIP_3[79]. Protein Kinase Cα (PKCα) contains a highly conserved C2 domain which usually functions in Ca^{2+} dependent membrane docking and helps to activate a range of other intracellular protein-lipid events[84]. While PKCα was known to bind to the negatively charged lipid, phosphatidylserine (PS), it was discovered that PIP_2 was essential for the membrane targeting role of PKCα[84]. EPR studies has been done to look at the

membrane docking mechanism of C2 domains of PKCα and Synaptotagmin since it has been reported to associate with the membranes with higher specificity and affinity[85, 76]. It has been reported in both studies that the highly conserved residues in the poly-lysine strand mediate the interaction of C2 domain to the PIP_2 containing lipid bilayer. Kuo et al., was able to show that the addition of 1 mole percent acidic phospholipid $PI(4,5)P_2$ to 3:1 POPC:POPC large unilamellar vesicles (LUVs) causes Ca^{2+} bound Syt1 to drive bilayers closer from 43Å to 35Å[76]. This ability to drive membranes closer could indicate a mechanism by which the C2 domains in Synaptotagmin trigger fusion.

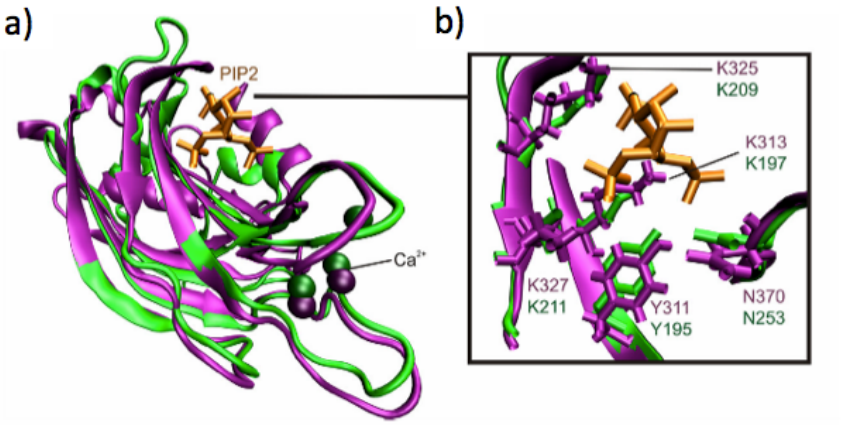

Figure 13. Superimposition of Syt1 C2B domain with C2 domain of PKCα bound to PIP_2 (taken from Bogaart 2012)

As seen in figure 13, the residues involved in the crystal structure of PKCα binding to PIP_2 include lysine residues K197, K209 and K211, which corresponds to residues K325, K327 and K313 in Syt C2B conserved polybasic strand [70]. It was proposed that there is cooperativity between PIP_2 and Ca^{2+} binding of Synaptotagmin which may be a process underlying Ca^{2+} triggered membrane fusion[70].

Membrane electrostatic interactions and binding energetics

Membrane binding of proteins is driven by a number of forces, such as the hydrophobic effect and electrostatic interactions[14]. It has been shown through in vivo and in vitro studies that a number of proteins need hydrophobic residues and a basic cluster of residues to associate with the plasma membrane for their crucial biological function[82]. In particular, the presence of highly negatively charged lipid PIP_2, which is localized in the plasma membrane, has been shown to be a membrane target for peripheral membrane proteins like PKCα, myristoylated alanine-rich C kinase substrate (MARCKS) and Synaptotagmin. An electrostatic 'switch' mechanism has also been proposed to account for the membrane association of proteins [86]. Do all of the electrostatic interactions work through nonspecific association to membrane surfaces? Several studies have indicated that poly-lysine residues in C2 protein domains have specificity to phosphatidylinositides [77, 87; 88, 88].

Electrostatic interactions play a role in the interaction of positively charged peptides or proteins to negatively charged membrane surfaces. This interaction is due to a long-range Coulombic interaction that becomes stronger as the distance gets shorter. Once the protein gets very close to the membrane surface, there is a desolvation penalty caused by the repulsion of polar water molecules[14]. This penalty is due to the energy cost in displacing the water molecules from the membrane surface. The free energy minimum of this electrostatic attraction occurs at the thickness of a water layer where the long-range coulombic

attraction is balanced by the short-range desolvation repulsion[14]. While electrostatic interactions can be specific between certain charged functional groups or molecules as shown by crystal structure of bound ligands, the 'nonspecific' interaction is more accurately defined by a molar partition coefficient instead of a binding constant since there is no stoichiometric relationship in the complex[14]. This specificity can be tested by using different isoforms with another molecular structure of the ligand such as $PI(4,5)P_2$ to $PI(3,5)P_2$.

Ben-Tal et al. reported the binding energetics of basic lysine peptides to 2:1 PC/PS membranes at different ionic concentrations[89]. It was found that peptides with varying number of multiple Lysine residues (Lys3, Lys5 and Lys7) in 100mM KCl resulted in binding energy of -1 kcal/mol per lysine residue[89]. It is understood that this value would change in different concentration and type of negatively charged lipids like PS and PIP_2.

Research Aims

Several important proteins in the cell are able to bind to membranes through a process driven by both hydrophobic and charged residues. It was reported by Xue et al. that the C2B domain of Synaptagmin has two highly conserved key arginine residues, R398 and R399, in the opposite face of its Ca^{2+} binding loops[90]. They showed that mutating these two key arginine residues virtually abolished the synchronous release in mice hippocampal neurons. They

hypothesized that the highly conserved positively charged residues are important in a membrane-bridging role for the C2B domain that is necessary for vesicle fusion. But they provided no data regarding the importance of these residues in the docking of C2B. There are also a number of unanswered questions. For example, how do two positively charged residues opposite the Ca^{2+} binding site alter the Ca^{2+}-dependent phenotype? Do these residues interact with the membrane or is there a more specific protein association, perhaps with the SNAREs, involved in the action of C2B in exocytosis?

In another study, Park et al. established that ATP present in the cytoplasm modulates Synaptotagmin's ability to bind in a cis or trans conformation in the presence of PIP_2 in the plasma membrane[91]. ATP with its four phosphate groups is highly negatively charged (-4) and could compete with PIP_2 in binding to the polybasic strand in C2B domain. While it is known that the highly conserved polybasic strand has a higher affinity for phosphoinositides, it was proposed that either ATP or PIP_2 has site coordination within the poly-lysine region, and that (binding of ATP or PIP_2) accounts for the different binding modes of synaptotagmin[91]. One question that will be addressed in this thesis is whether interactions with membrane associated PIP_2 are specific or non-specific, and whether binding is driven purely by electrostatic interactions.

Along with these important questions, another general goal of the research in this thesis was to understand protein – membrane electrostatic interactions. How do

the negatively charged residues in Synaptotagmin I (C2B) contribute to the binding energetics to membranes in the cell? What are the roles of the critical double arginines in neuronal fusion, and how are they different from positive charged residues in the polybasic strand? Is the membrane binding of C2B truly governed by specific coordination between the lysine residues in the polybasic strand with PIP_2. And do other polyelectrolytes like ATP modulate the binding mode of Synaptotagmin by competing for the same binding sites? Do we need to consider the effect of other physiologically available cations like Mg^{2+} for the role of ATP? And finally can we correlate the binding affinities between Synaptatagmin and the charged species to the membrane binding mechanism of Synaptotagmin?

Most importantly, the role of unspecific electrostatic interactions of proteins with the lipid bilayer or other proteins is investigated to allow one to connect the dynamic interplay of a cell signaling ‘switch’ mechanism, membrane fusion and more. The questions above are investigated in this research thesis, and they provide insight into the nature of the synaptotagmin 1 – membrane interaction, which we believe is fundamental in triggering the neuronal fusion event. Hopefully this work will facilitate future studies to unravel the events that ultimately facilitate membrane fusion in the neuron.

2. Materials and Methods

Expression and Purification:

DNA manipulation by site-directed mutagenesis

DNA of rat Syt1 (P12707) was acquired from Dr. Carl Creutz (Pharmacology Department, University of Virginia) in the PGEX-KG vector encoding amino acid residues 136-260 (Syt1 C2A), 249 -421 (Syt1 C2B), 96-421 (Syt1 C2AB) and 136-421 (Syt1 short C2AB: shC2AB). To produce the necessary plasmid, the gene encoding residues 136–265 (~17.4 KD) from the wild type C2A domain was ligated into the plasmid vector pGEX-kG following the coding region for GST[92]. The single native cysteine residue at position 277 was mutated to alanine by typical PCR strategies. Quick-change site-directed mutagenesis was performed to produce the single and double glutamine mutants (R398Q and R398QR399Q) on the C2AB T285C plasmid. Single cysteine mutants M173C, V304C, L323C, K327C and T329C were produced on the shC2AB construct (136-421) and the double mutants N396C and A415C were made on the C2B domain. For the binding assay experiment, the arginine double mutants (R398QR399Q) and the single and double lysine mutants (K326A and K326A K327A) were mutated on the C2AB construct. All mutagenesis was confirmed by DNA sequencing.

Protein expression and purification

The syt1 C2A, C2B, C2AB constructs were encoded in a frame with glutathione-S-transferase (GST tag)[50]. The wildtype and mutant plasmids were expressed in BL21 (DE3) pLysS cells (Invitrogen), and cells were grown in LB media until OD_{600nm} of 0.8 -1.0 was achieved and induced with 0.1M IPTG. After cells were

let to shake for at least 6hrs at 20°C, they were spun down. Protein inhibitors, AEBSF, leupeptin, aprotinin and Benzonase nuclease were added to the resuspended cell pellet before being french-pressed to lyse the cell walls. The cell debris was then spun down at 18 000rpm for half an hour. The resulting supernatant was run through the GST affinity column to trap the GST-tagged protein of interest. Thrombin cleavage of GST tag was also done in the purification procedure, after which, steps were taken to remove the thrombin and GST tag from the protein sample. After eluting with elution buffer (NaCl, MOPS, pH), the protein was buffer exchanged with respective A (100mM NaCl) and B buffer (800mM NaCl) as a preparatory step for ion-exchange chromatography.

The molecular weights (MW) of shC2A, C2B, shC2AB, and C2AB were 17.4kDa, 20.8kDa, 34.5kDa and 37.3kDa, respectively. SDS PAGE gels were run to ensure the protein of interest was clean and of correct molecular size. The maximum absorbance at 278nm was checked to make sure protein fractions were pure from any nucleic acid contamination. The protein concentration was determined with the Bradford Assay.

The isotopically labeled N^{15} C2A and C2B domain for the NMR experiment had some variation to how the cells were grown for protein expression. C2B and C2A constructs were expressed in BL21 (DE3) pLysS cells and grown in minimal media where $^{15}NH_4Cl$ was the sole nitrogen source. It was induced at OD_{600nm} of 0.6-0.8 with 0.5M IPTG. The cells were let to further shake for 6 hours in 20°C

before being pelleted for lysis. The cell lysate was spun down in a similar manner as above and the supernatant extracted for affinity column purification and an ion-exchange column.

The purified protein with a concentration of 0.4-0.8mM in NMR buffer (3mM $CaCl_2$, 150mM NaCl, 50mM MES, pH 6.3) was used to perform 2D HSQC NMR experiments. Titration of the ligands (o-phosphoserine, ATP, IP_3) was done at concentrations ranging from 0.05 – 4mM. The final protein sample had 10% D_2O and the NMR samples were placed in Shigemi tubes. The experiment was conducted in Bruker 600MHz NMR spectrometer at temperature 27°C. The standard was 50 μM DSS in the same buffer conditions.

The NMR data were processed in NMRpipe. The assignments were matched in Sparky from the PDB NMR resonance assignments of C2A (PDB 1BYN) and C2B (PDB 1K5W) from Rizo's group[52, 93].

Lipid Preparation

1-palmitoyl-2-oleoyl-sn-glycero-3-phosphocholine (POPC), 1-palmitoyl-2-oleoyl-sn-glycero-3-phospho-L-serine (POPS), L-α-phosphatidylinositol-4,5 bisphosphate (brain $PI(4,5)P_2$) and 1-palmitoyl-2-stearoyl-(5-doxyl)-sn-glycero-3-phosphocholine (5-doxyl PC) were purchased from Avanti Polar Lipids. Large Unilamellar Vesicles (LUVs) of 100mM concentration at the following molar ratios were prepared:

PCPS (3:1), PCPS (85:15), PCPS (4:1), PCPIP$_2$ (98:2), PCPIP$_2$ (95:5), PCPSPIP$_2$ (87.5:10:2.5), PCPSPIP$_2$ (84.5:5:0.5), PCPS5-doxyl PC (74:25:1), PCPIP$_2$5doxylPC (97:2:1)

The lipids were dissolved in chloroform in a round bottom flask and mixed uniformly in a rotary evaporator, while a vacuum was applied to dry the lipid mixture into a thin film. The lipid film was vacuum desiccated overnight to remove any residual chloroform. The dried down lipid mixture was resuspended in either sucrose buffer (176mM sucrose, 1mM MOPS, pH7.0) or Ca^{2+} buffer (1mM $CaCl_2$, 1mM MOPS, 100mM KCl, pH 7.0), and the lipid mixture was freeze-thawed five times before being extruded through a 100nm polycarbonate filter.

For sucrose loaded LUVs, another wash step with Ca^{2+} buffer was incorporated to remove the external sucrose solution through an ultracentrifugation technique, and then resuspended in Ca^{2+} buffer. For experimental conditions that were Ca^{2+}-free, a no- Ca^{2+} buffer (1mM MOPS, 100mM KCl, pH 7.0) was added to the LUVs instead.

For the doxyl-labeled PC experiment, 10mM NiEDDA was added to the buffer for resuspending the dried-down lipid mixture so that Ni was accessible to both the inner and outer leaflet of the spin-labeled PC.

Vesicle Sedimentation Assay

Peripheral membrane proteins often become active when they bind to membrane surfaces. Methods to quantitate this binding and determine the effects of functional groups or lipid composition on binding can be very useful in determining the molecular function of the protein. The equilibrium membrane binding affinity may be measured using a vesicle sedimentation assay, and the ultracentrifugation method established by Buser and Mchlaughlin in 1998 is a well-documented approach to quantitate the protein membrane interactions[94]. Equilibrium conditions are applied when doing this assay, which accurately reports the lipid partition coefficient, making this technique extremely useful.

The conditions under which binding experiments are performed are important in order to obtain accurate and meaningful results. The ionic strength has to be physiological and the lipid to protein mole ratio has to be high enough to take make sure the overall net surface charge density on the membrane is not altered by protein binding.

The membrane binding assay used makes use of sucrose-loaded vesicles and ultracentrifugation. Following the equilibration of the protein, the lipid vesicles are pelleted and the concentration of the unbound protein is measured using intrinsic protein tryptophan emission or the emission from a protein attached fluorophore. Since the initial total protein concentration is known, the bound protein can be

calculated to determine the fraction of protein bound. This is then used to plot a binding isotherm with respect to the lipid concentration.

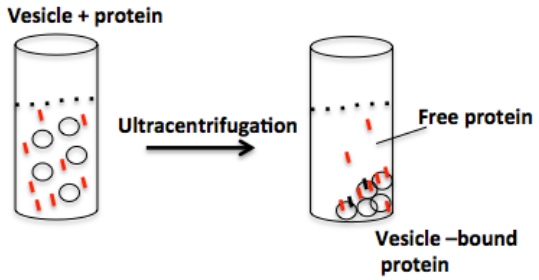

Figure 14. Ultracentrifugation technique to separate the membrane bound protein from the unbound (free) protein

This ultracentrifugation technique was used to measure the membrane binding affinity, K, of C2AB mutants in different lipid compositions. For tryptophan-based emission experiments, a final protein concentration of 0.1uM were added to sucrose loaded LUVs at final concentrations ranging from 0.02-15mM lipid. They were incubated in room temperature for 10 minutes before being centrifuged at 160,000g for an hour. The supernatant was extracted and the concentration of unbound protein determined.

Bodipy FL C1-IA or bodipy maleimide labeling on C2AB was used to repeat the measurements at lower protein concentrations confirmed the minimum lipid to protein molar ratio necessary to obtain a true binding constant, K. Similar binding affinities, K, for PC:PS LUVs were achieved when lipid to protein ratio was at least 140:1.

For each experimental condition, at least two measurements of the fraction of bound protein, fb, were made to determine a molar partition coefficient, K, which is defined as:

$$[P]_m / [L] = K[P]$$

Equation 2.1

Where, [P] is the concentration of protein in the bulk aqueous phase, $[P]_m$ is the molar concentration of protein bound to the membrane, and [L] is the molar concentration of accessible lipid. Provided that the protein concentrations are dilute on the membrane surface ([lipid]>>[protein]), the fraction of protein, f_b, will be given by:

$$f_b = K[L]/1+K[L]$$

Equation 2.2

The value of K (M^{-1}) was derived when the data plot was fit using this equation in OriginPro 7.5.

Single cysteine mutations in C2AB (269C and A123C) were labeled with bodipy maleimide to examine the binding affinity at very low protein concentrations. This allowed us to determine whether the lipid: protein mole ratios were sufficiently large to obtain a binding constant that represented a true protein-membrane affinity. Under sufficiently dilute conditions, the binding constant, K, will remain unchanged as the lipid: protein ratio is increased. It was found that a minimum lipid to protein ratio of 140:1 gave a K that remained consistent. A phosphate

assay by Ames B.N., 1966 was performed on the sucrose-loaded vesicles to verify the lipid concentrations for each experimental preparation[95].

Phosphate Assay

A phosphate assay protocol is used to quantitate the amount or concentration of lipid for the different preparations of the large unilamellar vesicles (LUVs)[95]. First, eight tubes of phosphate standards (ranging from 0 to 0.2umol) were prepared from 0.1mM KH_2PO_4 and dried overnight in the oven. Next, 5uL of the 100mM sucrose-loaded vesicles were added to glass tubes in triplicates. These samples were dried down in the oven at 125°C for half an hour.

Then, 200uL of 10% $Mg(NO_3)_2$ solution was added to each of the standards as well as the sample tubes. This mixture was further dried down in the oven. The tubes were removed from the oven, and flamed at the bottom so that the reagents could further react and form a white solid byproduct. Then, to each tube, 1.0mL of 0.5N HCl was added and vortexed to completely dissolve the white solid.

The mixture in the tubes was further heated in the oven for half an hour while being covered by marbles. Next, 2mL of a mixture containing 6 part ammonium molybdate (dissolved in 10% H_2SO_4) and 1 part 10% ascorbic acid was added to each tube. The reaction samples were then incubated in a 45°C water bath for half an hour before being analyzed spectroscopically for the phosphate content. To quantitate the phosphate level in each sample, the absorbance of the

standards and samples were recorded at 820nm on UV/Vis spectrometer. The absorbance of the standards were used to create a linear calibration curve whereupon, the concentration of the samples could be analyzed from.

Spin-labeling and cw-EPR spectrum acquisition

The purified single cysteine mutants are spin labeled with MTSL. It was spin labeled with MTSL at a 1:1:10 molar ratio of protein:DTT:MTSL and incubated in the dark for 2 hours in room temperature or overnight at 4°C. The excess free spin was desalted out using a desalting column from HiPrep 16/10 desalting column from GE healthcare. The spin-labeled sample is then concentrated to 100-200uM in a 10K ultra-centrifugal unit (Amicon Ultra 10).

About 8uL of the concentrate sample were loaded onto glass capillaries with an outer diameter (o.d.) of 0.84mm (VitroCom, NJ). The Varian E-line X-band spectrometer fitted with a loop-gap resonator (Medical Advance, Milawakee, WI) or a Bruker EMX spectrometer with a ER 4123D dielectric resonator were used to acquire the EPR spectra[96]. The spectra were recorded at a 2mW microwave power with a magnetic field sweep width of 100 gauss. The spectra were normalized for the total spin number so that the peak amplitude would approximate the extent of the motional averaging of the R1 side-chain[50]. The program BasePhaseNT by Dr. Christian Altenbach was used to normalize the spectra.

Power Saturation

Continuous wave (CW) power saturation measurements were carried out using the Bruker EMX spectrometer (ER 4123D dielectric resonator). Accessibility parameters, Π, and depth parameters, Φ, were calculated by getting the $P_{1/2}$ (figure 22) values from the saturating behavior of samples with respect to secondary paramagnetic reagents: Ni(II)EDDA and O_2 [97]. Power saturation experiments were done by measuring the peak-to-peak amplitude [98] (Figure 24) of the central line of the first derivative EPR spectra in progressive incident microwave power (MW) ranging from 0.25 to 64 mW in 12 steps. The power saturation curves were obtained in the three different conditions of O_2, N_2 and 10mM Ni(II)EDDA . The $P_{1/2}$ value is the microwave power that gives the resonance amplitude at half of its unsaturated value of a sample.

A semi-permeable TPX capillary is used to hold about 6uL of the sample. The $P_{1/2}$ (N_2) is obtained after purging the sample with N_2 gas for 15 minutes and power saturating the sample in the presence of the N_2 gas. This way $P_{1/2}$ (N_2) can be used to account for signal arising from the background. The power saturation measurement with the Ni(II)EDDA probe was also carried out in the presence of the N_2 gas after purging the sample with N_2 gas for 15 minutes to displace the oxygen from sample. Though 10mM of Ni(II)EDDA was used, the $\Delta P_{1/2}$ values were scaled to an effective concentration of 20mM [97]. The accessibility parameter, Π, of O_2 and Ni(II)EDDA , can be calculated from Eqn

2.20. Consequently, the depth parameter, Φ, can be calculated from Eqn 2.23. The depth parameter, Φ, can tell us the location of the protein-bound spin label with respect to the membrane surface.

DEER samples

The double mutant, N396C A415C, on C2B was purified using the regular purification protocol as mentioned in the earlier section. Running a SDS gel and using UV-vis spectrometer for maximum absorbance at 278nm checked for the protein purity. The protein was spin-labeled such that the mole ratio of protein:DTT:MTSL was 1:1:10. The spin-labeling efficiency on both sites were checked by running the cw-EPR spectrum of the individual single labeled C2B 415R1 and C2B 396R1 and adding the spectra together to yield the resultant spectrum from both labels. This additive spectra from the single labeled C2B 415R1 and C2B 396R1 was compared with the double labeled C2B 396R1 415R1.

The double labeled C2B 396R1 415R1 was then used to prepare the DEER sample which had a final concentration of 10% or 50% (by weight) deuterated glycerol (d-glycerol). The glycerol acts as a cryoprotectant as well as a glassing agent since the samples are flash-frozen to be run for the DEER experiment (see EPR Pulse DEER section)[99]. For the membrane bound protein sample, LUVs were added to the protein sample at a 1:200 protein: lipid mole ratio.

Magnetic Resonance

Spectroscopic methods utilize the absorption of radiation by a molecule to initiate energy-level transitions. Among spectroscopic techniques, magnetic resonance spectroscopy lies in the lower energy microwave and radiofrequency range of the electromagnetic spectrum[100]. Magnetic resonance makes use of the intrinsic spins of nuclei and electrons to measure their interactions with an external magnetic field which is relatively weak compared to the higher frequency X -rays and UV-Vis interactions[100]. Magnetic resonance can yield valuable information on the molecule's local electrical and magnetic environment.

Nuclear and Electronic Spin

Electrons and nuclei have an angular momentum or spin that is quantized. In the absence of a magnetic field, the energy levels of the different spin states are degenerate, but in the presence of an applied magnetic field, B, the energy levels of different spin states result are different. [101].

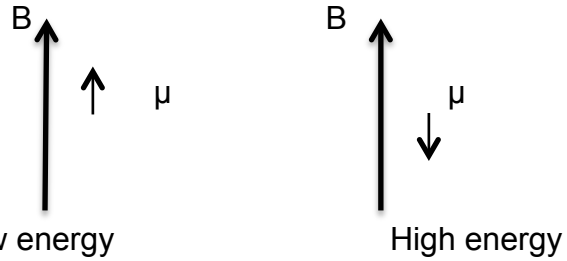

Figure 15. Spin quantum states of magnetic energy

If the spin magnetic moment, μ, is aligned parallel to the vector of the magnetic field, B, the spin is in its lowest energy state[101]. While the anti-parallel projection of μ along the magnetic field, B, dictates a high energy state.

The electromagnetic field in its classical description has two vectors, the electric field and the magnetic field[101]. Unlike other forms of spectroscopy, the magnetic field component is what perturbs the behavior of the spins and allows us to study the spin interaction with the electromagnetic radiation[102]. In order to understand the phenomenon that induces the transition of spins in the lower stable state to the higher, one must understand that the energy required is in the form of one discrete packet - a photon[102]. The idea of a photon or "packet" of energy is that the energy of the radiation must be exactly the energy difference, ΔE, between the two states. This is given by Planck's law, $\Delta E = h\nu$, where h is the universal Planck's constant and ν is the electromagnetic radiation frequency[100].

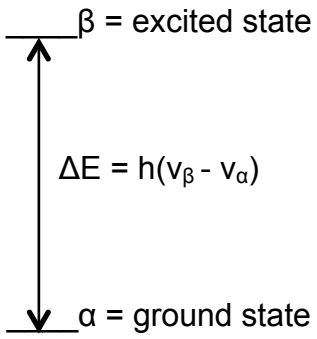

Figure 16. Resonance spin transition in a magnetic field

Only the electromagnetic radiation of the correct frequency, $\nu_{\alpha\beta,}$ can excite the spin and induce an energy transition hence creating resonance[102]. The energy, E, of the magnetic moment, μ, oriented in the magnetic field is denoted by:

$$E = -\mu \cdot B$$

Equation 2.3

The relation between the nucleus or electron magnetic moment and its spin is:

$$\mu = -g\beta S$$

Equation 2.4

Where g is the proportionality constant, β is the Bohr magneton and S is the spin for the electron.

$$\mu = g_n \beta_n I$$

Equation 1.5

Here g_n is the nuclear proportionality constant, β_n is the nuclear magneton and I is the nuclear spin. The minus sign for the electron magnetic moment is due to its magnetic moment and its spin being in opposite directions[100]. The mass of the electron is about 2000 times larger than the proton and taking into account the gyromagnetic ratios between the electron and the proton, the sensitivity of the electron is 700 times more than ^1H [100].

The Zeeman Effect

In order to understand the energy transition of spins, we have to go back to the interactions with the applied magnetic field, B. The spin states of electrons and the nucleus that have a net spin will split its energy levels from a degenerate, energetically equivalent state to a non-degenerate state in the presence of a magnetic field[102]. This primary interaction of the spin with the magnetic field is known as the Zeeman effect.

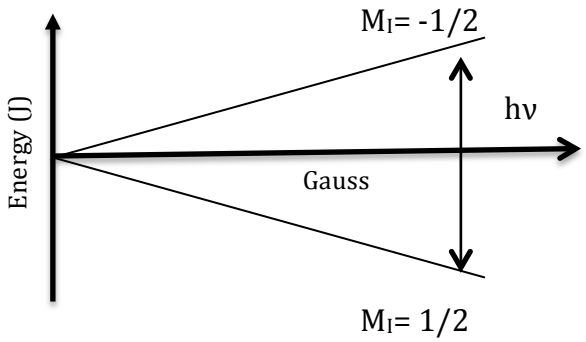

Figure 17. The Zeeman effect – energy level splitting in increasing magnetic field

It is important to understand the fundamental behavior of this energy splitting of a nuclei and electron which depends on the quantized property of the spin[100]. The nuclear spin quantum number, I, dictates the number of allowed transition states or orientations relative to the magnetic field that the spins can occupy[102, 100]. Hence, the number of levels (n) is equal to (2I+1). For a nuclei or electron with I= 1/2, the allowed energy states are given by the values of M_I = -1/2, 0, +1/2. The diagram in figure 17, shows the increasing energy difference of the two spin quantum states M_s= -1/2 and M_s= +1/2 dependent on the magnetic field magnitude.

The energy absorbed for the excitation of the spin to the higher energy level, β, is also denoted by:

$$\Delta E_{\alpha\beta} = \hbar\gamma B$$

Equation 2.6

where ħ is Planck's constant divided by 2π, and γ is the gyromagnetic ratio of the nucleus and is a constant for a specific magnetic species[100, 102]. Translating the

energy from the frequency of the transition to the angular frequency, ω, which is often used in NMR:

$$2\pi v_{\alpha\beta} = \omega_{\alpha\beta}$$

Equation 2.7

$$\Delta E_{\alpha\beta} = \hbar\, \omega_{\alpha\beta}$$

Equation 2.8

Hence, $\omega_{\alpha\beta} = \gamma B$

The classical Boltzmann equation determines the relative population in the low energy, α, and the higher energy, β, states at thermal equilibrium:

$$N_\beta/N_\alpha = e\text{^} (-\Delta E_{\alpha\beta}/kT)$$

Equation 2.9

Where k is the Boltzmann constant and T is the temperature in Kelvin. The $\Delta N_{\alpha\beta}$ between the two energy states typically yields a very tiny population difference at room temperature which correlates to a weak sensitivity of the absorption technique[102]. Hence applying a higher frequency, v, or increasing the magnetic field (B) directly results in an increase in the energy level and a bigger population difference, $\Delta N_{\alpha\beta}$, which gives better sensitivity and resolution.

Hyperfine splitting

While the external magnetic field, B, is required to generate the non-degenerate energy states, there are also other local smaller magnetic interactions that influence the energy splitting of quantum states[100]. The term ‘hyperfine’ arises

from the further splitting of the zeeman peak due to the electron spin interactions with the neighboring nuclei spin[100]. This is otherwise known as 'Spin-Spin' splitting in NMR. When the electron spin, S, experiences the applied field, B, it is also subjected to the magnetic field, B_I, from the nearby nuclear magnetic moment. Hence, for nuclear spin I= ½, this causes the electron spin to essentially experience both the different magnetic fields resulting in the splitting of the EPR line into two[100].

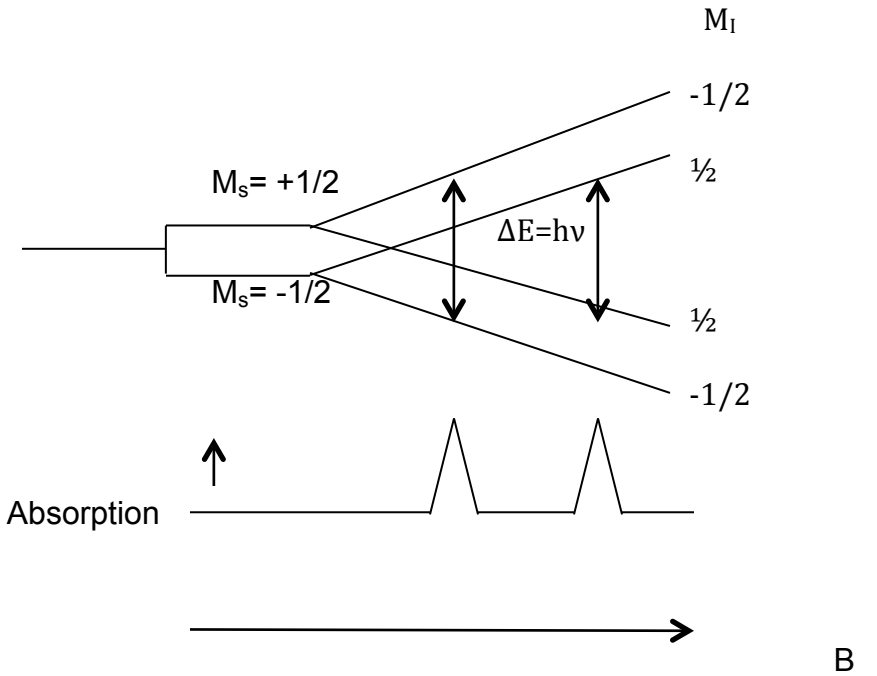

Figure 18. Hyperfine interaction splits energy levels at a constant frequency, v

Figure 18 illustrates how the hyperfine interaction with neighboring nuclei (I= ½) can split a single transition $\Delta E_{\alpha\beta}$ into a doublet. In the diagram, the electron spin quantum states, M_s, splits into the nuclear spin quantum states, M_I. The absorption of the energy with a radiation of fixed frequency corresponds to the excitation along the magnetic field, B. Such spin-spin interaction can further be

influenced by the presence of other nearby nuclei inducing more splitting of energy levels.

Spin-Lattice relaxation

As we discussed how the transition from the ground state to the higher energy level occurs and how the population differences are determined, we verified that it is the Boltzmann distribution, which allows us to understand this relationship. The population at thermal equilibrium is the more energetically favorable condition and the ratio of the number of spins in the two levels can be calculated by using the thermal energy, kT for the equation (Boltzmann). In order to detect a considerable magnetic absorption, it is customary that spins are excited as a group instead as an individual entity.

As mentioned in the earlier section, the population difference is so tiny due to the insufficient energy splitting, especially in NMR, that the ratio can be close to unity in normal room temperature[100]. Hence, some experiments are conducted at low temperatures to enhance this sensitivity. During the experiment where resonance absorbance is taking place, the spin populations will start to saturate and equalize and no further excitation can take place. This is alleviated by other mechanisms for spin relaxation where the induced energy is lost and the spin returns to the low energy level. One of the mechanisms for this is the spin-lattice relaxation and it is characterized by its spin-lattice relaxation time, T_1. In its simple definition, it is the loss of the energy of the spin to its external group of molecules (crystal lattice) surrounding the spin[100]. The time constant, T_1, is also

known as the longitudinal relaxation time constant since the magnetization establishes in the same direction (longitudinally) as the applied field, B[101].

Spin-Spin relaxation

The other mechanism of spin relaxation is due to the effect of neighboring nuclei in NMR and a secondary electron spin in ESR and how the absorption peak can be affected by the dipolar interaction between similar spins[100]. The time constant, T_2, is known as the spin-spin relaxation time or transverse relaxation time[101].

Spin-spin relaxation occurs when the interacting spins experiences different magnetic fields causing them to experience different frequencies that ultimately cause the dephasing of the transverse magnetization or relaxation of the spins[101]. The spin-spin relaxation, T_2, due to its inability to reduce saturation contributes to the broadening of the absorption line and hence determines the instrinsic linewidth, ΔH_{pp}, as shown:

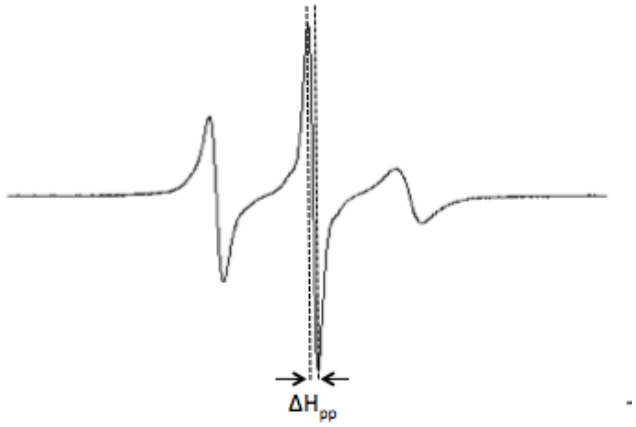

Figure 19. Linewidth of central peak, ΔH_{pp}

$$1/\Delta H_{pp} \approx 1/T_2$$

Equation 2.10

Electron Paramagnetic Resonance (EPR)

An unpaired electron has an intrinsic spin state that yields a net magnetic moment in the presence of an external magnetic field. This can be manipulated to study the dynamics and properties of nitroxide spin labels like methanethiosulfonate spin label, MTSL. The paramagnetic nature of a radical that is stable is a valuable property that scientists can influence by external perturbation through electromagnetic radiation to generate resonance states of the electron spin.

The common nitroxide that has been used to spin label protein is MTSL, which yields an R1 side chain upon forming a disulfide bond with a cysteine in the protein. Site-directed spin labeling is used to generate the R1 side chain on a site of interest in the protein. First, any native cysteine is mutated into an alanine or serine residue to eliminate background labeling of the wild type protein. Then, a cysteine is substituted to the site of interest in the protein by site-directed mutagenesis. Typically the site to be labeled is solvent accessible and outward facing in the protein structure.

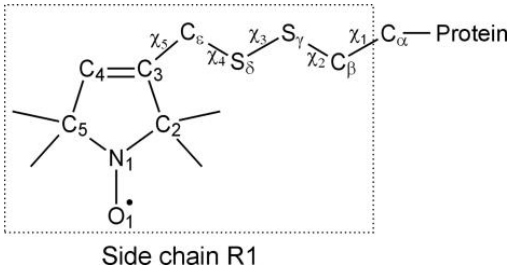

Figure 20. Site-directed spin labeling of MTSL on protein and the R1 side chain structure (adopted from Dr. Altenbach, 2004)

The structure of the nitroxide side chain R1 in figure 20 show the corresponding carbon and sulphur atoms in the side-chain and their dihedral angles (χ)[103]. It was found by crystallographic evidence of the MTSL bound to a helical protein site that a weak H-bond exists between the distal sulphur, S_δ, and the proton on the C_α[104].It was shown that about 2.8 Å distance separates the C_α and S_δ [104]. This suggests that the dihedral angles χ_1, χ_2 and χ_3 have a relatively fixed conformation. While the majority of the spin label spectral line shape is due to the free rotational motion about χ_4 and χ_5.

To further expand on the hyperfine interactions, it is useful to observe the effective magnetic field (B_{eff}) felt by the lone electron as:

$$B_{eff} = B + B_{local}$$

Equation 2.11

Where B is the applied field and B_{local} arises typically from local field caused by the nearby nitrogen nucleus of the spin label. While most lone electrons in free radicals are delocalized over the entire molecule, the unpaired electron in nitroxides is mainly localized on the nitrogen atom p orbital[100]. As discussed in the earlier section, the magnetic moment of an electron spin can interact with the spin of a nearby nuclei resulting in the hyperfine splitting. Similarly, as shown in figure 20, the unpaired electron in the MTSL nitroxide group interacts with the nitrogen nucleus giving rise to the classical three splitting of the absorption peak[100]. This is due to the hyperfine splitting of the electron spin energy levels

into three as determined by the nuclear spin quantum number of nitrogen, I=1. Hence the nuclear spin quantum states are: M_I = -1, 0, 1.

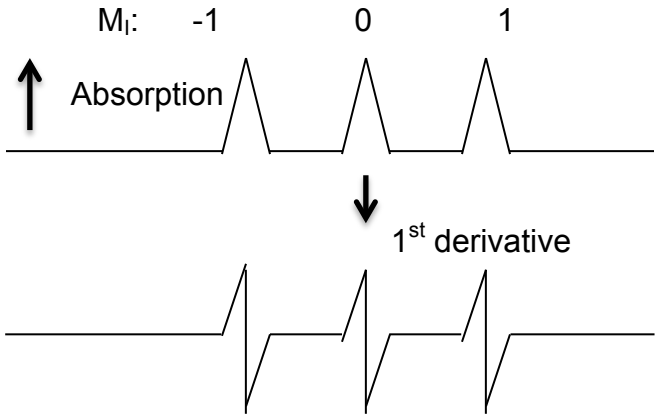

Figure 21. EPR MTSL first derivative spectrum from hyperfine splitting

The EPR spectrum as seen in figure 21, is typically recorded as a first derivative of the absorption peak. This is due the phase-sensitive detection system in the EPR spectrometer. This detection technique increases sensitivity by eliminating noise contribution at other frequencies by modulating the field at a small amplitude of 100kHz[100, 105]. The noise produced by the crystal detector diode at this frequency is also at a minimum hence eliminating the majority of the noise inherent to the device. In order to avoid broadening of the lineshape, the modulation amplitude has to be small since it would mean modulating a small range of the lineshape at a time[100]. A phase sensitive receiver detects signals in phase with the modulation and results in an output current that is first derivative.

Line shape analysis: mobility and backbone dynamics

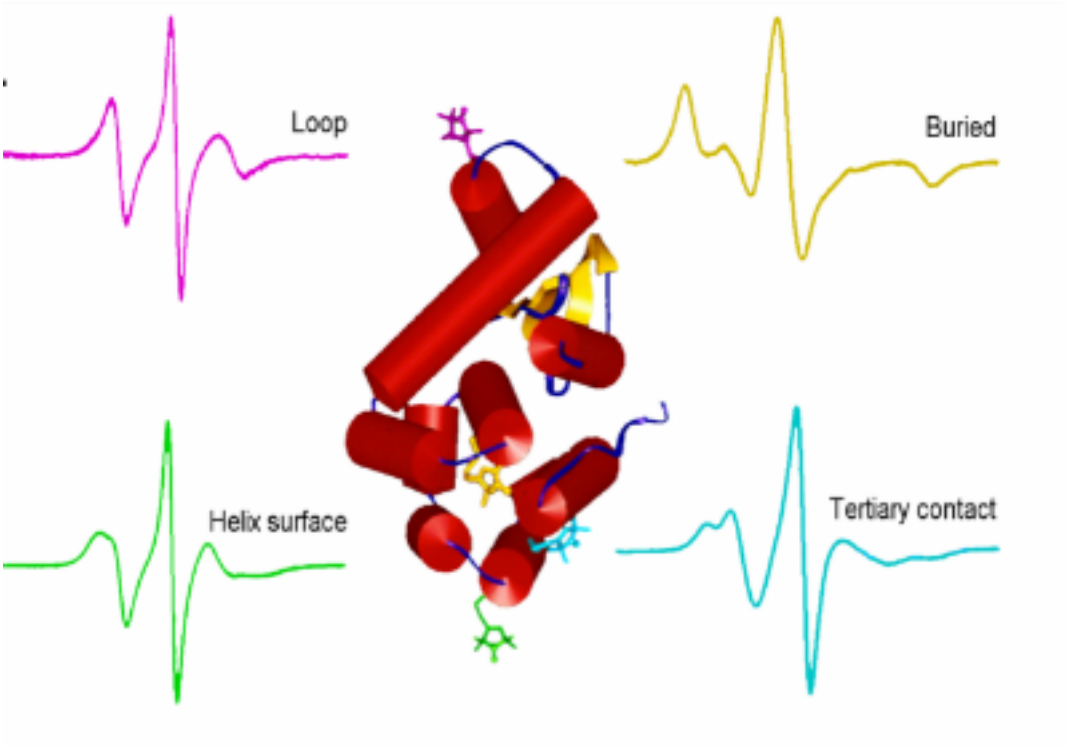

Figure 22. Motional side chain spectrum of spin labeled sites in T4 lysozyme (image courtesy of Wayne Hubbell (UCLA)).

The three things that affect the motion of the spin label on the protein are the overall motion of the protein, the motion of the side chain, and the motion of the protein backbone. Hence, the motion of the spin label can exist in the very fast timescale of 10ps to a rigid limit of 200ns[106, 107]. One disadvantage of the nitroxide spin labeling is the introduction of the R1 side chain that can perturb the structure and cause misfolding of the protein. Often circular dichroism is performed to check the secondary structure and fold of the protein, and functional assays to verify the protein's activity. Thermal unfolding of T4

lysozyme was performed and found that only spin label attached in the protein interior affects its stability and unfolding energy [103].

Figure 22 is a classic example of what happens when a spin label side chain R1 is incorporated into different T4 lysozyme sites. The spin label on the loop, pink spectrum, exhibits a line shape that is fairly narrow due to the flexible loops with a correlation time of low nanosecond timescale. While the helix surface site, green, encounters a slight restriction on the rotational motion of the label and hence has a broadened peak most noticeably on the low field resonance. When the spin label is in tertiary contact, cyan, there is broadening of the low field peak into two components, which is due to anisotropic motion (directionally dependent) of spin-label. The buried site in yellow would mean very little motional averaging and is indicated by a very broad spectrum with a large immobile component in the low field peak as well as in the high field. These classic examples of a spin-label on a helical protein structure show that the spectral lineshape is sensitive to the local environment of the spin label. The broadening of EPR lineshape of a spin-labeled protein upon membrane association have been found to be most likely due to the spin-label interaction with the protein surface [108; 109, 108, 110].

Power saturation and membrane depth parameter

Power saturation can provide information about the solvent accessibility of a specific site on the protein, which is spin-labeled with an MTSL nitroxide. This technique can be used to determine the membrane depth and orientation of spin-labeled membrane associated protein in the presence of paramagnetic reagents such as NiEDDA and O_2.

The Boltzmann distribution determines the populations of spin in each energy level at thermal equilibrium, and the populations can become equalized or saturated if the induced transitions overcome the intrinsic relaxation processes that return the spin system back to equilibrium. In a progressive power saturation measurement, the saturation behavior of the nitroxide depends upon the rate at which spins to relax to equilibrium. Thus, the method provides a measure of the relaxation rate of a spin system[100].

To determine membrane depth, the power saturation method employs a secondary paramagnetic reagent that promotes spin-lattice relaxation. Relaxation is induced by the secondary paramagnetic species through a 'Heisenberg spin exchange' that shortens the nitroxide T_1 relaxation time. Addition of the secondary relaxation enhancing agents like Ni^{2+} and O_2 provide a very effective spin-lattice relaxation mechanism for excited nitroxide spins[100]. This is due to the spins being strongly coupled to their 'lattice' which would

include these paramagnetic ions[100]. The spin-lattice relaxation pathway through collisions with the external spins is a much stronger effect than the contributions from the dipole-dipole interaction or the spin-spin relaxation, T_2[100]. The collision effect results in effectively switching the wave functions between the two magnetic species. It is analogous to the instance of an electron jumping from one spin system and exchanging with the other and it results from orbital overlap between the molecules containing unpaired electron spins. This exchange interaction is identical to a chemical exchange, where the nitroxide exchanges its long T_1 with the short T_1 of the paramagnetic reagent. This causes the nitroxide spins to require more power to attain saturation due to a more efficient relaxation pathway created by the paramagnetic relaxing agents.

These measurements of collision frequency with a paramagnetic reagent can be used to examine the membrane insertion of a spin-labeled protein that binds to membranes. Paramagnetic relaxation agents like NiEDDA and O_2 have short T_1 values and also have a preferential partitioning in the membrane hydrocarbon based on their polarity. NiEDDA, which is polar partitions into the aqueous phase, while O_2, which is hydrophobic partitions into the membrane bilayer. These reagents can be used to obtain information about nitroxide accessibility and about nitroxide membrane depth.

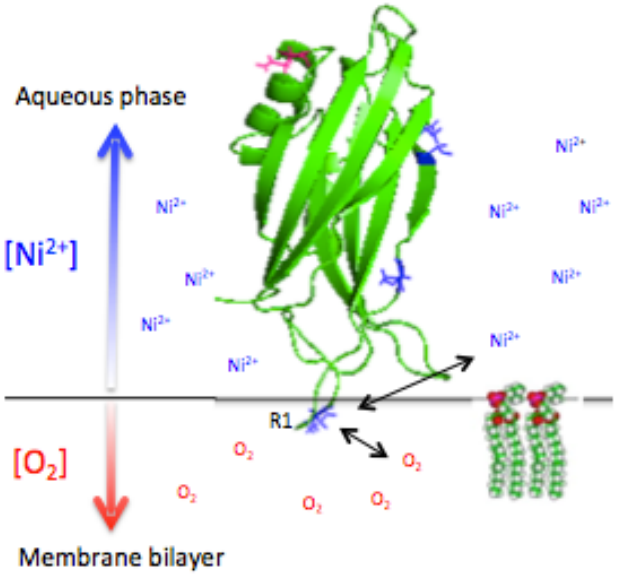

Figure 23. cw-EPR power saturation experiments. The collision frequency of the nitroxide side chain R1 with the secondary paramagnetic reagents, O_2 and Ni^{2+}, can give accessibility information, Π, as well as the depth parameter, Φ, of the spin-labeled site with respect to lipid bilayer.

By measuring the collision frequency and the $P_{1/2}$ parameter, one can determine if the spin-label is positioned into or away from the membrane. Based on the above principles, it will be difficult to saturate the spin-labeled protein that is exposed to either O_2 or Ni^{2+} depending on its solvent accessibility. The membrane depth parameter, Φ, is defined with respect to the lipid phosphate head groups. This depth parameter is directly related to the concentration of the secondary paramagnetic species, C_i. The concentration gradient of the secondary paramagnetic species at equilibrium is directly related to the standard chemical potentials, μ, of the reagents which is dependent on hydrophobic bilayer depth:

$$C_{i,m}(x)= C_{i,w}e^{(\mu_{i,w}(x)/RT)}e^{-(\mu_{i,m}(x)/RT)}$$

Equation 2.12

Where $C_{i,m}(x)$ is the concentration of the species i in the membrane at x distance from the lipid interface, $C_{i,w}$ is the concentration of i in the water (aqueous phase), $\mu_{i,w}$ is the standard chemical potential of i in water and $\mu_{i,m}$ is the standard chemical potential in membrane at a certain distance, x.

The theory for power saturation involves a number of equations, starting with the Bloch equations that describe the magnetization as a function of time. The central line peak-to-peak amplitude, A_{pp}, of the EPR spectrum is determined by the Bloch equations:

$$A_{pp} \alpha B/ (1+B^2\gamma^2T_1T_2)$$

Equation 2.13

Where B is the applied magnetic field and γ is the gyromagnetic ratio of the unpaired electron. B is also described by:

$$B = \Lambda\sqrt{P}$$

Equation 2.14

Where Λ is the constant depending on resonator properties and is related to the efficiency of the resonator in translating power. √P is the incident microwave power and often the value $P_{1/2}$ is used in power saturation experiments. $P_{1/2}$ is the microwave power required to saturate the signal to half the amplitude, A_{pp}, it would be if there were no saturation.

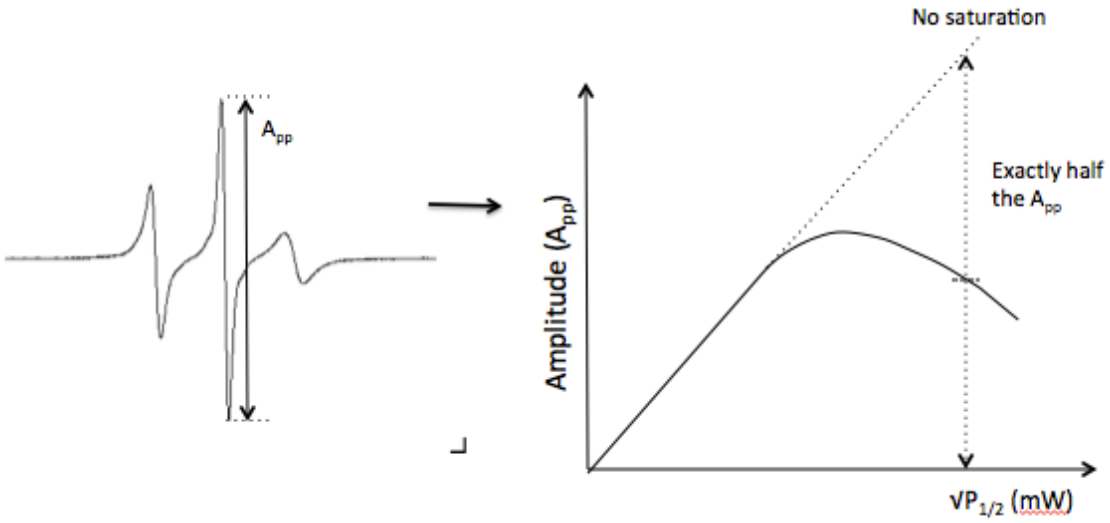

Figure 24. Power saturation curve plotted A_{pp} vs. √P. In power saturation experiments, peak-to-peak amplitudes [98] of the central EPR spectrum is plotted against the square root of the incident microwave power. The dashed linear line represents the amplitude, A_{pp}, relationship in increasing power in the absence of saturation. The $P_{1/2}$ value for each condition (O_2, N_2 and NiEDDA) is the √P at which the signal would be half the A_{pp} if there were no saturation occurring.

Computing a power saturation curve, figure 24, which is plotted with the intensity of the peak-to-peak central line amplitude against √P, gives the parameter $P_{1/2}$. The relationship between the central resonance line, A_{pp}, and $P_{1/2}$ is:

$$A_{pp} = IP^{1/2}\,[1+(2^{1/\varepsilon}-1)\,P/P_{1/2}]^{-\varepsilon}$$

Equation 2.15

Where I is a scaling factor and ε is a measure of homogeneity of the saturation. From equations 2.13 and 2.14, $P_{1/2}$ is a function of the relaxation times of the nitroxide (T_{1e} and T_{2e}) and can be described as[97]:

$$P_{1/2} \alpha\ 1/(T_{1e}T_{2e})$$

Equation 2.16

Next, the collision frequency, W_{ex}, between the nitroxide and secondary paramagnetic exchange reagents directly determines the Heisenberg exchange

rate. The collision frequency is directly related to the concentration of the secondary paramagnetic exchange species, C_i:

$$W_{ex} = k_{ex} C_i$$

Equation 2.17

Where k_{ex} is the exchange rate constant.

$$W_{ex} = \Delta (1/T_{1e}) = \Delta (1/T_{2e})$$

Equation 2.18

W_{ex} is also affected by a change in the nitroxide's T_{1e} and T_{2e}. Bringing equations 2.15, 2.16 and 2.18 together makes $\Delta P_{1/2}$ directly proportional to W_{ex}.

$$W_{ex} \alpha \Delta P_{1/2}$$

Equation 2.19

$\Delta P_{1/2}$ is experimentally calculated by:

$$\Delta P_{1/2} = P_{1/2} - P^{o}_{1/2}$$

Equation 2.20

Where, $P_{1/2}$ and $P^{o}_{1/2}$ denotes the microwave power in the presence and absence of the paramagnetic exchange species, i.

There are also other factors that influence this rate of collision, W_{ex}, between the nitroxide and the relaxing agent, i. They are the exchange probability (p), the steric factor (g), the collision diameter (d) and the relative diffusion coefficient based on position of spin-label ($D_m(x)$). The steric factor, g, assumes a particular accessible orientation between the exchangeable spins. The exchange probability, p, is the effective collisions with the relaxing agent and it may be compromised by the local environment of the spin-label on the protein.

$$W_{ex} = 4\Pi pgdD_m(x)C_m(x)$$

Equation 2.21

From equation 2.12, the depth parameter, Φ, is accurately a measure of the concentration of O_2 or NiEDDA with respect to the membrane interface and is directly related to their standard chemical potential, μ(i).

$$\Phi = - [(\mu(O_2) – \mu(Ni^{2+})/RT] + constant$$

Equation 2.22

This leads to equation 2.17 and 2.19, where the concentration of the exchange species, C_i, the collision frequency, W_{ex}, and $\Delta P_{1/2}$ are related. This allows the expression of the depth parameter as:

$$\Phi = \ln [(\Delta P_{1/2}(O_2)/ (\Delta P_{1/2}(Ni^{2+}))]$$

Equation 2.23

The accessibility parameter, Π, is also used to give information about the level of accessibility of the nitroxide label to the solvent. Dividing $P_{1/2}$ by the central linewidth, ΔH_{pp}, accounts for any line broadening due to T_{2e} (Eqn 2.16) and using the $P_{1/2}$ of a reference sample accounts for variation in the performance of different resonators. Thus Π is defined as:

$$\Pi = [\Delta P_{1/2}/\Delta H_{pp}]/ [P_{1/2}/\Delta H_{pp}]_{reference}$$

Equation 2.24

Pulse EPR –DEER

Double electron-electron resonance (DEER) is the measure of the dipole-dipole interaction between two electron spins that are separated by a distance, r. The practical applications of DEER in biophysical studies are to study interactions between biological macromolecules, protein conformational change and characterization of protein complexes. Unlike the popular Förster Resonance Energy Transfer (FRET) experiments, the advantage of measuring distance using nitroxide spin labels is that you are introducing a smaller side chain compared to the bulkier fluorophores and the uncertainty of the fluorophore position is higher due to its long flexible linker [111].

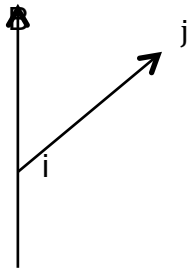

Figure 25. Two electrons i and j separated by distance, r, where r_{ij} is aligned along B

The total energy, $E_{dipolar}$, for the dipolar interaction of two spin-labeled sites is given by:

$$E_{dipolar} = (\mu_i \mu_j / r_{ij}^3) (1-3\cos^2 \theta)$$

Equation 2.25

Where the magnetic dipole moments, μ_i and μ_j, of spins i and j are directly dependent on the interspin distance, r_{ij}, and the angle of orientation, θ, with

respect to the magnetic field applied. A further expansion into equation 2.25 using equation 2.4 ($\mu = g\beta S$) describes the quantum energy of the system you are measuring:

$$E_{dipolar} = (g_i g_j \beta_e^2 S_i S_j / r_{ij}^3)(1-3\cos^2\theta)$$

Equation 2.26

Where g_i and g_j are the g-values of the interacting spins i and j respectively, β_e is the Bohr Magneton of the electron and S_i and S_j are the spin for the electrons i and j respectively along the z-axis. Hence, the coupling between the two unpaired electrons is a function of the distance between the two and the frequency of the dipolar interaction is inversely proportional to the cube of the distance[112, 113]. This distance or separation of the dipolar interaction is dependent on the angle of the inner spin vector of the electron and the applied magnetic field[113].

$$\omega_{ij} \alpha (1/r_{ij}^3)(1-3\cos^2\theta)$$

Equation 2.27

Where ω_{ij} is the dipolar coupling frequency between electron pair, i and j. From figure 25 and equation 2.25, the angular dependence of the electron orientation relative to the magnetic field also contributes to the dipolar signal.

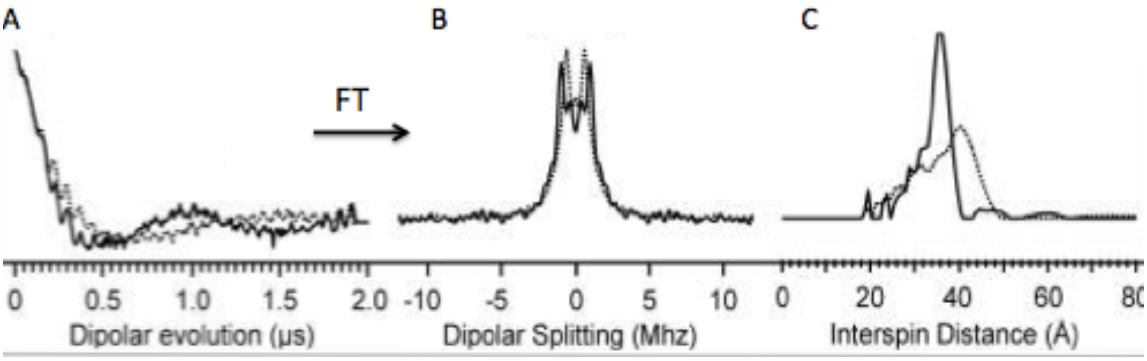

Figure 26. EPR raw DEER signal, Pake pattern and distance distribution. A) The background subtraction dipolar evolution DEER signal. B) Pake pattern after fourier transformation of A. C) Distance distribution (adapted from Altenbach 2008)

In figure 26, the splitting of the two peaks in a pake pattern is dependent on the distance and angle between the spin pair and is given by frequency of echo oscillation, ω_{ij} (Mhz)[114]. The fourier deconvolution of the pake pattern can give the average interspin distance as described in Equation 2.27 which in practice is a distribution[112, 113].

Pulsed EPR techniques differ from continuous wave (CW) EPR in that instead of scanning the magnetic field and keeping the frequency constant, a short pulse consisting of a range of frequencies is used to perturb the spins at a constant magnetic field[111]. When running DEER on a biological sample, the best sensitivity and signal is obtained when the temperature is 50-80K[115]. This low temperature enhances the T_1 and T_2 relaxation as well as increases the energy and population difference in Boltzmann equilibrium distribution. A longer T_2 allows for DEER echo modulation (signal) from weak interactions and longer distances.

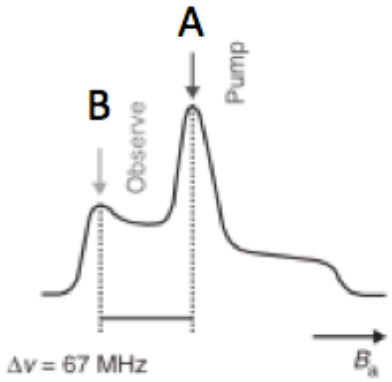

Figure 27. Nitroxide spectrum in X-band, excitation by the v_{pump} (A) and $v_{observe}$ (B) (adopted from Azarkh 2013)

An echo detected field swept nitroxide spectrum like in figure 27 gives the position of observe ($v_{observe}$) and pump (v_{pump}) frequencies that are used to conduct the DEER experiment[116]. In the biological sample, the two spin populations A and B are the nitroxide spin labels that are coupled. The spin ensemble A is excited using the v_{pump} inversion pulse. While the $v_{observe}$ is the detection pulse used to excite the spin ensemble B. The DEER signal is essentially the Hahn echo of the B spins recorded for a series of 180 degree pulses applied to the A spins that invert the sign of the dipolar coupling between A and B spins. The resulting echo oscillates with a dipolar evolution time, t, in the raw time domain spectrum as shown in figure 26A. This can be Fourier transformed to yield the frequency of the echo oscillation and as given in equation 2.27, the interspin distance, r (nm), can be derived from this frequency-domain spectrum, typically using a Tikhonov regularization fitting of the time-domain signal to obtain a distribution of distances[113, 115].

2D HSQC NMR

Nuclear spins interact with the magnetic field to produce a net magnetization and a signal is generated following the application of a radiofrequency pulse. In a 1D NMR experiment, signal acquisition occurs once the pulse sequence is complete. However in 2D NMR, the magnetization transfer between different nuclei is measured[117]. This yields a 2D map with signals from two different frequencies. 2D experiments can be magnetic interaction through bond, J coupling, or through space such as the nuclear Overhauser effect, NOE. J coupling can occur in the same type of nucleus, like in COSY (Correlated Spectroscopy), or another type of nucleus, such as HSQC (Heteronuclear single quantum coherence)[118].

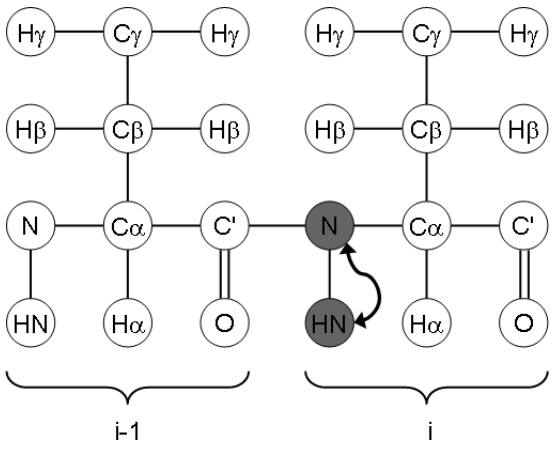

Figure 28. 2D HSQC - magnetization transfer from proton to ^{15}N (taken from Victoria A. Higman)

Heteronuclear correlation in 2D NMR involves transferring polarization or magnetization from ^{1}H, the most sensitive common nucleus, to a different nucleus of less sensitivity[102]. HSQC experiment is also termed the 'inverse' detection of sensitive nucleus from an insensitive nucleus. The proton (S) and ^{15}N nucleus (I) are coupled, and excited S spins are used to provide polarization

to the insensitive nucleus (I), which is transferred back to the proton S for detection[118, 102].

In a typical 2D map of the spectrum, the resonance cross peaks are a representation of the H-N correlation of each amide backbone in a protein. Hence, one can observe the molecular evidence of a protein since all amino acid residues other than proline will yield an amide resonance peak.

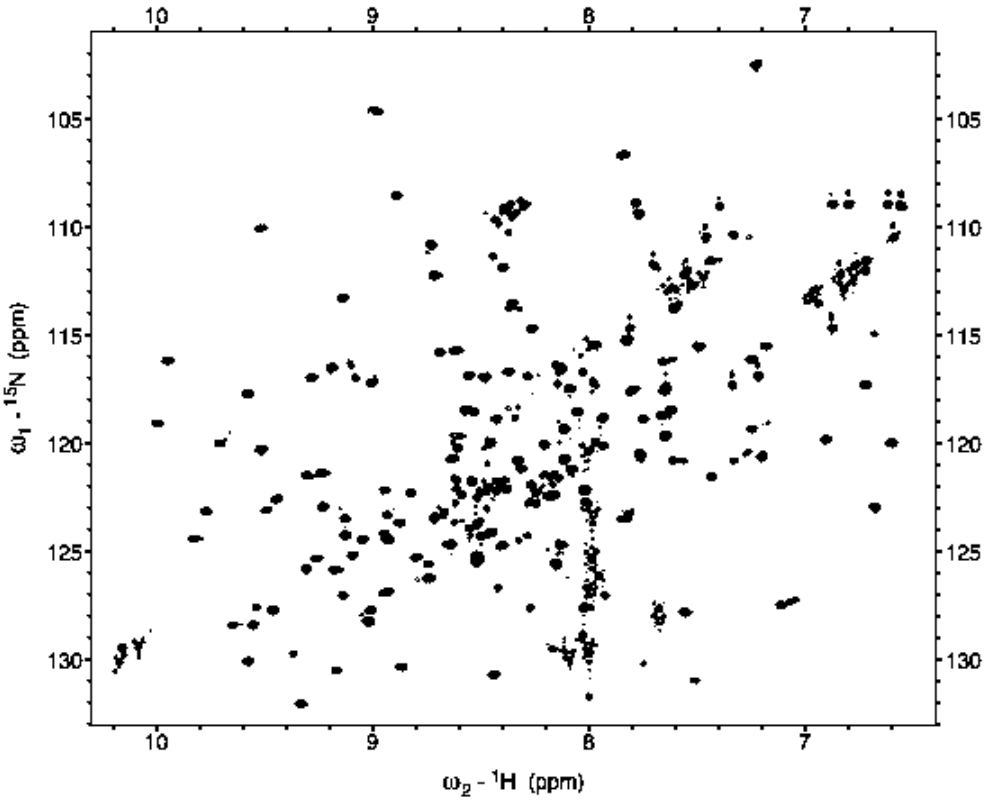

Figure 29. ^{1}H-^{15}N spectrum with cross peaks displayed in the proton chemical shift (ppm) in the x-axis and the nitrogen ppm in the y-axis

As shown in figure 29, the resonance peak of each residue has a ^{1}H and ^{15}N chemical shift value that is very sensitive to the local magnetic and electronic environment of the protein. Hence chemical shift perturbations of a ^{15}N labeled

protein is a sensitive technique to observe when there is binding of a ligand to the protein. Mapping chemical shift changes of proteins can characterize the binding sites of their partners and also give information on the relative intensity or affinity of the binding[119, 120].

When the binding or interaction of the ligand is weak, the protein is usually in fast exchange with the ligand. This usually occurs in the millisecond time and will give a peak corresponding to the weighted average chemical shift of the free protein and the complex form. Upon titration with excess ligand the protein will be completely in its complex form resulting in a chemical shift of the complex. If the binding of the ligand with the protein is tight, then the chemical exchange will slow. This usually leads to broadening or disappearance of the peak until a new peak emerges at a different chemical shift, making it hard to attain K_d values. The slow exchange rate is given by $K_d < 10^{-6}$ compared to $K_d > 10^{-5}$ for the fast exchange[121, 120]. While chemical shifts are representative of the molecular level of changes in the protein, a change in chemical shift does not imply a direct binding site but a possible indirect perturbation due to other local magnetic field adjustment[117].

Most chemical shift changes or the maximum perturbations are reported using a weighted average chemical-shift s for heteronuclear chemical shifts, since ^{1}H and ^{15}N have different ppm scales[119]. This is taken into account by introducing a

scaling factor, α, to the ^{15}N shifts and the calculating the average distance the cross peak changed.

$$\Delta (H_N, N) = \sqrt{} (\delta^2 H + \alpha \delta^2 N)$$

Equation 2.28

Where $\Delta (H_N, N)$ is the weighted average chemical shift, and $\alpha = 0.154$ (based on the average variance of structures in PDB)[122] .

3. The double Arginine mutant R398Q R399Q

Introduction

Xue et al. first found that the two highly conserved arginine residues (R398 and R399) on the opposite face of the calcium binding loops of C2B are crucial in neurotransmitter release, figure 9 of the introduction [90]. Lipid mixing assays showed there was a decrease in the rate of lipid mixing between reconstituted SNARE proteo-liposomes and Syt1 C2B upon the mutation of the two arginine residues into glutamines (R398Q R399Q). Furthermore, electrophysiological studies showed that this R398Q R399Q mutant was unable to rescue evoked release in Syt1 null autaptic neurons[90, 123]. They also found that the two-arginine mutations impair membrane interactions, as the wild-type C2B domain was able to cluster vesicles rapidly while the C2B double arginine mutant was unable to do so. The cooperative role of R398 and R399 was observed even when the single mutation of one of the two arginine residues resulted in a huge decrease in release.

Chapman's group reported from their scanning alanine mutagenesis of C2AB that the R398A mutant decreases the binding of C2AB to t-SNARE (membrane anchored syntaxin and SNAP-25) and the Ca^{2+} triggered fusion in vitro [124]. This reduced interaction with t-SNARE was observed without affecting the Ca^{2+} dependent membrane binding of C2AB or vesicle aggregation, suggesting its importance more in SNARE interaction than membrane binding for the fusion event. Brunger's group later proposed a model wherein these two key arginines

are responsible for making a specific interaction with the SNARE complex (figure 8) [71].

The research in this chapter was directed at characterizing the membrane interactions of C2AB that are mediated by an electrostatic attraction between the two basic arginine residues on Syt1 and the anionic plasma membrane. Site-directed spin labeling using electron paramagnetic resonance (EPR) spectroscopy can be used to observe EPR line shape changes and accessibility parameters as a way of testing the roles of R398 and R399 in the membrane interaction of Syt1 C2B. Since the EPR lineshapes are sensitive to the spin label mobility and tertiary contact, the extent of protein-lipid and protein-protein interactions can be observed. Previous work showed that the spin labeled site T285 (C2B domain), which is on the loop adjacent to the two conserved arginine residues R398 and R399 showed a noticeable EPR lineshape broadening in the presence of large unilamellar vesicles (LUVs)[50]. Site T285 on the C2B domain also exhibits EPR lineshape changes in the presence of the soluble SNARE complex[74].

By using secondary paramagnetic reagents, such as Ni(II)EDDA and O_2, power saturation measurements can be performed to determine bilayer depth of the protein-bound spin label. The data would be beneficial in testing the hypothesis that the critical function of the two conserved R398 and R399 residues is to promote membrane interactions. Consequently, a single mutation, R398Q, and

double mutations, R398QR399Q, on the soluble fragment of Syt1 (C2AB) were generated to study the effect of these mutations on Syt1 membrane binding.

The model proposed by Herrick et al. showed that Ca^{2+} binding loops of C2A and C2B are oriented in opposite directions binding apposing bilayers[50]. This model supports the role of the two conserved arginine residues in membrane binding and bringing apposing bilayers together.

Results

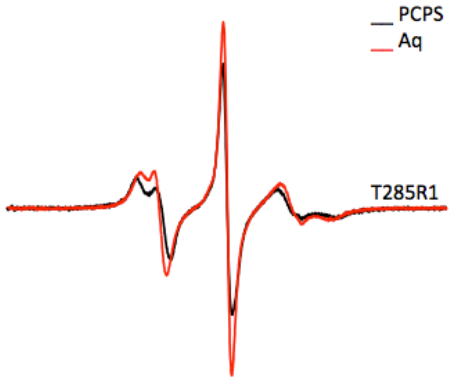

Figure 30. EPR spectra of C2AB T285R1 (near the arginine apex) in aqueous form (black) and in the presence of PCPS (3:1) LUVs (red)

The site 285, in close proximity to the two key arginine residues (arginine apex), in the presence of LUVs indicates contact with the lipid membrane, causing a decrease in the spin label mobility and less averaging of the signal. This site 285 is used to observe changes in membrane interaction due to the arginine apex on the opposite face of C2B domain.

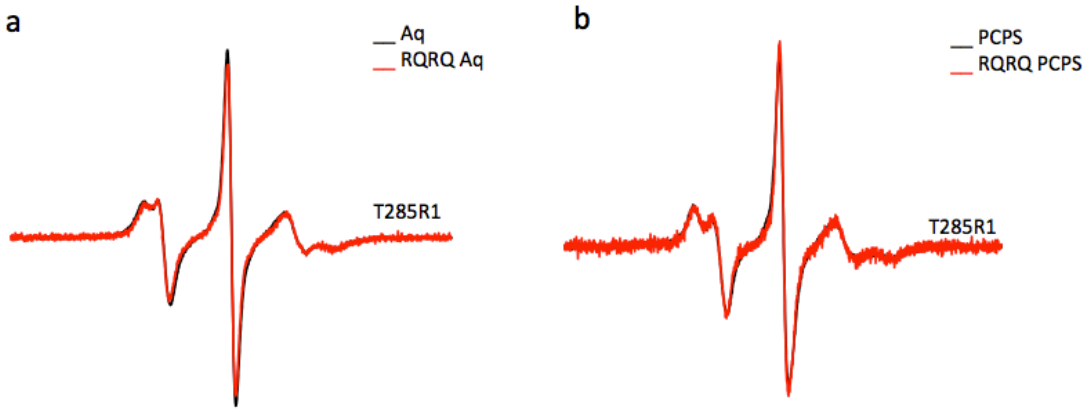

Figure 31. EPR spectra of C2AB 285R1 and C2AB 285R1 R398QR399Q. a) The black spectrum is of the wild-type (C2AB 285R1) and the red spectrum is the double arginine mutants (R398QR399Q) in their aqueous form. b) The wild-type (black traces) and double arginine mutant (red traces) in the presence of PCPS (3:1) LUVs.

The experimental conditions included 1mM Ca^{2+} and POPC:POPS LUV at a protein to lipid mole ratio of 1:1000. Figure 31a shows identical line shapes of the wild-type C2AB spin-labeled at 285R1 (i.e. C2AB 285R1) and the double arginine mutants (C2AB 285R1 R398Q R399Q) in their aqueous form suggesting that the arginine substitutions into glutamine do not perturb the protein secondary structure and dynamics. The spectra of the double arginine mutant (red traces) in the presence of PCPS LUVs, in figure 31b, did not change with respect to the wild-type (black traces) giving no conclusive result on the extent of membrane association upon mutation of the two arginine residues.

Power saturation experiments were performed to get more information on the bilayer depth of the spin label upon R398Q and R398QR399Q mutations. The collision rate with secondary paramagnetic reagents, O_2 and Ni(II) EDDA, yields

the accessibility parameter (Φ). Consequently, the bilayer depth parameter of the protein-bound spin label can be obtained from these accessibility parameters.

C2AB Mutant in POPC:POPS LUV 1mM Ca^{2+}	Depth Parameter (Φ)
285R1	-1.4 ±0.03
285R1 398Q	-1.9 ± 0.05
285R1 398Q 399Q	-2.0 ±0.05

Table 1. Depth parameters (Φ) of the C2AB arginine mutants. Depth parameters for C2AB are the average of 3 measurements, and errors represent standard deviations for the data. Previous work has shown that the depth parameters are in the range of approximately −2.0 to −2.5 for labels in the aqueous phase [125].

The data in table 1 are an average of at least three measurements. A larger negative Φ indicates that the spin label is further into the aqueous phase from the lipid interface while a larger positive Φ indicates an increase in the depth of spin label in the hydrocarbon membrane. Since the basic arginine residues were mutated to glutamine, a neutral but polar residue, it is expected that the electrostatic attraction between the basic R398 and R399 with the acidic phospholipids PC:PS would be abolished causing the spin label on site 285 to encounter less membrane interaction since it is also sitting at the same proximity from the membrane as the two conserved arginine residues.

Controls: Depth parameter (Φ) of C2AB mutants without PC:PS LUV.

C2AB Mutant in Aqueous form 1mM Ca^{2+}	Depth Parameter (Φ)
285R1 R398Q	-2.1 ± 0.1
285R1 R398Q R399Q	-2.2 ±0.1

Table 2. Depth parameters (Φ) in aqueous solution of the different arginine mutants spin labeled at site 285.

The data in table 2 are an average of three measurements. The negative Φ values indicate that the spin label is in the aqueous phase hence, indicating good control results. Hence, this demonstrates there are no steric effects of the spin label from the protein, which can alter its accessibility to the relaxing agents.

Method:

Continuous wave (CW) power saturation measurements were carried out using the Bruker EMX spectrometer. Accessibility parameters, Π, and depth parameters, Φ, were calculated by obtaining the $P_{1/2}$ (figure 24) values from the saturating behavior of the samples with respect to secondary paramagnetic reagents: Ni(II)EDDA and O_2 [97]. The power saturation curves for O_2, N_2, Ni(II)EDDA (figure 24) can provide the $P_{1/2}$ value . The $P_{1/2}$ value is the microwave power that gives the resonance amplitude at half of its unsaturated value of a sample.

A semi-permeable TPX capillary is used to hold about 6μL of the sample. The $P_{1/2}$ (N_2) is obtained after purging the sample with N_2 gas for 15 minutes and power saturating the sample in the presence of the N_2 gas. This way $P_{1/2}$ (N_2)

can be used to account for signal arising from the non-paramagnetic relaxation. The power saturation measurement with the Ni(II)EDDA probe was also carried out in the presence of the N_2 gas after purging the sample with N_2 gas for 15 minutes to displace the oxygen from sample. Though 10mM of Ni(II)EDDA was used, the $\Delta P_{1/2}$ values were scaled to an effective concentration of 20mM [97]. The accessibility parameter, Π, of O_2 and Ni(II)EDDA , can be calculated from Eqn 2.24. Consequently, the depth parameter, Φ, can be calculated from Eqn 2.23. The depth parameter, Φ, can tell us the location of the protein-bound spin label with respect to the membrane surface.

Discussion

The cw-EPR spectra of the single and double arginine mutants spin-labeled at site 285R1 do not indicate any changes compared to the wild-type (C2AB 285R1) when bound to membranes. However, the depth parameter suggests that site 285R1 next to the arginine apex is near the membrane interface where the phosphate headgroups lie. In addition, once the arginines are mutated to glutamine, the arginine apex lies in the bulk aqueous phase. It is possible that since the two arginines are charged and there are no hydrophobic residues in this region to cause penetration into the bilayer, the role of the two arginines is to help bridge bilayers by associating peripherally to the membrane. It has been found by studies on the effector domain from MARCKS that charged proteins lacking hydrophobic or aromatic side chains only bind peripherally, and that they do not penetrate, but reside in the ionic double layer adjacent to the bilayer[89]. It is possible that the mechanism by which the two arginines on Syt1 function in the

synaptic fusion event is through an electrostatic interaction with the membrane surface.

A possible extension to this would be to work with the C2B domain fragment alone since this would avoid the tethering effect by C2A that also could be resulting in the undefined interaction with the arginine apex in C2B. This would show a better relationship between the non-arginine mutant and the arginine mutants in the cw-EPR spectra.

4. C2B domain structural analysis through DEER

Introduction

It is generally believed that the C2 domain does not undergo any major structural changes upon Ca^{2+} binding, with only the Ca^{2+} binding loops exhibiting some ordering upon binding [126, 127, 51]. However there is no direct structural data regarding conformational changes in the C2 domains upon Ca^{2+}-dependent phospholipid binding. Malmberg et al. examine the membrane docked state of cPLA2 C2 domain through EPR studies and concluded that no large rearrangements of the membrane binding loops was observed upon Ca^{2+} binding [128].

Similarly, Chae et al. deduced from their NMR experiments that the Ca^{2+} bound C2A domain only showed perturbations in the binding loops in the presence of short acyl chain 6:0 PS (6PS) which were thought to become fully ordered only upon binding to phospholipid[129].

However, a recent study using molecular dynamics simulations proposed that the C2B domain in syt1 undergoes a conformational change upon membrane binding and that this change (which promotes membrane binding of a C-terminal helix) induces membrane curvature[130]. They reasoned that while both C2A and C2B possessed a polybasic strand, the Hβ helix near the C-terminal end of C2B stood out when comparing the sequence homology between the two tandem domains. It was suspected that the Hβ helix, unique to C2B alone, resulted in the stronger

propensity of C2B to be critical in membrane fusion. Hence a conformational transition of the Hβ helix was proposed to bind to membrane which would disorder the lipid leaflets and allow for hemifusion[130].

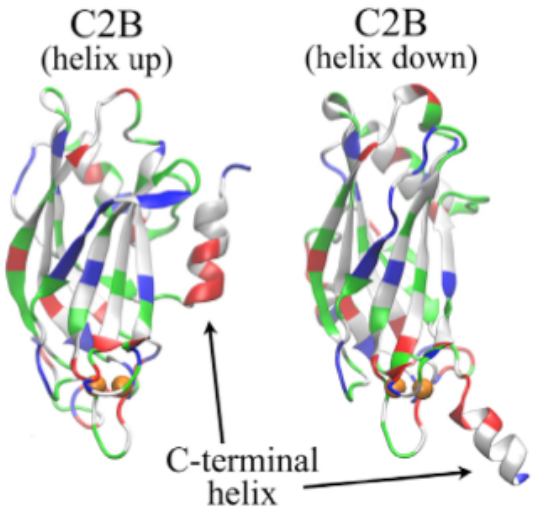

Figure 32. Simulated structures of C2B domain with Ca^{2+} bound. The C-terminal helix is shown to undergo conformational transition by coming down into the membrane from its up orientation (adopted from Wu et al. 2014).

The DEER experiment provides distance restraints as observed by the electron spin coupling between two nitroxide side chains out to 60 Angstroms and beyond. Hence this allows us to investigate the distance change between the Hβ helix and the structured regions of C2B upon membrane binding. EPR based DEER studies investigating the structural change of the C2A domain upon Ca^{2+} dependent membrane binding showed little evidence of any conformational changes upon membrane association (unpublished data by Herrick et al). Similarly, the C2B domain was also investigated where residues A415, on the Hβ helix, and N396, near the arginine apex, were spin-labeled with MTSL. All DEER data were analyzed using the software package DeerAnalysis (Jeschke et al. 2006).

Results

The CW spectrum of the double labeled C2B (415R1 and 396R1) was collected to verify that both sites were equally labeled by adding together the spectra of the single labeled C2B 415R1 and C2B 396R1. Once that was verified, the double mutant was purified and the spin labeled protein was concentrated down to 150μM. It is important that the lipid to protein molar ratio is significantly large to observe interactions as close to its native environment. For the PC:PS (3:1) condition, LUVs composed of the relevant PCPS concentration was added at a 200:1 lipid to protein ratio. The final DEER samples were made up by adding 10% (by weight) d-glycerol (deuterated form of glycerol). The samples were flash-frozen in a mixture of dry ice and isopropanol for the DEER experiment.

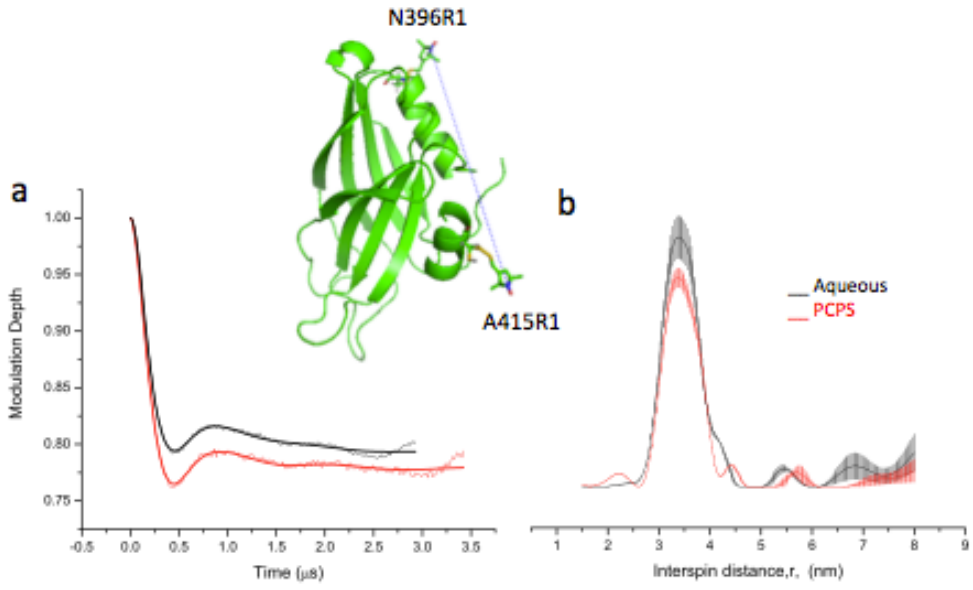

Figure 33. C2B 396R1 415R1 distance comparison in the presence and absence of 3:1 PCPS vesicles. a) The time domain of the echo modulation of the protein in aqueous (black traces) and PCPS LUVs (red traces). b) The deconvulated spectra of the dipolar echo evolution, a, resulting in the interspin distance, r (nm), between the aqueous form (black traces) and membrane bound form (red traces).

Figure 33a shows the time domain of the dipolar echo evolution from the DEER experiment for the aqueous (black trace) and PCPS (red trace) samples in 10% glycerol. Both the samples have comparable modulation depths of the echo oscillation indicating that an equal population of spins A and B are interacting. The echo signal was fit using Tikhonov regularization to provide a distance distribution. Figure 33b shows that the presence of vesicles containing 25% PS did not change the distance distribution (mean of 3.3nm) in C2B domain.

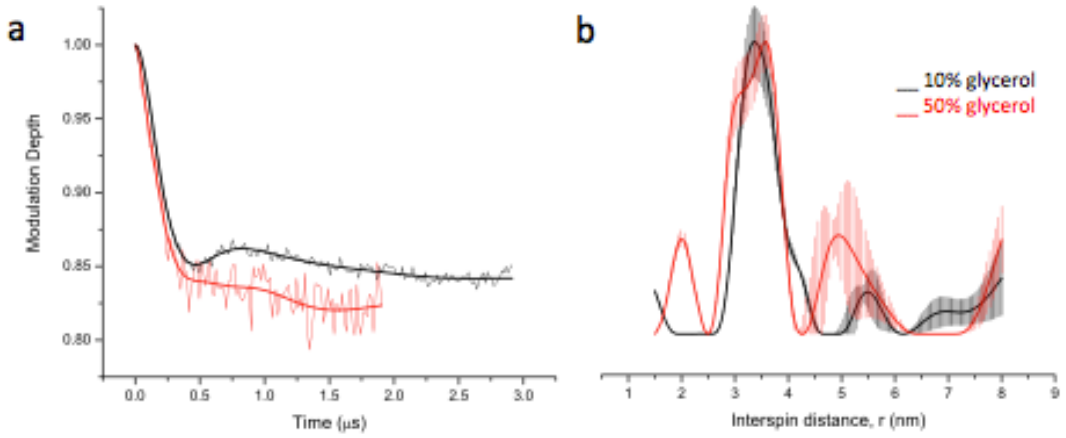

Figure 34. C2B 396R1 415R1 in the presence of 50%PS LUVs. a) In 10% (by weight) glycerol concentration in black traces and b) in 50% (by weight) glycerol concentration in red traces. There is an increase in the small population with longer distance of 5nm when the glycerol concentration is increased to 50%.

Next, the experiment was conducted in 50% PS instead of the regular 25%PS to compare to the experimental condition of Wu et al. which was at a much higher PS concentration [130]. The DEER distance distribution of the sample in 10% d-glycerol (black trace) for the 50%PS is comparable to the 25% PS lipid composition (figure 33). Glycerol is used as a cryoprotectant and glassing agent

since the protein samples are frozen to increase its phase memory time (T_M) or the T_2 relaxation[99, 115]. A glassing agent is needed to prevent formation of ice-crystals that would result in high local protein concentrations[99]. When the experiment was conducted in 50% d-glycerol for the 50% PS vesicles, evidence of a longer distance appeared. When the signal was fit, the distance distribution showed a small population at a longer interspin distance of 5.1nm, however, the error was high for this fraction of the distribution.

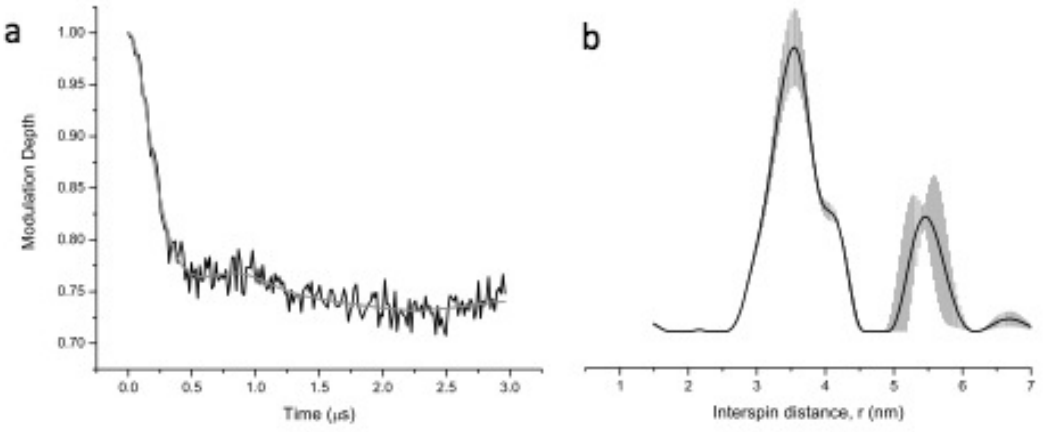

Figure 35. DEER spectra C2B 396R1 415R1 in addition of 5% PIP_2 to PCPS vesicles in 50% glycerol

In order to incorporate other acidic lipids and increase the charge density, 5% PIP_2 was incorporated into PCPS vesicles with a final lipid composition of 75:20:5 PC:PS:PIP_2. The sample in figure 35 was run in 50% d-glycerol since a longer distance component had been observed at this glycerol concentration which could have facilitated the detection signals due to longer interspin distances. Another small population at a long distance of 5.5nm was observed for this sample. However, the noise generated as a result of sample dilution (by the

addition of lipid and the 50% glycerol) implies a significant error of the long distance and it may therefore not be real.

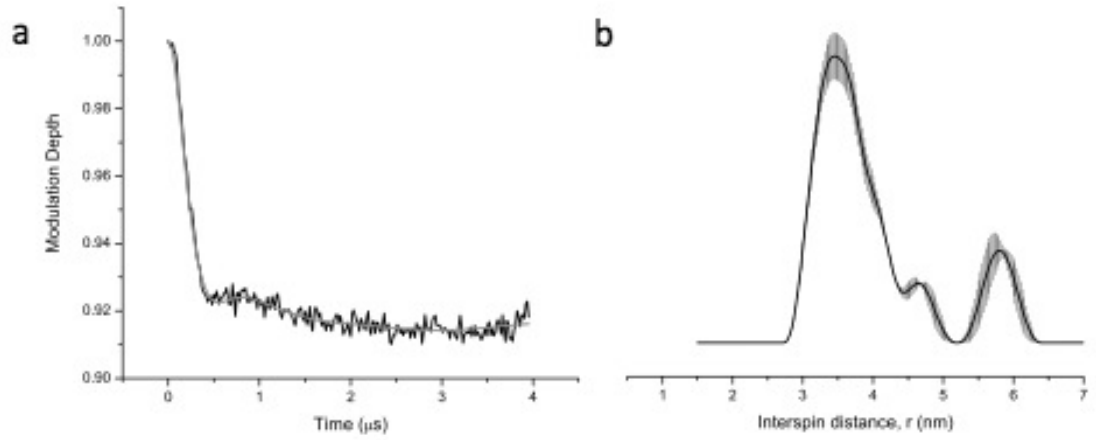

Figure 36. Control experiment of C2B 396R1 415R1 in 50% glycerol without LUVs

A control experiment was performed to see if the longer distance population was due to the change in negative charge density in the membrane surface or to the effect of a high glycerol concentration (50% by weight). As shown in figure 36, even in the absence of lipid but in the presence of 50% d-glycerol, there was a small population sampling a longer distance between the coupled spins. A high negatively charged lipid surface might trigger a conformational transition in the C-terminal helix in a small population of C2B domains, however the DEER data demonstrate that there are no major changes in the distance distribution between the two spin-labeled sites. The longer distance of 5nm in 50% glycerol could be due to glycerol modifying the solvation and dynamic properties of the protein as studies by Georgieva et al suggest [99].

Additional DEER experiments with single labeled C2AB 283R1 and C2B 415R1 were also done to verify the lack intermolecular interactions between the protein domains. Both produced a DEER signal with zero echo modulation, which confirm that there was no aggregation or oligomerization occurring.

Discussion

Mutations in the C2B domain of Syt1 have been found to be more deleterious to Syt1 function in electrophysiological experiments compared to the C2A domain[124]. It also makes a greater contribution to membrane binding than does the C2A domain. Hence, the possibility that the C2B domain might undergo a conformational transition upon the Ca^{2+} dependent membrane binding is more likely than for the C2A domain. Structural changes upon membrane association are not without precedent. Other proteins like PLC-δ1 and EGF receptor have been reported to undergo conformational changes upon membrane binding[131, 132].

With the conserved polybasic face and the key arginines thought to be crucial for Syt1 function, C2B may be capable of undergoing structural rearrangements or conformational transitions that are important for the function. However, in contrast to the molecular dynamics studies, our DEER measurements show that the C-terminal helix of the C2B domain does not undergo any significant distance changes or rearrangements even when subjected to highly negatively charged membrane surfaces. Only one spin-labeled pair was tested, and an investigation

of other sites would provide a more complete picture of the structural integrity of C2B upon membrane binding. Similar work performed on a number of sites in C2A (unpublished data of Dawn Herrick) clearly show that C2A domain does not undergo any structural transitions upon membrane association as well.

5. Polyelectrolytes and phosphoinositides modulate the membrane interactions through the polybasic face of C2B

Introduction:

In order for neuronal exocytosis to be triggered by the influx of Ca^{2+}, Synaptotagmin 1 (Syt1) has to bind to Ca^{2+} and interact with its target instantaneously. The mechanism of how the Ca^{2+} dependent binding of Syt1 facilitates the rapid fusion of hundreds of vesicles is still unclear, however, the membrane binding of Syt1 is likely to be a critical event for fusion. The other proposed Ca^{2+} dependent role for Syt1 is to bind to the core SNARE complex or the individual SNARE proteins like Syntaxin [20, 133; 134, 133]. The membrane binding activity of some C2 domains, such as in PKCα and Syt1, requires the presence of Ca^{2+} and a negatively charged lipid such as phosphatidylserine (PS) [135 136, 77, 137]. Electrostatics is known to be the driving force by which this binding mechanism occurs. The binding of Ca^{2+} changes the electrostatic potential on the membrane interacting loops of the domain and regulates its membrane interaction[138, 139, 41]. The extent of phospholipid binding is correlated with the negative charge density on the membrane surface[138]. Electrostatic screening experiments to shield charges by increasing salt concentration have also shown a dependence on electrostatic interactions for these C2 domains[91]. While electrostatic interactions have been found to be important in Ca^{2+} dependent binding of C2 domains to phospholipids, there is also evidence that it may not be purely electrostatic [140, 139]. Mutating the acidic residues that bind the Ca^{2+} ions does not give similar membrane binding results in PKCβ[140, 139] It has been found through crystallographic studies that the C2 domain-bound Ca^{2+} ion provides coordination sites for the headgroup of PS in the membrane[93, 141, 138]. This is

consistent with the observation of an increased affinity for Ca^{2+} by Syt1 in the presence of negatively charged containing phospholipids[93, 78]. While the electrostatic and coordinating effects of the protein bound divalent cation have been found to be important, the hydrophobic residues on the binding loops also contribute to the binding energy required for the loops to penetrate into the membrane bilayer[128, 136].

Mutating the key arginine residues R398 and R398 in the C2B domain of Syt1 to glutamines was found to inhibit synaptic transmission in mice hippocampal neurons, disrupt liposome clustering in vitro and also inhibit its interaction with the t-SNAREs (target SNAREs on plasma membrane)[90, 124, 142]. The role of this arginine apex in membrane binding is thought to be electrostatic since the two basic residues would be attracted to the negatively charged bilayer. This also agrees with the model generated by Herrick et al. where Syt1 bridges opposing bilayers with the Ca^{2+} loops of two C2 domains are oriented in opposite directions to each other in a trans configuration [50]. In the present work, these two key arginine residues and the two basic residues, K326 and K327, on the poly-lysine strand of C2B domain were neutralized through mutagenesis and their membrane binding contribution to Syt1's role were measured. The mutants shC2AB R398Q R399Q and shC2AB K326A K327A were generated on the short C2AB construct 136-421 (shC2AB) and their membrane binding affinities under equilibrium conditions were determined using a well-established vesicle sedimentation assay[94]. Several studies on the modulation of PKCα and Syt1 in

their membrane-binding role by PIP_2 have been reported[141, 70; 78]. It has been shown that the polybasic strand in the C2B domain of Syt1 and C2α in PKC is unique to PIP_2 binding in both its Ca^{2+} - bound and Ca^{2+} - free form [141, 70; 78, 143]. The effects of the different negatively charged lipids, PS and PIP_2, on C2AB membrane binding were also investigated.

While electrostatic interactions are important, the role of a specific coordination between the protein-bound Ca^{2+} with PS containing membranes is not well characterized. The divalent cation, Sr^{2+}, was found to substitute for Ca^{2+} in inducing both the synchronous and asynchronous neurotransmitter release although with varying efficiency[144, 145, 146]. Recent work done by the Igumenova group provided NMR and crystallographic evidence that while certain divalent metal ions can substitute for Ca^{2+} to bind to the C2 domain of PKCα, it may or may not act as a surrogate for the membrane binding function of PKCα[77, 147]. While there is strong evidence that both Cd^{2+} and Pb^{2+} binds to the loops in PKCα, the Cd^{2+} bound PKCα does not bind to PS containing membranes unlike Ca^{2+} or Pb^{2+} [77, 147]. This provides strong evidence that the interaction between the protein bound metal-ion and the phospholipid membranes occurs in a specific coordinated manner rather than a non-specific electrostatic manner.

The role of negatively charged biomolecules like ATP was also investigated here since ATP was found to enhance the Ca^{2+} dependent binding to PIP_2 containing chromaffin granules and synaptic vesicles[148]. It was proposed that ATP acted to

shield electrostatic charges on PS-containing synaptic vesicles and prevent the cis-binding of Syt1 (where both the C2A and C2B domains preferred to bind back to the synaptic vesicles). However, in the presence of the PIP_2-containing plasma membrane, ATP is unable to compete for Syt1 binding and hence it facilitates the trans-binding mode of Syt1 (where the synaptic vesicle anchored Syt1 binds to the opposing plasma membrane). A coordination mechanism of the protein bound Ca^{2+} with ATP in the presence of PS and PIP_2 was also proposed. The bioavailability and cytoplasmic levels of ATP is reported to be around 2mM[149]. At these ATP concentrations, the membrane binding of C2AB in PS or PIP_2 in the presence of vesicles was investigated here using the vesicle sedimentation assay. The electrostatic or coordination mechanism of Syt1 to ATP were also addressed by doing NMR experiments to see if ATP and IP_3 (the headgroup of PIP_2) competed electrostatically for the same binding sites and to extract their respective binding affinities.

Results

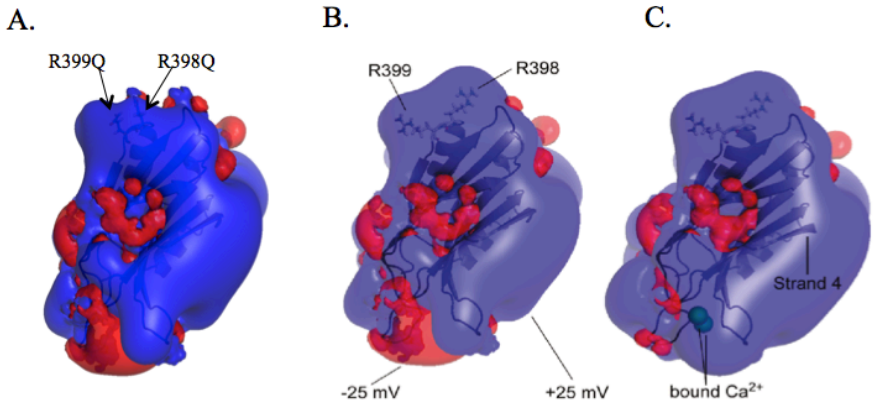

Figure 37. Equipotential electrostatic surfaces for the C2AB domain contributed by the two key arginine residues. (A) The R398Q R399Q mutation in the absence of Ca^{2+}(B) The wild--type in the absence of Ca^{2+} and (C) presence of Ca^{2+}.

The Adaptive Poisson-Boltzmann Solver (APBS) plugin in Pymol was used to calculate the electrostatic potential in 150mM monovalent ion concentration and display the potential isocontours on C2AB. The surfaces shown represent the +25 mV (blue) and the negative is -25 mV (red) isopotential surfaces.

The C2B domain is highly positively charged due to its highly conserved polybasic strand and the two conserved arginine residues located on the opposite face from the Ca^{2+} binding site. The positive surface potential on the apex is not as prevalent when the arginines are mutated to glutamines as seen in fig. 37A compared to 37B.

Ca^{2+} -dependent membrane binding

Charged residues opposite to the calcium binding loops do not play a significant role in controlling the calcium-dependent membrane affinity. Mutations in the arginine apex involving a double RQRQ mutation do not significantly alter the Ca^{2+}-dependent membrane affinity either in the absence or the presence of PIP_2.

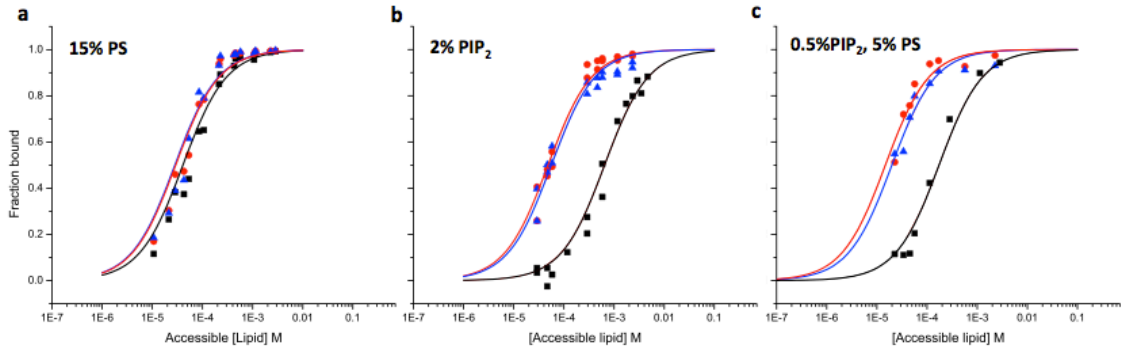

Figure 38. Comparison of the equilibrium Ca^{2+} -dependent binding for C2AB WT, RRQQ and KAKA mutants in different lipid compositions. (a) In 15% PS vesicles, the Ca^{2+} -dependent binding of C2AB is similar with the RQRQ mutant and is decreased by a fraction with the KAKA mutation; wild-type C2AB (▲), RQRQ (●), KAKA mutation (■). (b) In 2% PIP_2, the RQRQ mutation does little to alter the Ca^{2+} dependent membrane binding affinity compared with the KAKA mutation; wild-type C2AB (▲), RQRQ (●), KAKA mutation (■). (c) In 0.5% PIP_2, 5%PS bilayers the binding of C2AB is not strongly altered by the RQRQ mutation but is altered by the KAKA mutation; wild-type C2AB (▲), RQRQ (●), KAKA mutation (■).

The vesicle sedimentation assay, which is an ultracentrifugation technique, can quantitate membrane binding of proteins under equilibrium conditions. Large unilamellar vesicles (LUVs) are sucrose-loaded to help with the sedimentation of vesicles so that the unbound protein in the supernatant can be separated from the membrane-bound protein. It is important to make sure the lipid to protein ratio is large enough to ensure the true binding of the protein due to electrostatic interactions[94]. It was found that a minimum lipid to protein ratio of 140:1 gives a partition coefficient K (M^{-1}) that remains constant as the ratio is increased.

Several contributions to the membrane binding of Syt1 C2AB were investigated. In this study, this included two separate mutants on the short C2AB construct, R398Q R399Q (RQRQ) and K326A K327A (KAKA), and the double arginine mutants that were substituted to glutamines opposite the membrane binding surface[90]. The KAKA double lysine mutants have been found to impair the

membrane-binding role of Syt1[143]. Surprisingly, no change in the membrane binding affinity of RQRQ mutant was observed in comparison to the wild-type in the presence of 1mM Ca^{2+}. This result was consistent regardless of the use of the highly negatively charged PIP_2 in the lipid composition. The KAKA mutant bound 0.7 times as strong to vesicles composed of 15mol % PS. Though it did not exhibit a dramatic decrease in the presence of just PS, the KAKA mutant had a strong dependence on the level of PIP_2 in the membrane. In vesicles containing 0.5% PIP_2 and 5% PS, the partition coefficient of the KAKA mutant decreased by 5-fold (table 2). And in just 2% PIP_2 vesicles, the partition coefficient of the KAKA mutant decreased by almost 20-fold, table 2. This huge change in the partitioning coefficient of C2AB to bilayers containing just PIP_2 compared to both PIP_2 and PS illustrates the large contribution of the lysine residues in the polybasic strand to PIP_2 binding.

The roles of the charged residues in the calcium-independent binding of C2AB were also investigated. It has been reported that C2AB has a Ca^{2+} independent binding mode which allows it to tether to the membrane surface and act as an 'electrostatic switch' once activated in its Ca^{2+} bound form by bridging bilayers together [150, 134, 52]. The model proposed by Kuo et al. showed that R398 and R399 could also contribute electrostatically to the Ca^{2+} independent membrane binding of C2AB, which is mainly through the polybasic face[150].

Ca^{2+} -independent membrane binding

The KAKA mutant eliminates the Ca^{2+}-independent binding of C2AB to either PS or PIP_2 containing bilayers. The affinity of C2AB is greatly diminished in the absence of Ca^{2+}. By determining the membrane partition coefficient under equilibrium condition, the free energy contribution ($\Delta\Delta G_{binding}$) of Ca^{2+}, could be calculated. In PS containing bilayers, the affinity without Ca^{2+} is reduced approximately 3 kcal/mole and in 2 mol% PIP_2 containing bilayers it is reduced by 1.5 kcal/mol. Residues in the arginine apex have little effect upon the Ca^{2+}-independent binding of C2AB; however, mutations in the polybasic face have a profound effect in either the presence or absence of PIP_2.

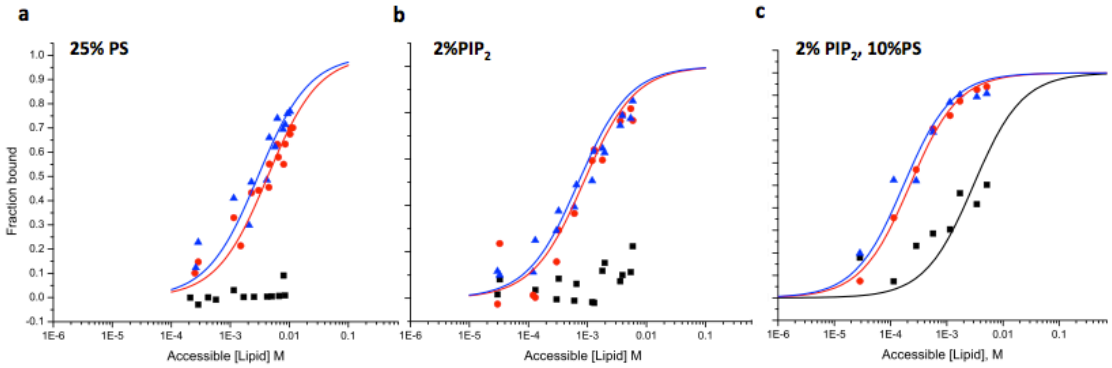

Figure 39. Comparison of wild-type RQRQ and KAKA mutant Ca^{2+} independent binding in PS or PIP_2 containing bilayers. (a) With bilayers composed of 25 mol% PS. The RQRQ mutation (●) produces a slight decrease in the Ca^{2+}-independent binding affinity compared to the wild-type protein (▲); however, binding is not detected for the KAKA mutant (■). (b) C2AB binding to bilayers composed of 2 mol% PIP_2 is slightly stronger than to bilayers composed of 25 mol% PS for either the wild-type (▲) or RQRQ mutant (●). The Ca^{2+}-independent binding of the KAKA mutant (■) to 2 mol% PIP_2 is very weak or absent. (c) In bilayers composed of both 2 mol% PIP_2 and 10 mol% PS, the wild-type (▲) and RQRQ mutant (●) both have an even more stronger binding compared to bilayers composed of just 2 mol% PIP_2. While a weak binding of the KAKA mutant (■) is observed by a decrease of 15-fold.

The partitioning of C2AB to membranes is weak in the absence of Ca^{2+}, except in the presence of PIP_2. Bilayers with mixtures of PIP_2 and PS produce the highest

affinities in the absence of Ca^{2+} while mutations in the polybasic face eliminate the Ca^{2+}-independent binding interaction.

Lipid Composition (Ca^{2+} free)	C2AB WT [M^{-1}]	C2AB RQRQ [M^{-1}]	C2AB KAKA [M^{-1}]
25 mol% PS	3.4 (±0.3) x 10^2	2.3 (±0.2) x 10^2	Not detected
2 mol% PIP_2	1.4 (±0.2) x 10^3	1.2 (±0.1) x 10^3	Not detected
2 mol% PIP_2 10 mol% PS	5.9 (±0.9) x 10^4	4.6 (±0.2) x 10^4	3.4 (±0.5) x 10^2

Table 1. Molar partition coefficients, K (M^{-1}), for the Ca^{2+} independent membrane affinity of Syt1 C2AB. The membrane affinity of the arginine mutant and lysine mutant are compared to the wild-type in the different anionic lipid compositions. The errors represent the uncertainty obtained from the non-linear regression fit using equation 2.2 in chapter 2 to yield K. The dissociation constant is the reciprocal of K, which is the accessible molar lipid concentration where 50% of the protein is bound to membrane.

Figure 39 and table 1 show that the RQRQ mutations do not change the membrane binding affinity of C2AB in its Ca^{2+} -free state either. The similar binding affinity of the RQRQ mutant to the wild type was prevalent in the different lipid compositions tested. The KAKA mutant however did not exhibit any binding to 25 mol% PS in the absence of Ca^{2+} and 2 mol% PIP_2 vesicles. Its binding is thought to be sufficiently weak so that little is bound given the lipid concentrations used in this experimental setup. There was a very weak binding of 340±0.5 M^{-1} that was observed when the negative charge density was increased by using 2% PIP_2 and 10% PS in the vesicle. This demonstrated a decrease by up to 15-fold compared to the wild type protein. All of the three lipid conditions indicate the importance of the lysine residues in the weak Ca^{2+} independent binding of C2AB. The binding energetics in 25% PS is reduced by 3 kcal/mole in the absence of

Ca^{2+}, whereas, the decrease in binding in 2% PIP_2 resulted in 1.5 kcal/mole in the absence of Ca^{2+} compared to the Ca^{2+} dependent binding. The lipid-to protein ratio was at least 250:1 for the Ca^{2+} independent binding of C2AB.

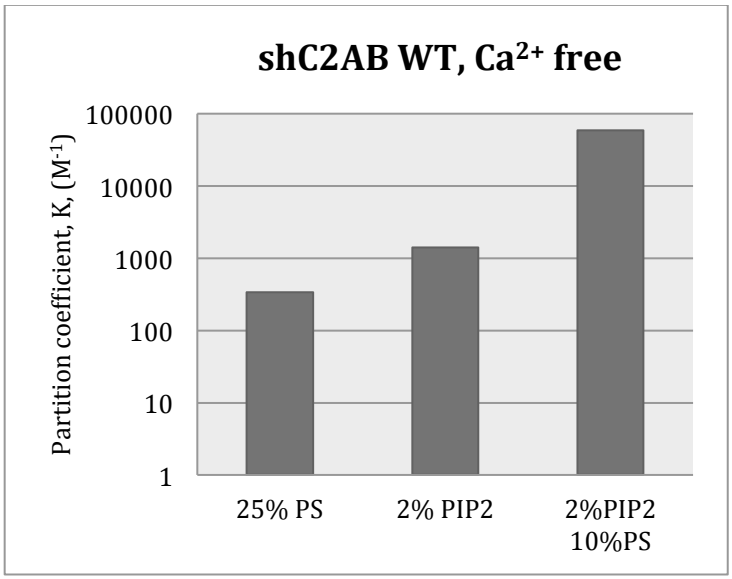

Figure 40. The molar partition coefficient, K, of Syt1 C2AB plotted in log scale: The effect of PIP_2 is several fold higher than just the PS containing membrane in the Ca^{2+} independent binding of C2AB.

Table 1 and figure 40 show the comparison of the molar partition coefficient, K, of C2AB with 25% PS and 2% PIP_2 and suggest that PIP_2 plays a predominant role in the weak membrane binding of Syt1. Even though the charge density is lower in 2% PIP_2 which would be equivalent to 8% monovalent negatively charged PS, the K value of 2% PIP_2 is 4 times higher than in 25% PS. This could be an example of the sequestration of PIP_2 by poly-lysines as seen in other proteins containing lysine repeats hence causing the local charge density to be much higher[151, 152]. Furthermore, it has also been hypothesized that though PIP_2 constitutes 1 mol% of the phospholipids in the cell plasma membranes, it can

reach up to 6 mol% due to sequestration effects in active sites of exocytosis in PC12 cells[153].

PS and PIP_2 act cooperatively to bind C2AB to bilayers. When membranes of equivalent charge densities are compared, C2AB has the greatest affinity to bilayers containing both PS and PIP_2.

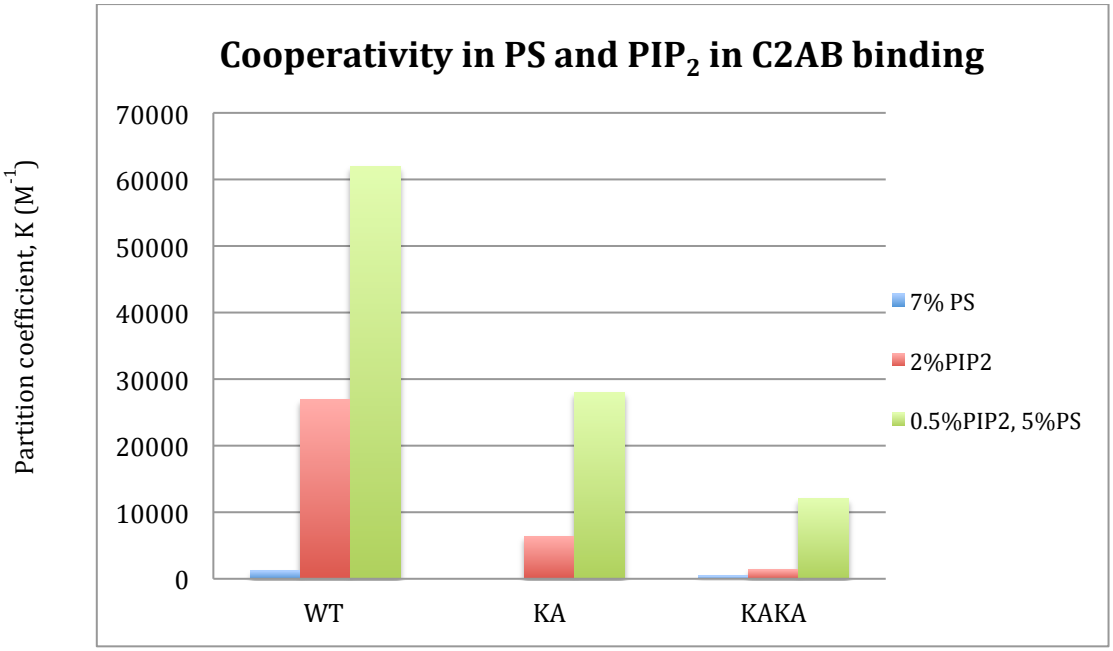

Figure 41. Cooperative effect of C2AB binding in lipids containing both PS and PIP_2. The single lysine mutant K326A (KA) and double lysine mutant K326A K327A (KAKA) were found to decrease binding accordingly in the three lipid compositions with equivalent mole charge density: 0.5%PIP_2 5%PS, 2% PIP_2 and 7% PS.

Lipid Composition (1mM Ca^{2+})	C2AB WT [M^{-1}]	C2AB KA [M^{-1}]	C2AB KAKA [M^{-1}]
7 mol% PS	1.2 (±0.1) x 10^3	--	4.2 (±0.4) x 10^2
2 mol% PIP_2	2.7 (±0.2) x 10^4	6.4 (±0.5) x 10^3	1.4 (±0.1) x 10^3
0.5 mol%PIP_2 5 mol% PS	6.2 (±0.7) x 10^4	2.8 (±0.3) x 10^4	1.2 (±0.1) x 10^4

Table 2. Molar partition coefficients, K, of Syt1 C2AB to lipid bilayers at comparable charge densities (7 mol% negative charge). The additive effect of a single lysine contribution to the binding affinity from the KA and KAKA mutants is prevalent in the three anionic lipid compositions. The cooperative effect of $PSPIP_2$ in all the different Syt1 C2AB forms is also observed.

It has been shown that incorporating PIP_2 into PCPS liposomes increases the membrane binding of certain sites in C2AB in the presence and absence of Ca^{2+} [76, 78]. However, it has not been demonstrated that the presence of both PIP_2 and PS in physiological concentrations can act synergistically in the membrane binding of C2AB. Previous work on Syt1 C2AB membrane binding in the presence of PIP_2 were done by adding 1 mol% PIP_2 to PCPS liposomes with a final composition of PC:PS:PIP_2 75:24:1 mole ratio[78, 76]. Hence, the proper evaluation of the cooperativity of PS and PIP_2 by keeping equivalent charge densities in membranes has not been accomplished. Unpublished data from Dr. Angel Perez in Prof Reinhard Jahn's group in Max Planck Institute (Gottïngen), using stopped flow binding data showed that the K_{off} (the rate of unbinding) is the most affected in bilayers containing both PIP_2 and PS even though the overall equivalent charge density is retained. Similarly, in the work herein (figure 39 and table 2), the Ca^{2+} dependent binding in the presence of an equivalent mole charge density of PS and PIP_2 shows a trend that 2% PIP_2 has a much stronger

partition coefficient, K, than 7% PS for the KAKA mutant, KA mutant (K326A) and wild-type. There is a dramatic increase of up to one order of magnitude in the K values when both PS and PIP_2 are present in the vesicle. This binding trend in the different lipid compositions is also consistent for the different mutants investigated. Hence, suggesting the cooperativity of PS and PIP_2 is prevalent in the membrane binding mechanism of C2AB.

The polybasic face of C2AB contributes to the calcium-dependent membrane binding of C2AB primarily when PIP_2 is present. No large differences in the C2AB membrane affinity to PS bilayers are seen when wild-type protein is compared to the KAKA mutant; however, when the bilayers contain PIP_2, differences in affinity appear. Each lysine residue contributes approximately 1 kcal/mole to the membrane affinity when bilayers are composed of 2 mol% PIP_2.

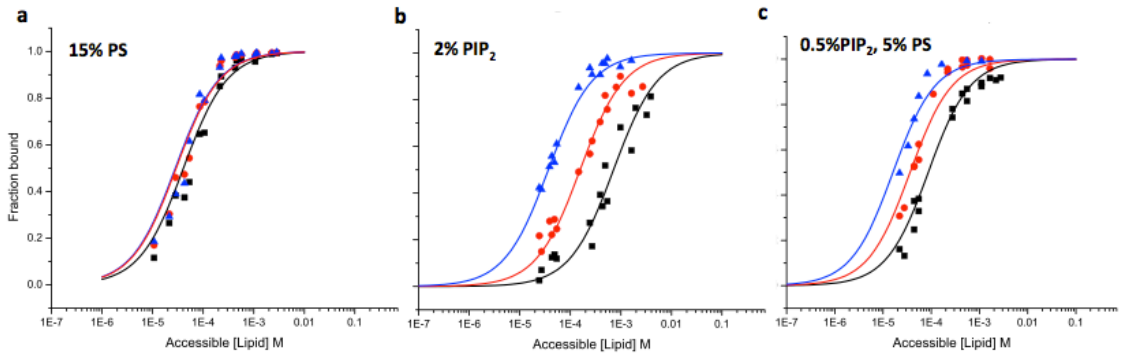

Figure 42. Equilibrium binding of C2AB and polybasic mutants to PC, PS, and PIP_2 bilayers. (a) In PS bilayers, the calcium-dependent binding of C2AB is not strongly modulated by the mutations in either the polybasic face or arginine apex (sites opposite the calcium-binding loops); wild-type C2AB (▲), RQRQ (●), KAKA mutation (■). (b) In 2% PIP_2 bilayers, the removal of one lysine residue alters the free energy of binding by about 900 cal/mole; wild-type C2AB (▲), KA mutation (●), KAKA mutation (■). Lipid bilayers in (b) and (c) have equivalent charge densities. (c) In PS:PIP_2 bilayers (5% PS, 0.5% PIP_2) removal of one lysine residue within the polybasic face alters the free energy of binding by about 500 cal/mole; wild-type C2AB (▲), KA mutation (●), KAKA mutation (■).

The contribution of a single lysine in the polybasic strand to the binding affinity of C2AB was investigated by comparing C2AB K326A (KA mutant) and the KAKA mutant to the wild-type. Not much has been reported on the contribution of an individual lysine in the polybasic moiety of C2B domain to the membrane binding capability of Syt1. Herein it was found that a single lysine mutation decreased binding by over 4 fold in 2% PIP_2 vesicles. By determining the membrane partition coefficient under equilibrium condition, the free energy contribution ($\Delta\Delta G_{binding}$) for a single lysine, could be calculated. Since the partition coefficients of the wild-type (K_{WT}), the KAKA mutant (K_{KAKA}), and KA mutant (K_{KA}) are known, the free energy of binding can be calculated:

$$\Delta\Delta G_{binding} = -RT \ln (K_{KA}/K_{WT})$$

and

$$\Delta\Delta G_{binding} = -RT \ln (K_{KAKA}/K_{KA})$$

This yielded a $\Delta\Delta G_{binding}$ of 0.9 kcal/mol in PIP_2 vesicles and 0.5 kcal/mole in $PSPIP_2$ vesicles by a single lysine residue. Since the PIP_2 and $PSPIP_2$ compositions are below physiological concentrations, the $\Delta\Delta G_{binding}$ is expected to be significantly more.

Effects of ATP and negatively charged polyelectrolytes

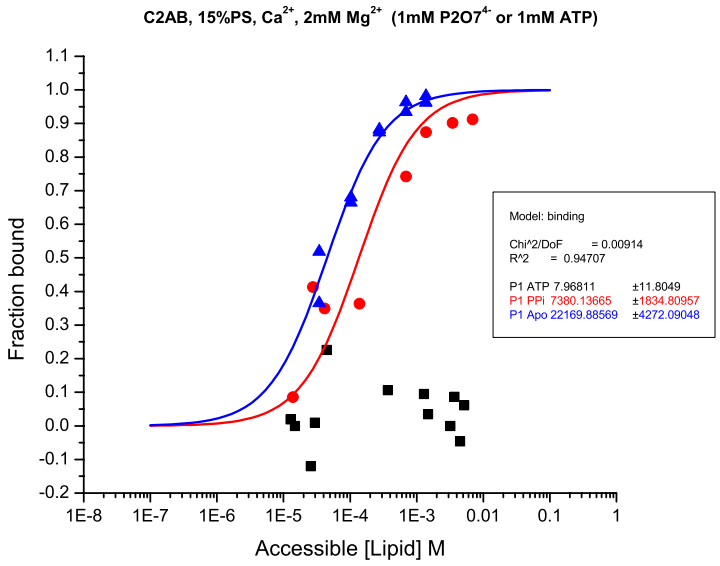

Figure 43. Addition of 1mM pyrophosphates shifts binding equilibrium to the right by three-fold while 1mM ATP diminishes binding completely. The binding of wild-type C2AB (▲) to 15%PS vesicles is three times stronger than in the presence of 1mM $P_2O_7^{4-}$ (●). Binding of wild-type C2AB to 15%PS vesicles in the presence of 1mM ATP (■) is completely eliminated. There was 1mM Ca^{2+} and 2mM $MgCl_2$ present in the samples.

It has been proposed that when Ca^{2+} is present, the membrane anchored synaptotagmin binds to its own membrane in the synaptic vesicle instead of undergoing tethering or bilayer bridging[154]. This binding back to its own membrane is termed *cis*-binding compared to the *trans*-tethering to the plasma membrane. This occurs due to the presence of ~12% PS in the synaptic vesicle[75]. It is postulated that addition of ATP would eliminate the *cis*-binding of synaptotagmin and enhance the *trans*-tethering to the plasma membrane that contains 1-3% PIP_2[91]. This modulation of synaptotagmin from the *cis*-binding to the *trans*-tethering to the target membrane by ATP is thought to regulate the fusion event in synaptic transmission. The inhibition of synaptotagmin binding to

the PS containing vesicle membrane by ATP is thought to be electrostatic in nature. This was observed in the complete loss of C2AB binding to 15%PS LUVs when 1mM ATP was added as shown by the black data points in the binding curve shown in figure 43. The addition of a similar charged 1mM pyrophosphate, $P_2O_7^{4-}$, shifted the binding isotherm to the right by three-fold as represented by the red curve. This illustrates that the binding mechanism of synaptotagmin is electrostatic in nature though the magnitude of the different polyphosphate is different between ATP-Mg and $P_2O_7^{4-}$.

Characterization of IP3 and ATP binding site on Syt1 C2B through NMR

The molecular mechanism for how ATP and PIP_2 exhibit the different interactions of Syt1 in the synapse-mimicking environment is postulated to be a factor of electrostatic interactions as well as formation of a coordination sphere with the Ca^{2+} [91]. It was proposed that since ATP and C2AB, in synaptic vesicles containing 15% anionic lipid, have a similar Ca^{2+} affinity (EC_{50} = 230μM, half maximal effective concentration), there is competition for Syt1-Ca^{2+} by charge shielding of ATP [91]. Ultimately this leads to disruption of the *cis*- binding, allowing Syt1- Ca^{2+} to interact in the *trans* configuration with the target membrane. And since PIP_2 present in the target plasma membrane has a much higher binding affinity for Ca^{2+} (EC_{50} = 56 μM), it is able to outcompete ATP for binding to Syt1. To better understand this mechanism of interactions, NMR experiments were performed to i) to understand if it is driven by a non-specific electrostatic

interaction, ii) characterize the binding sites of ATP and PIP_2 in Syt1, and iii) quantitate their binding affinity to Syt1 C2B.

The presence of IP3 (headgroup of PIP_2) or ATP produces chemical shifts in the heteronuclear HSQC spectra of C2AB or C2B.

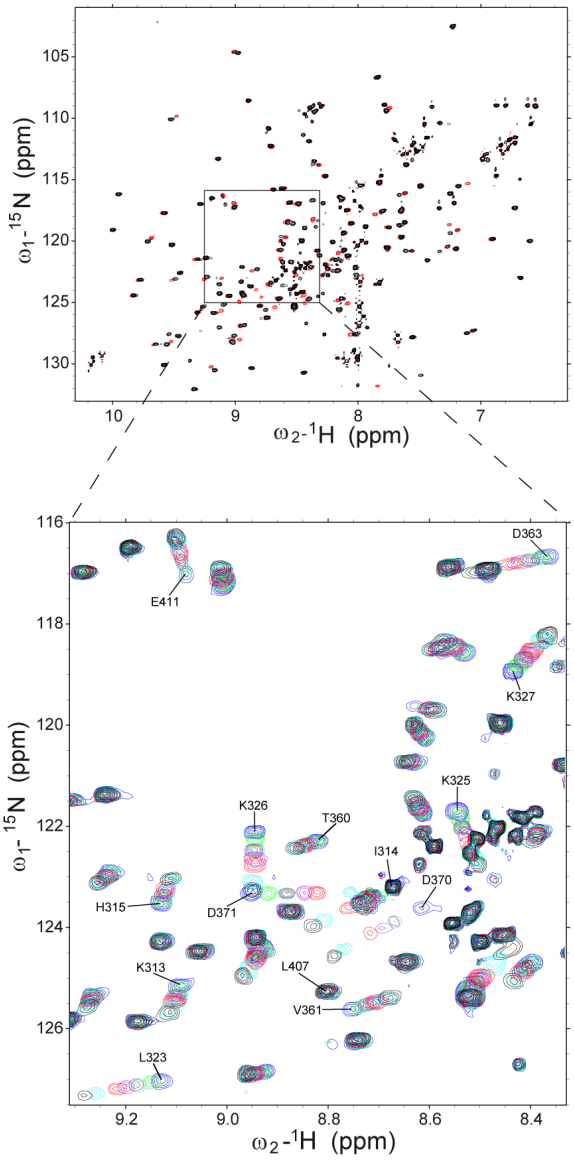

Figure 44. Overlay of 2D HSQC spectra to map chemical shift perturbation upon IP_3 titration. Apo C2AB (black), C2AB in the presence of 2 mM IP3 (red). Expanded section of the HSQC spectrum showing chemical shift changes upon titration with IP3 (0mM – blue, 0.1mM – green, 0.2mM – maroon, 0.3mM – purple, 0.5mM – red, 1mM – cyan, 2mM - black)

The effect of the ligands ATP and IP3 on the C2B domain of Syt1 was determined by performing a series of titration experiments through 2D HSQC NMR using isotopically ^{15}N labeled C2A and C2B individual domains. The C2A and C2B individual structure resonance assignments were acquired from the solution NMR structures deposited in the PDB by Rizo's group (PDB ID: C2A 1BYN; C2B 1K5W)[93, 52]. The 2D NMR experiment on the C2B domain yielded crosspeaks in which 85% were successfully matched with the resonance assignments provided by Rizo's group.

The final ^{15}N-labeled protein concentration was between 0.35- 0.6mM in 3mM $CaCl_2$, pH = 6.3 at 27°C. IP3 was titrated up to 2mM at increments of 0.1 and 0.2mM. ATP was titrated up to 4mM in 0.2mM increments until it was in slight excess of its physiological level. The overlay of the individual spectra at different ligand concentrations allowed the mapping of cross peaks that were perturbed following the assignment of resonance that was specific to the residue. The chemical shift was mapped for the ligands titrated as shown in figure 44. The maximum perturbation of each cross peak changing position upon excess ligand addition was measured. In figure 44, he residues that showed the most significant chemical shift change in IP3 belonged to the polybasic strand (L323, K325, K326 and K327) or the Ca^{2+} binding loops (D363, D370, D371).

Both IP3 (the PIP_2 headgroup) and ATP interact with the C2B domain polybasic face as well as with the Ca^{2+}-binding loops of C2A and C2B.

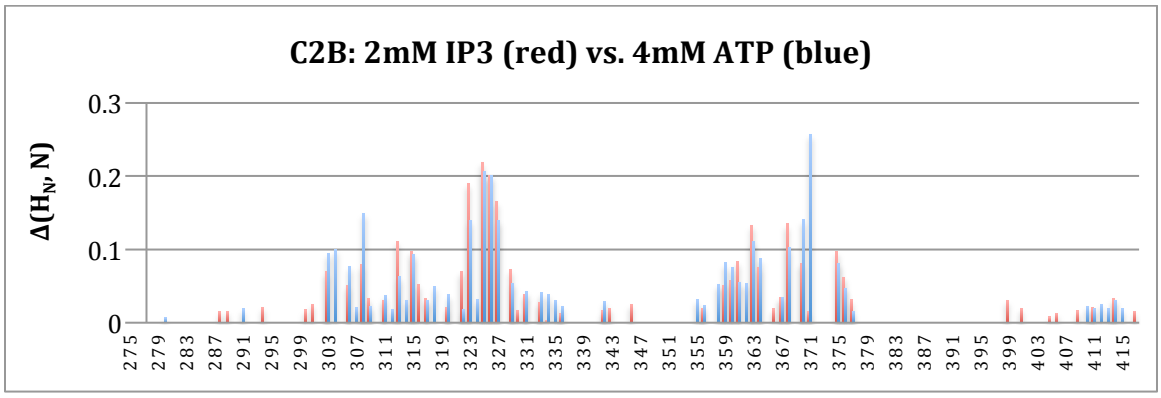

Figure 45. C2B amino acid sequence plotted against the maximum weighted average chemical shift change, $\Delta(H_N, N)$. The red bars represent the chemical shift change due to 2mM IP3 while the blue bars represent the chemical shift change from 4mM ATP. The overlaid graphs indicate that IP3 and ATP compete for the same binding sites probably due to unspecific electrostatic interactions on the positively charged regions on C2B.

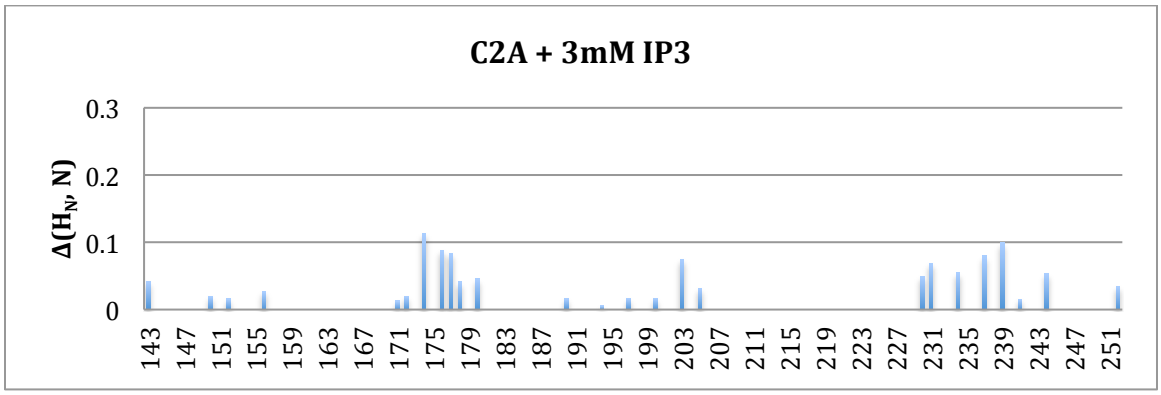

Figure 46. Residues in C2A exhibiting chemical shift perturbation in the presence of 3mM IP3. C2A is less sensitive to the interactions caused by IP3 suggesting weak unspecific interactions mainly on the Ca^{2+} binding loops.

The ligand induced chemical shift perturbation on specific sites on C2A and C2B domain were calculated using a weighted average chemical shift change (equation 2.28) $\Delta(H_N, N)$, to account for the different chemical shift (ppm) scale for ^{15}N vs. ^{1}H. In figure 45 and 46, the $\Delta(H_N, N)$ in the presence of IP3 or ATP is plotted as a function of the residue number for C2B and C2A respectively. Figure 45 is an overlay of the chemical shift perturbation of the residues in C2B due to

2mM IP3 in red bars and 4mM ATP in blue bars. The trend of the sites of interaction is generally similar between the two different polyphosphate anions. The residues showing the maximum weighted average chemical shift change is representative of the binding site of the ligand[87]. The red bars exhibit a maximum perturbation of $\Delta(H_N,N) > 0.15$ in residues L323, K325, K326 and K327 which are in the polybasic strand. The ATP induced maximum perturbation as denoted by the blue bars had a $\Delta(H_N,N) > 0.15$ in both the polybasic strand (residues K325 and K326) and the Ca^{2+} binding loops (residues S308 and D371) . The difference suggest that while IP3 is specific to the polybasic strand, ATP seems to have a more non-specific interaction with charged regions like the Ca^{2+} binding loops and the polybasic region. In comparison to the IP3 interaction with the C2A domain, figure 46, the residues with $\Delta(H_N,N) > 0.075$ in C2A are G174, T176, S177 and D203 which are in the Ca^{2+} binding loops.

In order to exclude chemical shift changes due to ATP induced aggregation of the C2B domain, DEER experiments were performed. They were done on the singly spin-labeled C2AB (283R1) and C2B (415R1) domains to see if ATP caused aggregation of the protein. However, there was no DEER signal detected and hence, was concluded that the 2mM ATP did not cause either the single labeled C2AB or C2B to aggregate.

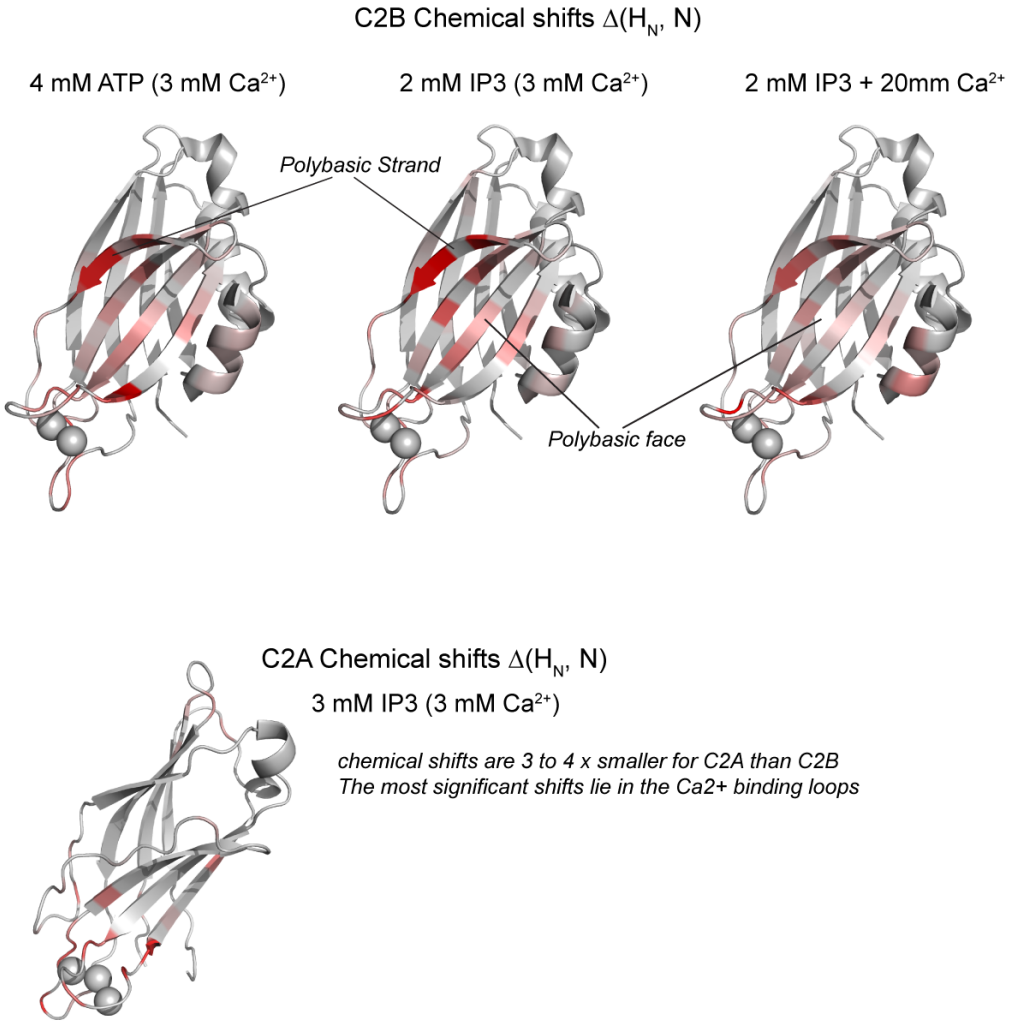

Figure 47. Mapping of the perturbed sites (red) induced by IP3 and ATP onto the structure of C2A (PDB 1BYN) and C2B (PDB 1K5W) domain. The intensity of the red color corresponds to the larger chemical shift change, $\Delta(H_N, N)$.

The red color coded chemical shift change $\Delta(H_N, N)$ was mapped onto the NMR structures of C2B and C2A for ATP and IP3. The largest chemical shifts are seen for C2B, smaller chemical shifts are seen for C2A. The chemical shift changes are widely distributed in the C2B polybasic region for both ATP and IP3. The binding of the polyphosphates is not limited to the polybasic strand but is also observed on the calcium binding loops. The little perturbation on C2A

domain shows that binding is not only weak but also centered mainly on the charged Ca^{2+} loops probably due to unspecific electrostatic interaction.

IP3 shows a higher affinity for the synaptotagmin C2B domain than does ATP.

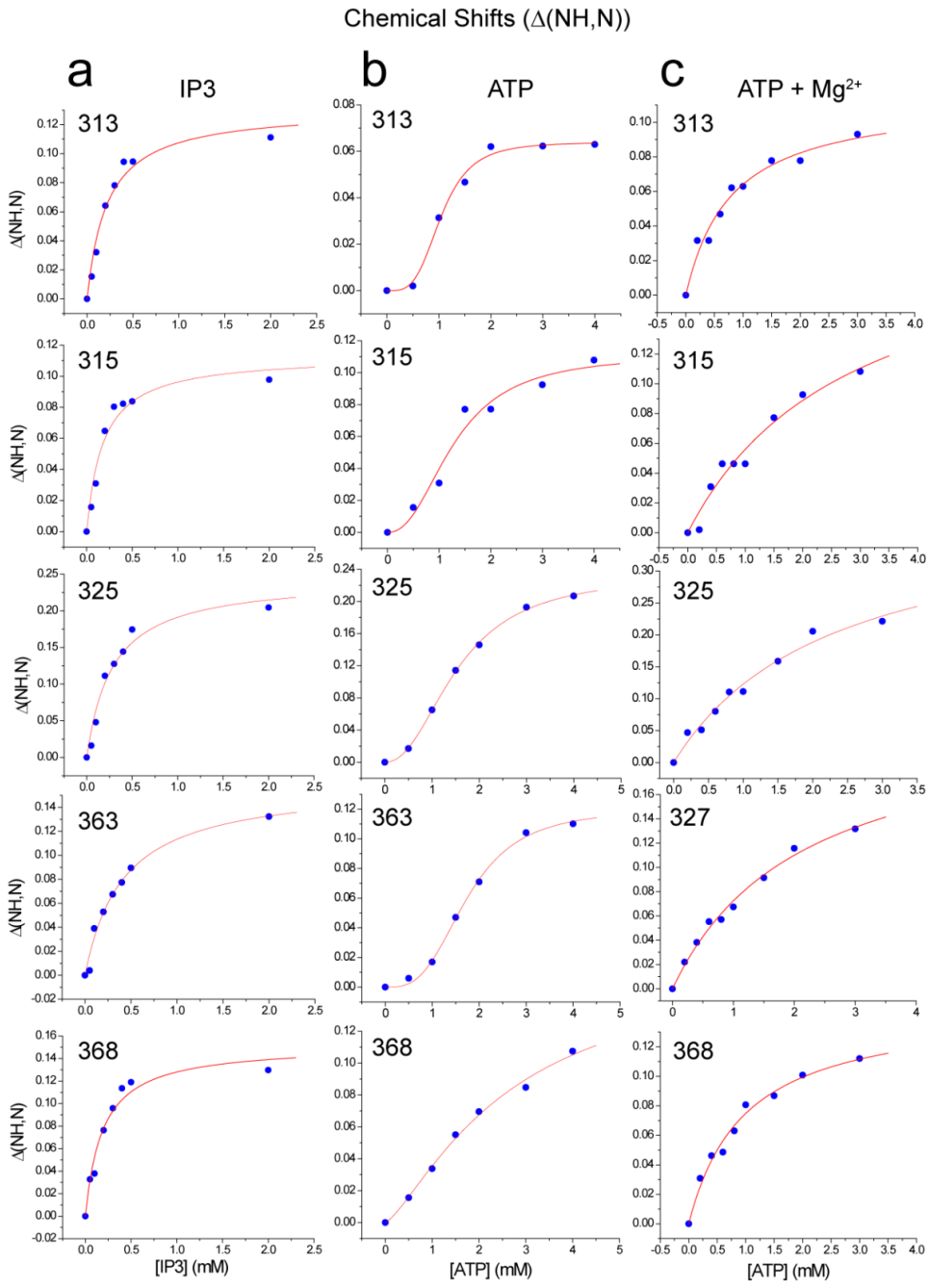

Figure 48. Comparison of the residues that exhibited the most chemical shift change upon addition of each ligand, IP3, ATP and ATP-Mg^{2+}.(a) Titration of the chemical shift changes with IP3 yields good fits to single site binding model (red line). The affinity calculated from each site is similar, with an affinity of 230 μM observed for sites at the polybasic face and Ca^{2+}- binding loops. In (b) the binding to ATP is cooperative with an average affinity of 1.6 ± 0.5 mM and a binding site (n) of 2. The addition of Mg^{2+} during the ATP titration (c) eliminates this cooperativity, but does not significantly change the affinity, 0.8 mM ± 0.5 mM.

Binding curves were constructed by plotting the $\Delta(H_N, N)$ as a function of the titrated ligand concentration as shown in figure 48. The observation of a single set of peaks and the slow saturation of the protein chemical shifts upon titration with ligand is consistent with fast exchange and relatively weak binding K_d ~10^{-5} M[120].The residues exhibiting the most chemical shift change in the fast exchange regime were chosen to construct binding curves with to determine the binding affinity, K_d, of the ligands. The IP3 binding curve was fitted to a hyperbolic tangent curve yielding a K_d of 230μM. This also indicated a single-site binding isotherm. The ATP binding curve was sigmoidal in nature suggesting a cooperative binding mode with multiple binding sites. It could only be fitted to a Hill equation, which gave a K_d of 1.6 ± 0.5 mM and a binding site (n) of 2.

Since the majority of ATP present in the cell exists as a complex with Mg^{2+} the ATP titration experiment was repeated in the presence of 1mM Mg^{2+} [155]. Here the cooperativity of ATP binding to the C2B domain was no longer observed (figure 48c). The binding data could be fitted to a hyperbolic equation for single site binding and yielded a slightly higher K_d of 0.8 mM ± 0.5 mM, however, the binding affinity of C2B to IP3 was still significantly higher.

Discussion and future experiments:

The interaction of IP6 and the human Syt1 C2B was characterized through similar NMR experiments [87]. It was found that residues in the polybasic face and the Ca^{2+} loops had the highest chemical shift perturbation, which is indicative of the binding site of the ligand. Their findings are similar to what we found for the rat Syt1 C2B domain and IP3. Furthermore, work done by Igumenova's group on C2α and C4-PIP_2 binding indicated that the poly-lysine region, homologous to the polybasic strand in the Syt1 C2B, as well as the Ca^{2+} binding loops were the most perturbed [77]. The results are consistent for domains that contain clusters of basic residue and Ca^{2+} bound regions where the overall electrostatic potential is positive. The highly negatively charged polyphosphate anions (IP3, C4-PIP_2, IP6 and ATP) would be attracted to the positive protein surfaces. Increasing the ionic strength to eliminate unspecific electrostatic interactions can also be done to see if similar perturbations still occur which would be indicative of IP3 forming a complex with C2B domain.

The binding site may or may not be a 1:1 complex between PIP_2 and C2B (i.e. specific binding) with the ligand site comprising both the polybasic face and Ca^{2+} loops as proposed by Joung et al. and Morales et al. with their NMR findings [87, 77] . The number of binding sites of PIP_2 has been proposed to be 1 by ITC binding measurements (Angel Perez unpublished data) and it may just be the polybasic strand that is facilitating the main interaction in the C2B domain. It

is presumed that in the presence of PS in the membrane, the Ca^{2+} loops penetrate into the bilayer leaving only the polybasic strand available for interaction with PIP_2 in the target membrane. To support this hypothesis, my power saturation data indicates specificity of the binding loops to PS versus PIP_2. More of this membrane orientation and docking of C2AB to bilayers containing PS and PIP_2 will be covered in the next chapter.

The binding affinity of IP3 was found to be 4 times stronger than ATP in the presence of Mg^{2+}. Though the overall charge on ATP-Mg^{2-} is less than IP_3, it is thought that PIP_2 would be dominantly specific to the polybasic face of C2B due to the local effective concentration on the plasma membrane compared to the spatial concentration of ATP in the cell.

The results of the sedimentation assay to quantitate C2AB membrane binding suggest that PIP_2 prefers the polybasic strand of C2B. This was applicable in both the presence and absence of Ca^{2+}. The double arginine mutants on the other hand did not seem to govern the membrane binding affinity of C2AB. Though turbidity assays and vesicle aggregation assays in high-protein-to-lipid concentrations show that the two arginines are important in the membrane binding role of C2AB, we were not able to see strong effects of the two key arginines. Other groups have also reported that there is no correlation between the membrane binding role of C2AB and the two arginines[156]. Furthermore, if interactions were driven by electrostatic interactions, then my NMR experiment

done using highly negatively charged IP_3 (PIP_2 head group) and ATP would show significant perturbations on the two arginines cross peaks as well, however very little chemical shift change observed. Though the expression and the proper folding of the Syt1 arginine mutants (R398Q and R398Q R399Q) were checked and their correct targeting to the synapses were verified, the defects in the intrinsic Ca^{2+} sensitivity of release could not be checked as done in the experimental set up by Xue et al [90, 123]. Young et al. postulated that the loss of function phenotype observed by Xue et al from the R398QR398Q Syt1 mutant could be due to defects in synaptic vesicle positioning or defects in the intrinsic calcium sensitivity[123]. This correct positioning of the synaptic vesicles also known as 'positional priming' has been reported to be important for synchronous release[157].

From the power saturation measurements in chapter 3, the membrane binding on the C2B arginine apex may be electrostatic and just interfacial to the lipid phosphates. This interfacial association of the two conserved arginine residues could still contribute to the binding of Syt 1 as models of Syt bridging bilayers have been implicated to be important for synaptotagmin's function [50, 158].

The membrane binding energy contributed by a single lysine was higher in vesicles containing just PIP_2 at 0.9 kcal/mol compared to 0.5 kcal/mol when PS was included in the vesicles. This suggested that the binding energy of the poly-lysine strand is influenced predominantly by PIP_2 than by PS, which is thought to

be specific to the binding loops. Overall, accounting for the number of lysines/arginine in the polybasic strand, the binding energy contribution of this important region would be close 3 kcal/mol in PCPSPIP_2 bilayers.

One of the mechanisms of membrane binding of C2AB is proposed to be non-specific electrostatic interactions between the positively charged Ca^{2+} loops of C2 domains and the negatively charged lipid in the bilayer. The extent of membrane binding was observed to be larger for vesicles containing PIP_2 compared to PS at equivalent in charge densities. This is consistent with an electrostatic mechanism where discreteness of charge effects are important for lipids such as PIP_2. The several-fold enhancement in C2AB binding when both PS and PIP_2 are present indicate that there may be a cooperative role of the two anionic lipids in membrane fusion. It would illustrate that both PS and PIP_2 are required to effectively coordinate the membrane binding of Syt1 before and after the Ca^{2+} influx.

6. Molecular mechanism of C2AB docking with membranes

Introduction

As discussed earlier (see Introduction), the C2B domain of synaptotagmin 1 and other C2 domains show specificity for polyphosphoinositides, such as $PI(4,5)P_2$ [79, 83, 143, 159]. A Ca^{2+} dependent and Ca^{2+} independent binding of the synaptotagmin 1 C2 domains to $PI(4,5)P_2$ phospholipids has been observed in these studies[143, 70, 78]. In collaboration with Dr. Angel Perez in Prof Reinhard Jahn's group in Max Planck Institute (Gottïngen), we tested several hypotheses regarding the membrane binding of C2AB. First, we tested the proposal that the binding affinity of C2AB to liposomes containing either PS or PIP_2 was different, even when each lipid was present at equivalent charge densities. Second, we tested the idea that there is cooperativity between PS and PIP_2 when the membrane binding affinity of C2AB is quantitated. Third, we tested the proposal that the membrane binding mode or docking orientation of C2AB with respect to membranes containing either PS or PIP_2 is different. In order to perform these experiments, we examined EPR line shapes of spin labeled C2AB and performed power saturation experiments to obtain the membrane insertion depth of the domain in the different negatively charged lipid environments.

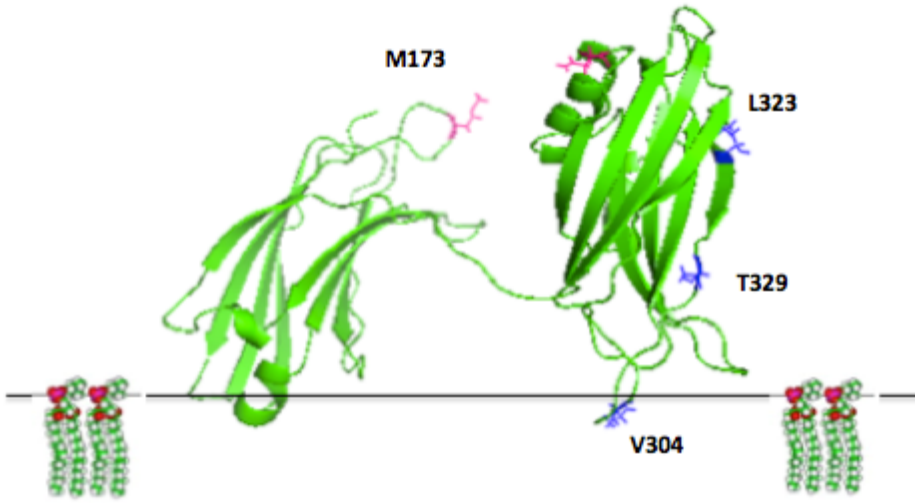

Figure 49. Sites on C2AB probed for membrane interaction and docking orientation by doing site-directed spin labeling EPR experiments. Each site on the Ca^{2+} binding loops on the individual C2A (M173) and C2B (V304) domain are chosen to be spin-labeled. Sites, L323 and T329, near the conserved polybasic strand on C2B are also spin-labeled.

Results:

CW EPR spectra

EPR line shapes provide information about the mobility of the spin label side-chain (R1). When attached to a protein that interacts with the membrane interface, such as a C2 domain, the R1 side chain exhibits a dramatic reduction in motion and a broadening of the EPR spectrum upon insertion into the lipid bilayer. In general, the extent of broadening in the EPR spectrum is dependent upon the depth of insertion. In these experiments, EPR spectra are obtained in aqueous solution, bound to large unilamellar vesicles (LUVs) and finally normalized to correct for the total spin number in each sample. The amplitudes measured will then reflect the motional averaging of the R1 side-chain and the extent of membrane penetration. The R1 labeled sites shown in figure 49 were

probed upon binding to membranes containing either mixtures of PS, PS and $PI(4,5)P_2$.

C2AB V304R1, Ca^{2+}

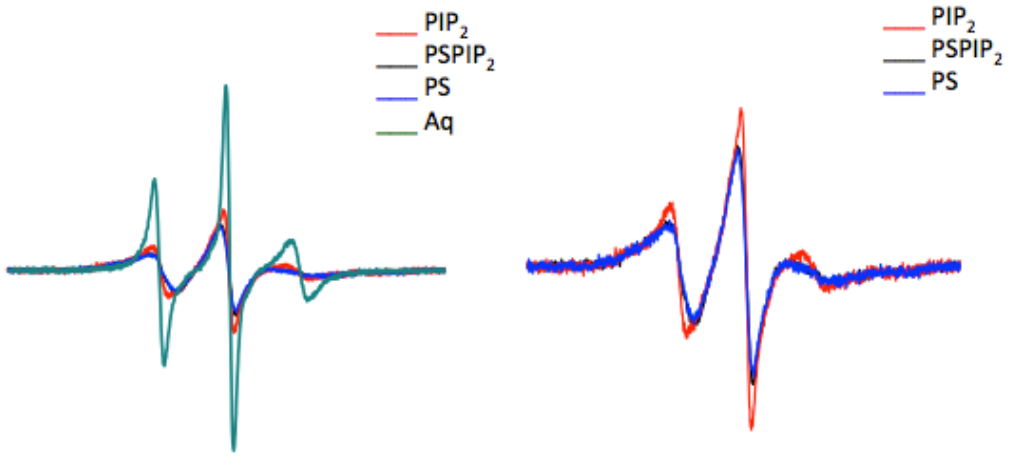

Figure 50. cw-EPR spectra for site V304R1 on C2AB in the different lipid compositions in the presence of Ca^{2+}. The aqueous form of the spin-labeled C2AB is in green while the line shapes due to PS, PIP_2 and $PSPIP_2$ are in blue, red and black respectively. The spectra on the right show that PS induces the most membrane contact on the Ca^{2+} binding loop 1 of C2B domain. This broadened line shape due to PS is very different to the spectrum due to just PIP_2 vesicles. The spectra are normalized against the total spin number so that the peak amplitudes are an approximate measure of the R1 side chain signal.

The spin-labeled site V304R1 is on Ca^{2+} binding loop 1 of the C2B domain. In contrast to the aqueous form of the C2AB V304R1 mutant (green trace), the EPR spectrum in the presence of PC:PS (4:1) LUVs shows significant broadening (blue trace, figure 50). This indicates that the motion of the spin-label on the binding loops has been restricted, due to insertion of this site into the membrane bilayer. Recent work indicates that the restricted motion and the broadening EPR line shapes at a protein-lipid interface is due to interactions of the R1 side chain with the protein surface rather than with the hydrocarbon chains[108, 109, 110]. The red traces are due to C2AB V304R1 bound to 5%PIP_2 containing PC vesicles.

There is also a broadening of the EPR spectrum and a decrease in the peak-to-peak amplitude of the central line in these vesicles even though PS is not present. However, comparing the line shape of the V304R1 mutant in the presence of vesicles containing either PS or PIP_2 suggests that the spin-labeled loops do not undergo an identical membrane association. Though similar in charge density, 20% PS appears to permit a greater membrane insertion of the V304R1 site on C2AB (figure 48 left) than does PIP_2. When both PS and PIP_2 are present at equi-molar charge densities 2.5%PIP_2 and 10% PS in the membrane, the line shape is identical to that obtained with 20% PS.

C2AB M173R1, Ca^{2+}

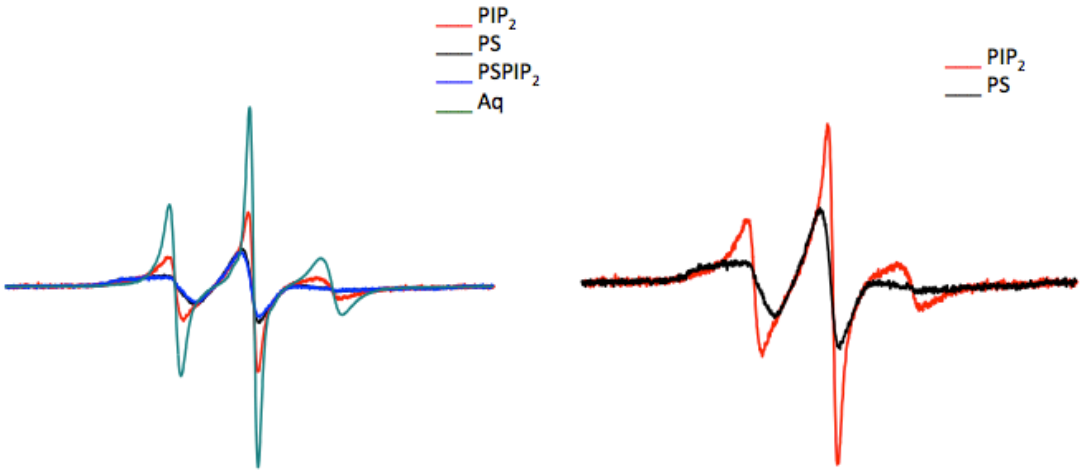

Figure 51. Site M173R1 on C2AB in the different lipid compositions in Ca^{2+}. The aqueous form of the R1 mutant is in green while the line shapes due to PS, PIP_2 and $PSPIP_2$ are in black, red and blue respectively. The Ca^{2+} loop 1 on the C2A domain show that a more dramatic line shape broadening occurs in PS vesicles (black) than in PIP_2 vesicles (red).

Similarly, the spin-label on the binding loops of C2A domain yielded EPR spectra that had the most broadening in PS containing vesicles (20% PS and 10%PS, 2.5%PIP_2). The green trace in figure 51 corresponds to the spin-labeled mutant

in its aqueous state and has sharp peaks due to a very mobile R1 side-chain. The red trace is the M173R1 mutant in the presence of 5% PIP_2 which also undergoes line shape broadening but not as drastically as in PS containing vesicles (blue and black traces). In the right spectra in figure 51, the lineshape between the 20% PS (black traces) and 5%PIP_2 (red traces) are overlaid. This is a good example of PS inducing very different docking of C2AB compared to PIP_2 and the spin-label experiences different mode of binding.

C2AB L323R1, Ca^{2+}

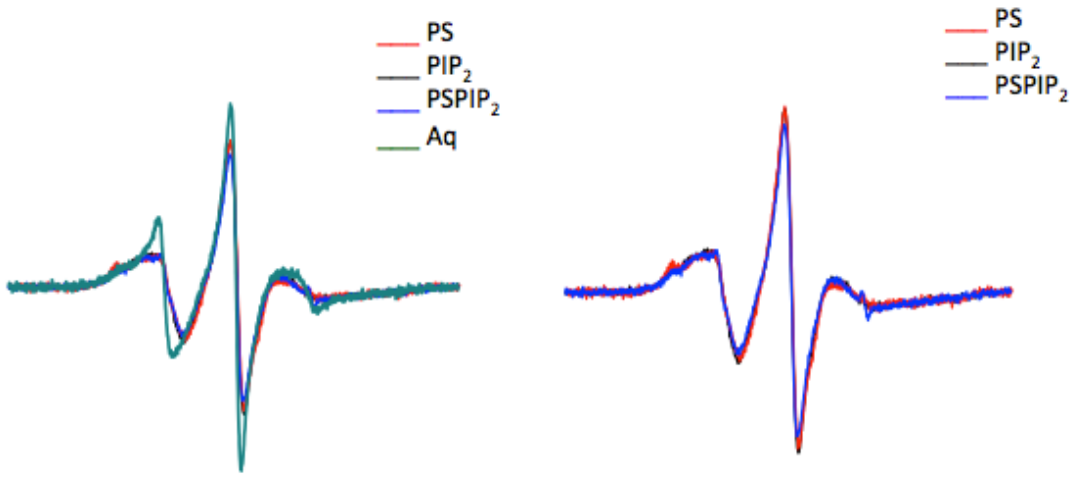

Figure 52. cw-EPR spectra for site L323R1 on C2AB in the different lipid compositions in Ca^{2+}. The aqueous form of the spin-labeled C2AB is in green while the line shapes due to PS, PIP_2 and $PSPIP_2$ are in red, black and blue respectively. On the right, the spectra in the different anionic lipids are identical suggesting little interaction with the membrane surface.

The site L323, which precedes the lysine clusters in the polybasic strand, was also chosen to be spin-labeled. However, the line shape of the site L323R1 changed little upon membrane association of the domain compared to the aqueous form (green traces in figure 52) and was not strongly affected by varying

the anionic lipid composition. The right spectra show identical line shapes in the three different lipid compositions that are color-coded as indicated. This indicates that site L323 in C2AB is not inserted into the membrane interface in the Ca^{2+} bound state of C2AB. It also means that the site 323 do not control the binding mode of C2AB.

C2AB T329R1, Ca^{2+}

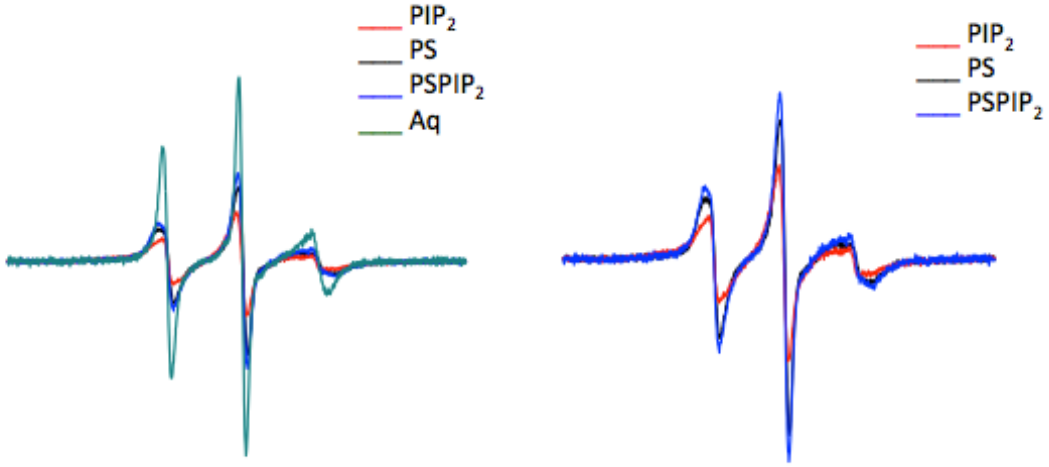

Figure 53. cw-EPR spectra for T329R1 on C2AB in the different lipid compositions with Ca^{2+}. The aqueous form of the R1 mutant is in green while the line shapes due to PS, PIP_2 and $PSPIP_2$ are in black, red and blue respectively. On the right, the PIP_2 spectrum (red) undergoes the most line shape broadening compared to the spectra due to PS. This suggests that the binding mode of this region near the polybasic strand is different and more specific to PIP_2 bilayers.

The site T329, which is positioned just after the lysine cluster in the polybasic strand, exhibited the most broadening in its EPR spectrum upon membrane association when these membranes contained 5% PIP_2 (red traces in figure 53). A less extensive line broadening was obtained when C2AB was bound to PS containing vesicles (black and blue traces). The green trace is the spectrum of

the mutant T329R1 in aqueous solution and it has a line shape characteristic of the R1 label attached to a flexible loop. In figure 53, on the right the spectra obtained in the three different lipid compositions are compared. The red trace is obtained in PIP_2 bilayers and indicates that this site near the polybasic strand exhibits the most contact with the membrane interface when compared to the 20% PS (black) and 10% PS, 2.5% PIP_2 (blue) samples. This was somewhat surprising for the case where both PS and PIP_2 (blue) were present. Though it was not expected that the presence of PS would decrease the lipid insertion of site 329R1 due to PIP_2, the addition of PS probably rearranged the binding loops such that the site T329R1 was outward facing with the binding loops more inserted.

In summary, the Ca^{2+} dependent membrane binding of C2AB spectra illustrated that the Ca^{2+} binding loops on C2A (M173R1) and C2B (V304R1) undergo the most line shape broadening when subjected to just PS containing LUVs. In contrast, the site T329R1 near the polybasic strand showed more broadening in PIP_2 containing LUVs. Though more sites need to be investigated, this preliminary data suggest that the membrane insertion of the Ca^{2+} binding loops is driven by the presence of PS, while insertion of the site near the polybasic region is driven by PIP_2.

C2AB K327R1

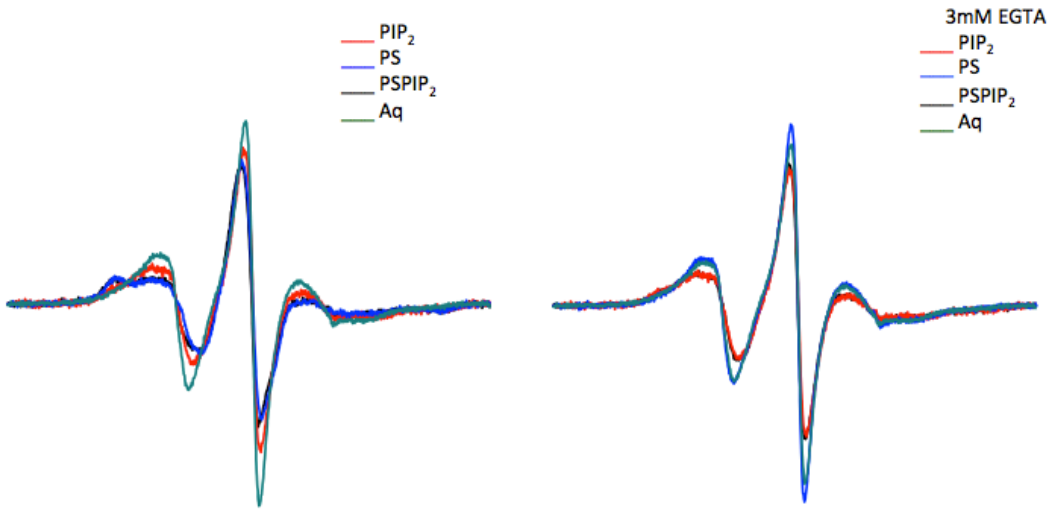

Figure 54. Site K327R1 on C2AB in different lipid compositions. The aqueous form of the R1 mutant is in green while the line shapes due to PS, PIP_2 and $PSPIP_2$ are in blue, red and black respectively. The left spectra are in the Ca^{2+} condition and show line shape broadening in the presence of membranes. While the right spectra, in the Ca^{2+}-free condition (EGTA), are generally mobile like the aqueous form but slightly broadened spectra of PIP_2 (red) and $PSPIP_2$ (black) conditions.

The left spectra in figure 54 are the cw-EPR spectra of site K327R1 in the presence of Ca^{2+}. Interestingly, the line shape of K327R1 in the presence of PS (blue traces) appeared to be the most immobile. The red trace of the spin-labeled protein in 5% PIP_2 vesicle also had a large line shape broadening however did not exhibit the residual hyperfine component in the low field resonance characteristic of an immobilized nitroxide. The spectra on the right are obtained from the K327R1 mutant when bound to different lipid compositions in the absence of Ca^{2+}. It appears that in this lower affinity Ca^{2+} independent binding mode of C2AB, the polybasic region exhibits stronger interactions to membranes

containing PIP_2 as seen by the broadened red line (5%PIP_2) and black line (10%PS, 2.5%PIP_2).

C2AB V304R1, Ca^{2+} -free

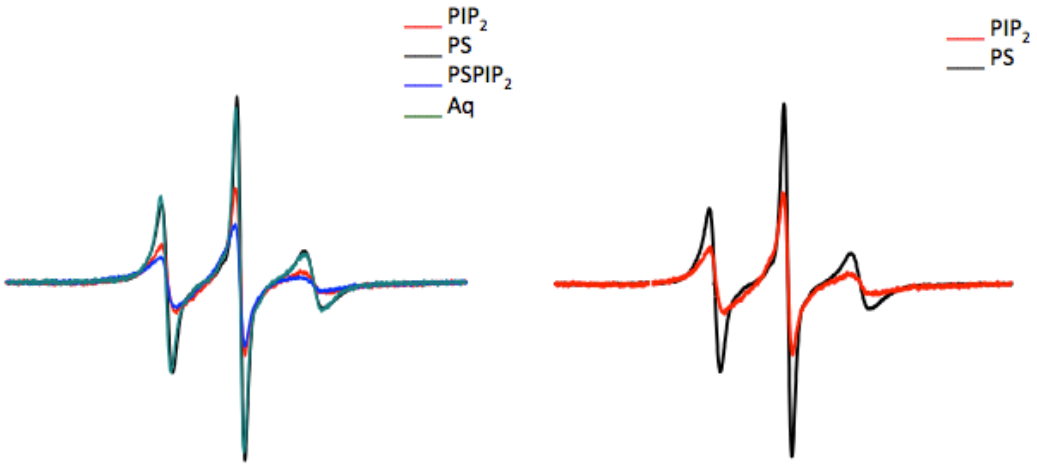

Figure 55. Ca^{2+} independent binding mode of C2AB 304R1. The aqueous form of the R1 mutant is in green while the line shapes due to PS, PIP_2 and $PSPIP_2$ are in black, red and blue respectively. The spectrum due to $PSPIP_2$ (blue) shows the most broadening, followed by PIP_2 (red).

The binding loop on C2B domain exhibited differing line shapes of the nitroxide R1 side-chain in the absence of Ca^{2+}. The mutant V304R1 in 20% PS vesicles, shown in the black trace in figure 55, has a mobile line shape identical to the aqueous state (green trace) of the mutant. The rotational motion of the nitroxide side-chain experiences some restriction due to membrane association in 5%PIP_2 vesicles (red trace). The most interaction with the membrane in the absence of Ca^{2+} is seen for $PSPIP_2$ vesicles (blue trace). This is the only time C2AB showed the most line shape broadening due to the $PSPIP_2$ lipid composition since this composition would seem to adopt the line shape of either the PS or PIP_2 bilayers

depending on where the spin-label was. Interesting, the Ca^{2+} loop on the C2B domain appears to associate with the membrane when PIP_2 is present in its Ca^{2+}- free form.

C2AB M173R1, Ca^{2+} - free

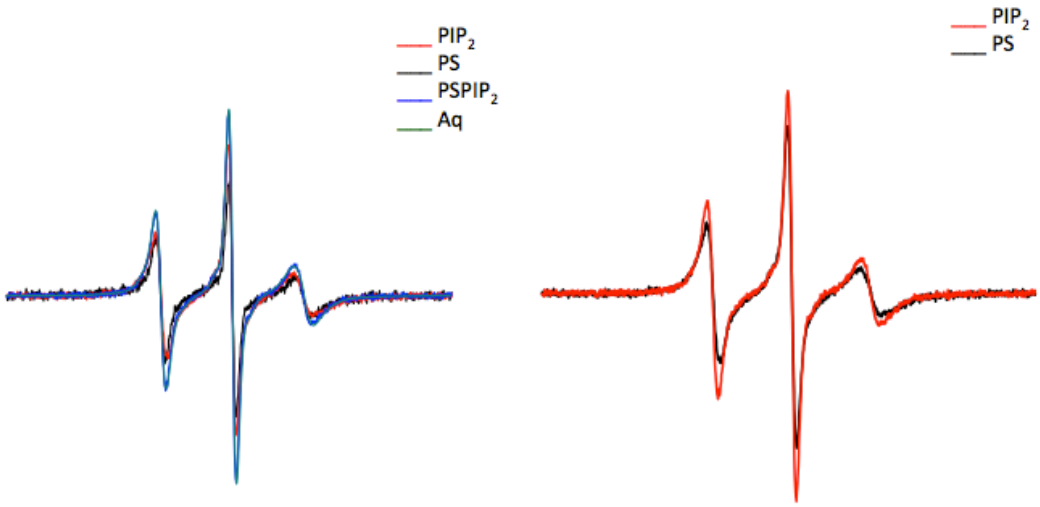

Figure 56. Ca^{2+} independent binding of 173R1 loops on C2AB. The aqueous form of the R1 mutant is in green while the line shapes due to PS, PIP_2 and $PSPIP_2$ are in black, red and blue respectively. The spectra in the different lipid compositions are generally mobile like in its aqueous form.

On the other hand, the Ca^{2+} loops on C2A domain did not experience a different mode of binding in the Ca^{2+} -free state when different lipid compositions were compared. The spectra on the left in figure 56 show that the spectrum from $PSPIP_2$ (black trace) has the largest decrease in peak-to-peak amplitude of the central line. On the right, the EPR line shapes due to PIP_2 (black trace) and PS (red trace) for membrane associated spin-labeled C2AB show little difference. Overall, the C2A domain Ca^{2+} binding loops do not seem to be immediately involved in the Ca^{2+} independent binding mode of Syt1.

C2AB T329R1, Ca^{2+} -free

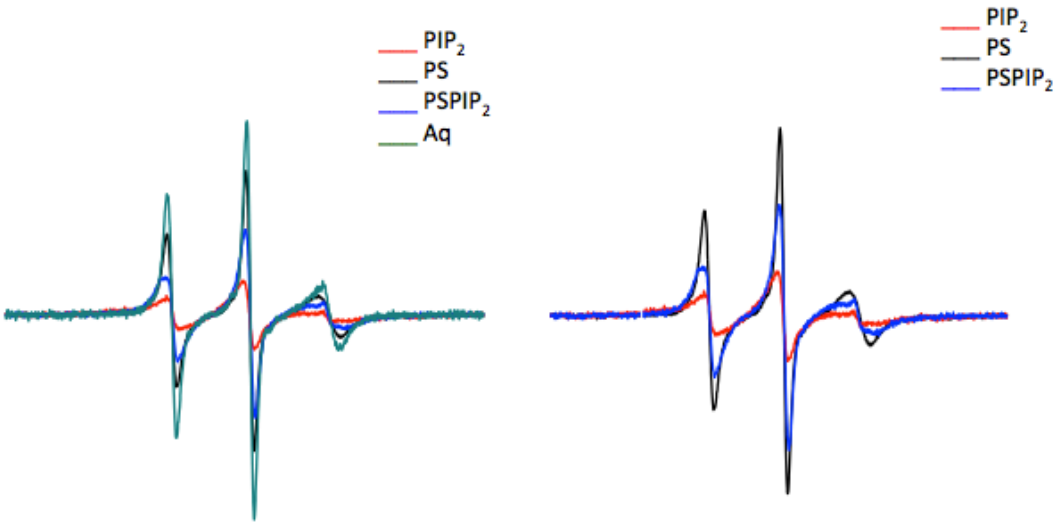

Figure 57. Ca^{2+} independent binding of 329R1 on C2AB. The aqueous form of the R1 mutant is in green while the line shapes due to PS, PIP_2 and $PSPIP_2$ are in black, red and blue respectively. On the right, the spectra from PIP_2 (red) is the most broadened indicating the most interaction with the membrane compared to the PS (black) and $PSPIP_2$ (blue).

The spectra on the left in figure 57 clearly show that the PIP_2 bound C2AB T329R1. The EPR line shape (red trace) displays the most significant broadening among the different lipid compositions. The red line shape has an immobile component in the low field resonance manifold indicating a tertiary contact of T329R1 in membrane vesicles containing only PIP_2. The least line shape broadening is seen for vesicles containing only PS (black trace). These results illustrate that the site near the polybasic region appears to be more specific to PIP_2 vesicles just as it is in its Ca^{2+} bound state.

C2AB L323R1, Ca^{2+} -free

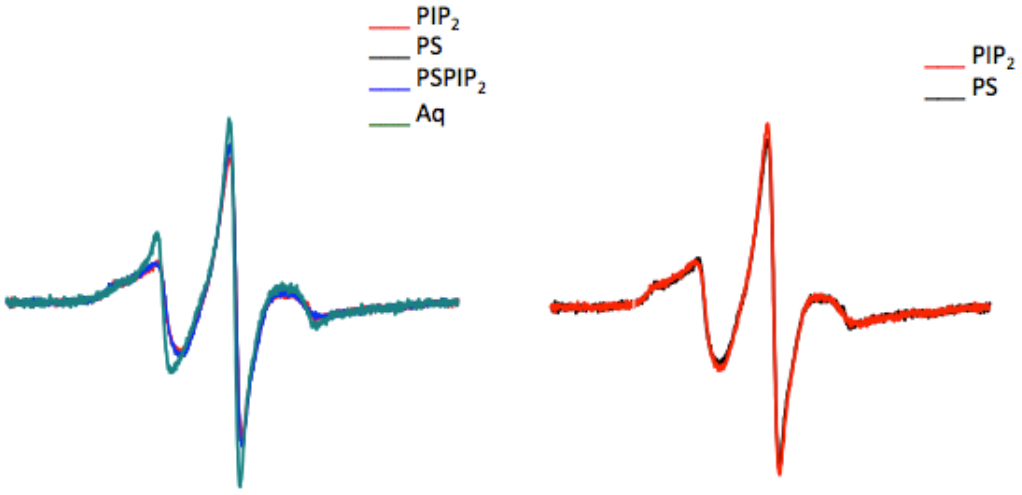

Figure 58. Ca^{2+} independent binding of L323R1 on C2AB. The aqueous form of the R1 mutant is in green while the line shapes due to PS, PIP_2 and $PSPIP_2$ are in black, red and blue respectively. The spectra in the different lipid compositions do not change from one another.

EPR spectra obtained for site L323R1 of C2AB when membrane bound in a Ca^{2+}- free form are shown in figure 58. These spectra do not exhibit any significant changes in line shape when different lipid compositions are compared. As seen on the right, the EPR line shapes due to PS (black trace) or PIP_2 (red trace) upon membrane association were virtually identical. This site lies above a cluster of lysine residues on the polybasic strand. This region did not seem to be interacting with the membrane interface in different acidic lipids in neither its Ca^{2+} bound nor Ca^{2+} free forms.

Power Saturation – bilayer depth data

The EPR power saturation technique is widely used to get depth information of spin-labeled sites on proteins when bound to a bilayer interface. This information is then used to generate docking orientation of the protein on the membrane interface. Utilizing the short T1 spin-lattice relaxation of a secondary paramagnetic reagent, like NiEDDA and O_2, the collision gradient of the nitroxide spin-label on the protein can be used to measure accessibility to the reagent and measure the distance of the spin-labeled site from the bilayer interface. The different spin-labeled sites on figure 49 were power saturated in the presence of 10mM NiEDDA and Air (20% oxygen). The samples are prepared in a TPX tube, which is semipermeable to gas since the sample needs to be purged in N_2 to get rid of O_2 while conducting the power saturation in the Ni^{2+} condition. Then the sample is purged with N_2 in the absence of Ni^{2+} to probe the relaxation rate in the absence of any paramagnetic reagent. For the O_2 condition, the experiment is conducted by softly blowing air into the TPX tube containing the sample. These three different conditions for each experiment will yield the $\Delta P_{1/2}$ for each reagent, Ni^{2+} or O_2.

$$\Delta P_{1/2}\,(\text{probe}) = P_{1/2}\,(\text{probe}) - P_{1/2}\,(N_2)$$

Equation 6.1

Since the experiment is done in 10mM NiEDDA, the $\Delta P_{1/2}$ is scaled to 20mM. The depth parameter, Φ, is derived from:

$$\Phi = \ln [\Delta P_{1/2} (O_2) / \Delta P_{1/2} (Ni^{2+})]$$

Equation 6.2

The depth parameter (Φ) can be either positive or negative, where the more positive values are representative of the spin-label in the membrane hydrocarbon. The distance (x) represents the distance from the lipid phosphates and is related to Φ by the following empirically derived hyperbolic tangent function[150]:

$$\Phi = 3.4 \tanh [(0.11 (x - 8.56)] + 1.1$$

Equation 6.3

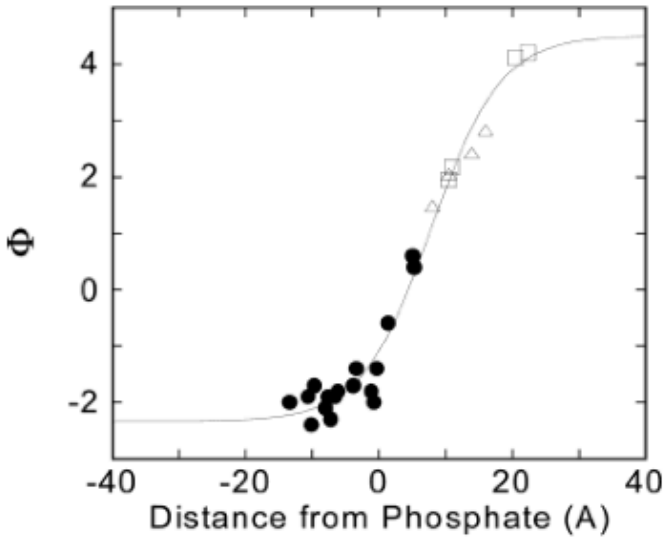

Figure 59. The empirically derived depth calibration curve that is fitted to equation 6.3 describes the dependence of Φ to the position from bilayer interface (Frazier 2003). The depth calibration curve was generated experimentally from doxyl-PC (Δ), Syt1 C2A (●) and bacteriorhodopsin (□) to yield the distance, x, from the lipid phosphates.

An empirical relationship between the depth parameter and the membrane depth was previously established by generating a calibration curve using doxyl-labeled phosphatidylcholine (PC), bacteriorhodhopsin (bR) and Syt1 C2A in PCPS (3:1)[136]. The calibration curve is shown in figure 59. The x value derived from the

empirical function in equation 6.3 gives the distance of the spin-label from the lipid phosphates (x =0). The negative x values represent the spin-label residing towards the aqueous phase while the positive distances represent the spin-label positioned in the bilayer hydrocarbon. Since the empirical hyperbolic tangent function was derived in bilayers containing 3:1 PCPS vesicles, the effect of PIP_2 in perturbing the Ni^{2+} or O_2 accessibility in the bilayer was also tested. Hence, control experiments were conducted with 5-doxyl PC incorporated into PCPS and $PCPIP_2$ membranes to confirm that the R1 side chains are undergoing similar accessibility to the relaxing agents, which would allow the use of the calibration curve, in figure 59, for my experimental conditions.

The $\Delta P_{1/2}$ (O_2) for 5-doxylPC (1 mol%) incorporated in 2% PIP_2 98% PC LUVs was acquired, along with the $\Delta P_{1/2}$ (O_2) for 5-doxyl PC in the standard 3:1 PCPS LUVs. It was found that my depth parameter (**Φ)** for 3:1 PCPS was 2.2 compared to 1.55 in April Frazier's lab notebook. This meant that I had a higher depth propensity with the same labeling method. My depth parameter for 98:2 $PCPIP_2$ was even more positive at 2.7. All experiments were repeated three times and the values were averaged. These differences in our **Φ** values could have been due to a number of variations to my experimental protocol. These variations could be due to the inaccurate concentration of our NiEDDA stock, or the time period in purging our sample with N_2, or the properties of the instrument resonator. Since I have been keeping the manner in how I conduct my experiment strictly consistent, the differences observed in my own experimental results are real. However, due to this discrepancy in the Φ values of the doxyl-PC

standards, scaling factors were multiplied into my x values that were derived from equation 6.3 for the respective different lipid compositions.

The membrane docking of C2AB is altered in the presence of PIP_2. The power saturation depth measurements of spin-labeled C2AB in different lipid compositions are given in table 4. The conditions were in 1mM Ca^{2+}, 100mM KCl (normal physiological conditions) and the lipid to protein mole ratio was at least 200:1.

Mutant	Lipid Composition (mol %)	Depth parameter (Φ)	Point to plane distance (Å)	Error (± Å)
M173R1	20% PS	+1.9	+7.7	0.33
	5% PIP_2	-1.1	+0.9	0.32
	10%PS 2.5%PIP_2	+1.6	+6.9	0.33
V304R1	20% PS	+1.5	+6.8	0.32
	5% PIP_2	-0.3	+2.7	0.23
	10%PS 2.5%PIP_2	+2.5	+8.8	0.64
K327R1	20% PS	-1.8	-2.3	0.69
	5% PIP_2	-2.3	-8.0	bulk aqueous
	10%PS 2.5%PIP_2	-1.8	-2.4	0.60
T329R1	20% PS	-2.0	-3.8	2.73
	5% PIP_2	-0.8	+1.6	0.31
	10%PS 2.5%PIP_2	-2.1	-4.9	3.90

Table 3. Ca^{2+} dependent membrane depth parameter and distance, x, of R1 side chain on C2AB. The distances, x, are from the R1 side chain to lipid phospholipid phosphates. Positive distances indicate the spin labels are inserting into the membrane. All experiments were repeated at least twice and the average of the Φ values were used to get the distance, x, using equation 6.3. The error (± Å) is the uncertainty in the distance (x) of the spin-label based on the uncertainty of the experimental depth parameter, Φ, value.

In its Ca^{2+}-bound state, the 1^{st} and 3^{rd} calcium binding loops of both C2A and

C2B penetrate the bilayer in the presence of 3:1 PC:PS, either with or without PIP_2 (see: Herrick et al[50], Kuo et al[76]). With PC:PIP_2 alone (no PS), the binding mode of C2AB is significantly different as shown in table 4 and figure 55. The Ca^{2+} binding loops of C2A and C2B (residues 173 and 304) fail to deeply penetrate to PC:PIP_2 bilayers and spin labels on these loops are shifted approximately 6 Å towards the aqueous phase. The C2B domain is also twisted to lift the polybasic face. This places residue 329 deeper into the interface, and twists residue 327 away from the interface.

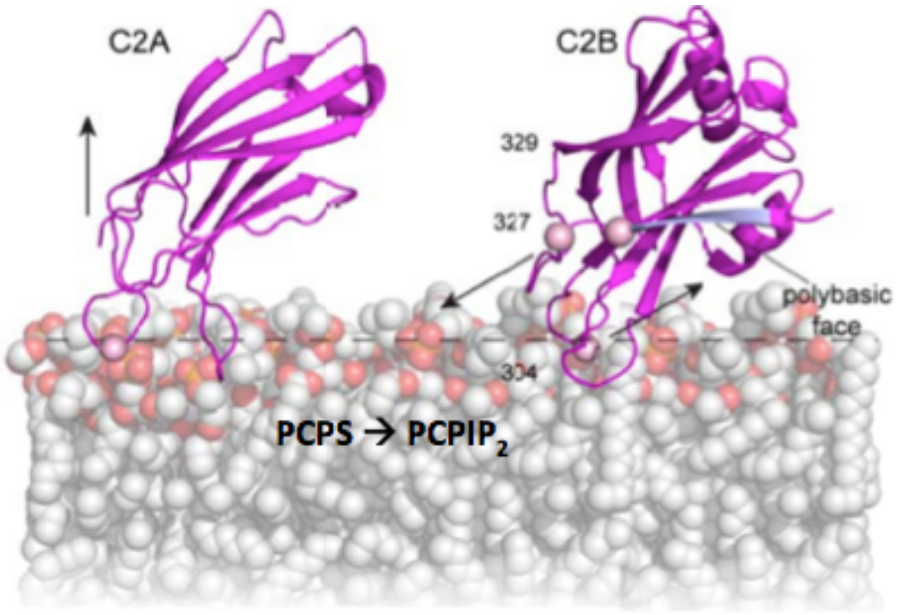

Figure 60. Docking orientations determined previously using EPR power saturation measurements for C2A and C2B bound to PC:PS bilayers. The movement of the docking orientation in the presence of PC:PIP_2 bilayers alone is indicated by the arrows.

The binding to PC bilayers, where PIP_2 is the only negatively charged lipid, results in a significantly different binding mode for syt1 C2AB, where neither C2A nor C2B penetrates as deeply into the interface, and the polybasic face of C2B is

lifted further into the aqueous phase. These power saturation results are consistent with EPR spectra from sites 173 (figure 51) and 304 (figure 50) which are shown above in solution or when bound to bilayers with PC:PS, PC:PS:PIP_2 or PC:PIP_2. The EPR spectra for 173 and 304 indicate that there is more motional averaging of the R1 label when C2AB is bound to PC:PIP_2 than when it is bound to bilayers containing some PS. This is consistent with power saturation data (Table 4), which indicate that the extent of membrane penetration is reduced by about 6 Å for PIP_2 alone.

PIP_2 modulates the Ca^{2+} independent binding mode of the C2B domain. Table 5 gives the bilayer depths of spin-labels on the C2AB when the domain is bound in the absence of Ca^{2+}. Here the positions of the spin labels were primarily in the aqueous phase or near the bilayer interface. The maximum positive distance was +2.7Å of site 329R1 in the PCPIP_2 bilayer followed by +2.3Å of site 304R1 in PCPSPIP_2 bilayers. First, this demonstrates that Ca^{2+} binding to C2AB domain is required for the domains to penetrate into the membrane hydrocarbon. Second, it shows that the Ca^{2+} independent binding of C2AB is weak and only interfacial to the membrane and requires the addition of PIP_2 to observe membrane contact of the C2B domain.

Mutant	Lipid Composition (mol %)	Depth parameter (Φ)	Point to plane Distance (Å)	Error (± Å)
M173R1	20% PS	-1.8	-2.0	1.0
	5% PIP_2	-2.1	-3.6	3.1
	10%PS 2.5%PIP_2	-1.5	-0.42	0.32
V304R1	20% PS	-1.8	-2.0	1.1
	5% PIP_2	-1.3	+0.32	0.43
	10%PS 2.5%PIP_2	-0.7	+2.3	0.38
K327R1	20% PS	-1.8	-2.2	0.58
	5% PIP_2	-2.1	-4.6	2.5
	10%PS 2.5%PIP_2	-1.6	-0.81	0.54
T329R1	20% PS	-1.9	-2.7	1.5
	5% PIP_2	-0.3	+2.7	0.28
	10%PS 2.5%PIP_2	-1.8	-2.4	1.3

Table 4. Ca^{2+} independent membrane depth parameter and distance, x, with error range of R1 side chain on C2AB. All experiments were repeated at least twice and the average of the Φ values were used to get the distance, x, using equation 6.3.

The Ca^{2+} independent mode of membrane binding by Syt1 is weaker than that in the presence of Ca^{2+}. As shown by my binding data on the energetics of membrane binding in the absence of Ca^{2+}, the binding free energy is reduced by 3 kcal/mol compared to the Ca^{2+} bound state. Unlike the cw-EPR spectra in figures 55 and 57, the distances from the depth parameter indicate that there is no insertion of C2AB occurring in this weaker Ca^{2+} independent binding mode.

This secondary binding mode of Syt1 is postulated to be driven by the electrostatic interaction primarily between the polybasic strand and anionic phospholipids present in the synaptic vesicle or plasma membrane[154, 137, 50]. The electrostatic switch mechanism of C2 domains has been proposed by different groups and with a recent model by Kuo et al[150]. Surprisingly, the binding loop 1, site 304R1, in C2B still showed membrane association especially in the presence of both PS and PIP_2.

The cooperative role of PS and PIP_2 even in the Ca^{2+} free state was seen in my binding data in chapter 5, and this interaction of the C2B loops may be a direct result of the cooperativity between the two negatively charged lipids. It probably results in how the domain is lying on the membrane surface comprised of $PCPSPIP_2$ instead of PCPS, where no membrane association was seen from the cw-EPR spectra (figure 53). The site 329R1 was positioned closest to the bilayer in $PCPIP_2$ without PS present, followed by $PCPSPIP_2$ and then PCPS. In both its Ca^{2+} activated and inactivated form, the site 329R1 had the most interfacial contact with only PIP_2 containing bilayers ($PCPIP_2$). The orientation of the domain is altered once PS is incorporated into the vesicles.

Discussion and future extensions

As illustrated by the cw-EPR spectra and power saturation data on various spin-labeled sites on C2AB, the Ca^{2+} dependent molecular mechanism of membrane binding of C2AB is considerably different between PS and PIP_2. The main conclusion from bilayers containing only PIP_2 as the negatively charged lipid is that there is no membrane penetration of the Ca^{2+} binding loops (in C2A and C2B), while the addition of PS into PIP_2 bilayers is able to recover the insertion of these loops. It is possible that the binding of C2AB due to PIP_2 is largely dependent in its interaction with the polybasic face and hence does not or cannot really facilitate the insertion of the binding loops. Though electrostatic repulsive forces come into play for charged protein-membrane interactions, the hydrophobic residues in the binding loops drive the membrane penetration of the Ca^{2+} binding loops in the bilayer [41, 160]. This is known to contribute favorably to the binding energy. EPR studies on cPLA2 and Syt1 show that, the Ca^{2+} binding loops 1 and 3 inserts into the membrane hydrocarbon[128, 136, 161].

It was found in EPR generated docking models of the PKCα in PIP_2 containing vesicles that the polybasic strand was pushed away from the membrane interface due to the steric hindrance of bulky headgroup of PIP_2[85]. The electrostatic contribution due to the large local charge density on the PIP_2 bound membrane may cause a higher unfavorable repulsion force due to desolvation effects.

The probing of more sites on other binding loops like loop 3 in both C2A and C2B would provide a complete picture of whether the loop penetration is impossible with only PIP_2 as the anionic lipid. More experiments should be done to address if PS is in fact modulating its binding mode and is required for the Ca^{2+}-bound loops to penetrate into PIP_2 containing vesicles. The use of other monovalent acidic lipids like PG, PA or PI instead of PS could be done. Increasing the salt concentration to test the electrostatic contribution of the coordination with PS could also be investigated.

7) Significance and Future Directions

The electrostatic interactions of proteins with membranes may be crucial for biological activity, and the energetic contributions made by electrostatics can be quite high. The sequence, structural and functional homology of the synaptotagmin family with other C2 domain containing proteins is strong. They have diverse roles in which they are involved in cell signaling to membrane fusion in the secretory pathway. It has been proposed that one of the important functions of Synaptotagmin 1 is to bind to Ca^{2+} and phospholipids in an electrostatic manner to trigger the membrane fusion event and exocytosis. The very complex set up in the neuronal exocytosis event is preceded by the instantaneous synchronous release upon transduction of the Ca^{2+} signal in the neuron. How Ca^{2+} and the tight coupling of Syt1 with the target plasma membrane triggers fusion is of great interest, and knowledge of the energetic contributions of Syt1 -membrane binding would help separate the different models for Syt1 function in the membrane fusion event.

One model for synaptotagmin function involves a direct interaction with the SNAREs in the presence of Ca^{2+}, which leads to the zippering of the SNAREs to drive complete fusion of primed (ready-to-go) vesicles with the plasma membrane [72, 71]. The other is its inherent membrane binding function that allows it to penetrate into membrane bilayers in the presence of Ca^{2+} [137, 154, 161, 162]. From our data, the insertion of the Ca^{2+} loops is specific to PS containing membranes and work done by Lai et al showed that C2AB can cluster PS, which

might induce the curvature stress required for the formation of hemi-fusion state between opposing bilayers[162]. The perturbation of the lipid bilayer due to protein insertion is thought to physically deform the lipid leaflet and reduce the energy necessary to merge opposing bilayers[130]. The synaptotagmin C2B domain also possesses a unique trait found in other C2 domains like PKCα, which is to recognize and strongly bind to target membranes containing PIP_2. The combination of these important characteristics of Syt1 indicates that they may be of central importance to membrane binding that triggers the fusion event.

By studying the role of the different functional groups in the C2AB domain of Syt1 play in membrane binding, we have provided evidence for the role that membrane association plays in fusion. The binding data for C2AB to membranes demonstrates specificity and preferences towards different negatively charged lipids in the cell membrane. Each lysine in the polybasic strand contributes 0.9 kcal/mol to the binding in $PCPIP_2$ vesicles while the addition of PS to the $PCPIP_2$ vesicles reduced the binding energy to 0.5 kcal/mol per lysine residue. This implies that the polybasic strand comprising of six basic residues could contribute up to 3 kcal/mol to the binding energy of Syt1 to the plasma membrane. The energy required to form the hemi-fused state between the synaptic vesicle and plasma membrane is approximately 45 k_BT or 27 kcal/mol [16,163]. The Ca^{2+} induced membrane binding energy was found to be more than 3 kcal/mol and this additional energy provided by the Ca^{2+} influx could be sufficient to trigger the fusion of the primed (ready-to-go) vesicles. The two

key arginines on the other hand did not appear to contribute in the membrane binding affinity of C2AB in any lipid composition. The power saturation data on the arginine apex indicated peripheral association of the two arginines with the lipid phosphates, which was lost upon neutralization of the basic residues. Maybe its role is to associate peripherally to the ionic double layer but not penetrate, mainly helping in the bridging of opposing bilayers or correctly orienting synaptotagmin. However, it is not clear why this does not contribute to the binding energetics. Conceivably, the differences could be due to the different conditions and lipid compositions used in the two sets of experiments.

The cooperative role of PS and PIP_2 was seen in the substantially higher binding affinity of C2AB in both the Ca^{2+} dependent and independent binding mode. This cooperativity did not contribute to the binding depth in membranes containing both PS and PIP_2; however, the Ca^{2+} binding loops and the polybasic region seem to be dominated either by PS or PIP_2, respectively. In the case of sites near the polybasic region, the EPR line shapes are unique when PIP_2 is present, while sites in the loops give unique signatures in PS. This was also evident in the power saturation depth data, which showed that the insertion of the Ca^{2+} binding loops required PS. The site near the polybasic region on the other hand, was closest only in PIP_2 containing bilayers.

The NMR data reflected the interactions made by C2B with charged polyphosphate anions under physiological conditions. Overall it was determined

that the interactions with PIP_2 and ATP are largely electrostatic in nature where the positively charged regions in C2B had the most chemical shift perturbations. Together with findings from Park et al., it is likely that PIP_2 would have a higher affinity than ATP in the cell as indicated by the IP3 affinities from the NMR titration and the fact that PIP_2 would be at a very high local concentration at the focal site of fusion[91]. By interfering with the electrostatic binding of C2AB to PCPS membranes, ATP could modulate C2AB function[91]. The interactions that have been observed by NMR and EPR between synaptotagmin and the SNAREs appear to occur through the polybasic face of C2B[72, 74]. As a result ATP, which interacts with the polybasic face, is also expected to interfere with the synaptotagmin – SNARE interaction and at normal cellular levels of ATP-$Mg^{2+,}$ Thus, the synaptotagmin 1 – SNARE interaction that has been examined in vitro, may not be relevant within the cell.

Both PIP_2 and PS are known to be important for neuronal exocytosis and the findings presented here on the role of the charged residues in Syt1 helps explain the importance of these residues as seen in both in-vivo and in-vitro systems for membrane fusion. The exact mechanism by which synaptotagmin 1 function is not entirely clear, but the data obtained here suggest that several models deserved consideration. We do not believe that direct synaptotagmin 1/SNARE interactions are important in triggering fusion, but it is possible that synaptotagmin may alter SNARE assembly in an indirect manner. As mentioned above, the C2AB domains have been observed to demix (sequester) PS upon

membrane binding[162]. This may either induce membrane curvature strain[162, 130] , or it may alter the membrane interactions of other proteins involved in fusion, such as the SNAREs. If the SNAREs exist in a partially assembled state prior to fusion, synaptotagmin 1 may act to drive membranes closer together, thereby triggering SNARE assembly and driving fusion. In this mechanism, ATP binding to synaptotagmin and the presence of PIP_2 in the target cytoplasmic membrane may function to direct synaptotagmin into a *trans*-binding mode so that synaptotagmin is able to bridge bilayers and close the distance between the vesicle and cytoplasmic membranes.

Appendix

1) The Ca^{2+} independent binding of long C2AB construct (96-421)

Introduction

Much of the work that has been carried out previously on a soluble fragment of C2AB utilized a construct (96-421) that contained an additional N-terminal fragment from the full-length protein that preceded the C2A and C2B domains (references). We compared the binding affinity of a shorter construct (136-421), which contains just the C2A and C2B domains, with the longer fragment. The two give comparable affinities when the Ca^{2+}-dependent binding to membranes of POPC and POPS is examined; however, when the Ca^{2+}-independent binding of this fragment is examined to POPC and POPS bilayers, the binding isotherm for this fragment does not behave properly. This contrasts with the shorter fragment lacking the N-terminal piece, which yields a well-behaved binding isotherm that can be used to accurately access the calcium-independent binding of C2AB. The longer fragment (96-421) contains a number of charged and acidic residues at the N-terminus and it is likely that this fragment interferes with the membrane binding to POPC:POPS in the absence of calcium.

In quantitating protein affinity to membranes, it is important that binding has reached equilibrium to truly characterize the binding behavior of the protein in the amount of lipid accessible to it. When the equilibrium condition is satisfied and enough lipid is titrated to saturate the complete binding of the protein, the binding

curve of the protein should reach a plateau. The binding curve, which should reach unity for the fraction of protein bound, is then fitted to the equilibrium binding equation 2.2 to yield a partition coefficient, K (M^{-1}), which gives the membrane binding affinity of the protein. The partition coefficient, K, corresponds to the accessible lipid concentration where 50% of the protein is bound. This binding affinity is useful in calculating the free energy of binding between the different conditions investigated.

If the protein is behaving correctly, the binding curve should be hyperbolic in nature and plateau in saturating conditions. However, when the Ca^{2+} independent binding was performed, the binding curve was not normal and did not have a saturating curve close to unity. Hence, it could not be used to fit the binding equation 2.2 and yield a partition coefficient, K, value to quantitate the binding affinity.

Result

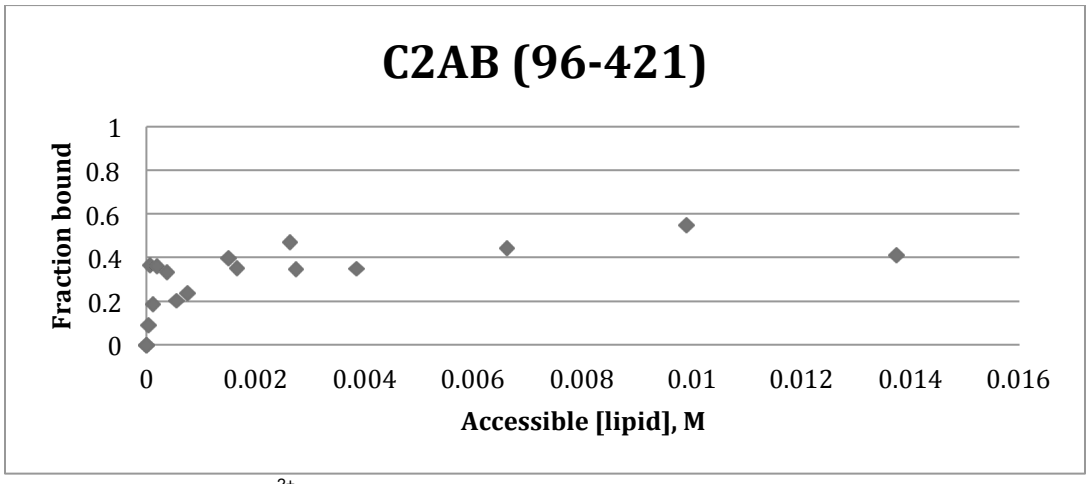

Figure 61. C2AB WT, Ca $^{2+}$ free membrane binding in 25%PS LUVs. Experimental data are a combination of two data sets.

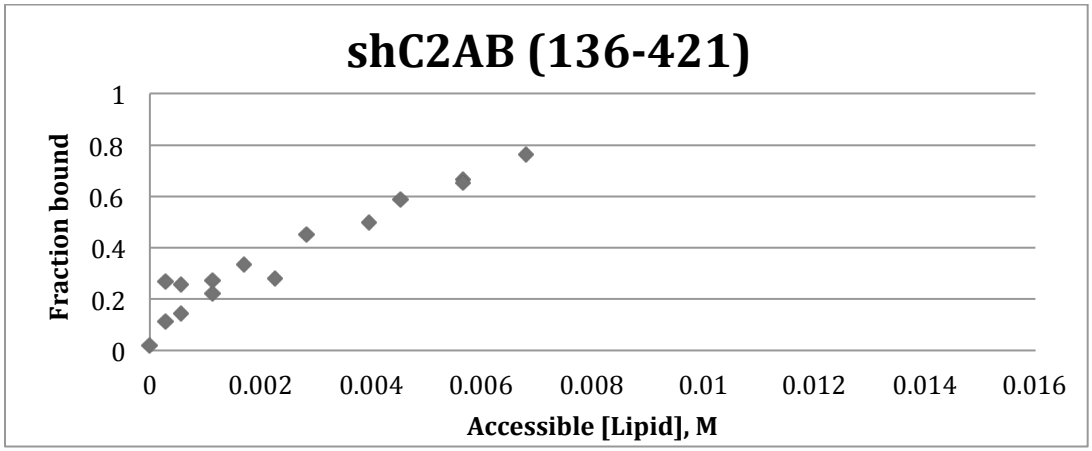

Figure 62. Short C2AB (shC2AB) WT, Ca^{2+} free membrane binding in 25%PS LUVs. Experimental data are a combination of two data sets.

The Ca^{2+} independent binding of C2AB is weak and hence requires a much higher lipid concentration to achieve binding. Several changes were made to purify the protein and get it completely clean from any residual nucleic acid contamination. The protein was expressed in cells grown in minimal media, which has been known to yield much cleaner protein fractions after ion exchange column. The protein was given a second run in the ion exchange column to double purify it. The silver nitrate experiment, to detect any trace nucleic acid contamination, was also conducted but yielded a negative result for nucleic acid. The protein and sucrose-loaded large unilamellar vesicles (LUVs) was also incubated for 6 hours before ultracentrifugation to let the membrane binding reach an equilibrium if the binding kinetics were slow. However under all those different preparations, the membrane binding of C2AB under very high lipid concentration was still not exhibiting a saturating binding behavior. Also, the mole percentage of the negatively charged phosphatidylserine was increased from 25% to 35% in order to observe a stronger binding effect but it failed to yield a

complete binding of the protein to membranes. The binding curve is in figure 30, where the fraction of protein bound is plotted against the accessible lipid concentration.

The shorter C2AB construct from residues 136-421 which does not have the N-terminal linker before C2A domain was used. It showed signs of an increasing binding isotherm though it was not perfect, as seen in figure 62.

Next, the possible interference from residual lipid in the supernatant causing light scattering and hence, signal noise was investigated. The total volume of buffer in each tube was increased from 500uL to 700- 800uL. Since 400uL is extracted from the supernatant after centrifugation, extra care can be taken to remove the top-most layer of the supernatant without disturbing the lipid pellet. This approach seemed to yield a much-expected hyperbolic binding isotherm in the short C2AB construct, figure 63.

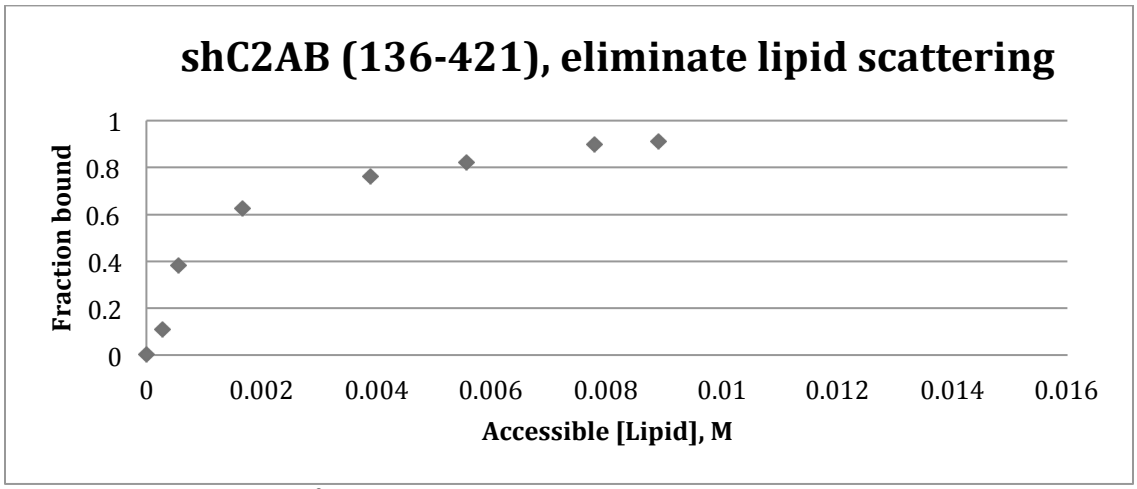

Figure 63. shC2AB WT in Ca^{2+} free binding with no lipid scattering

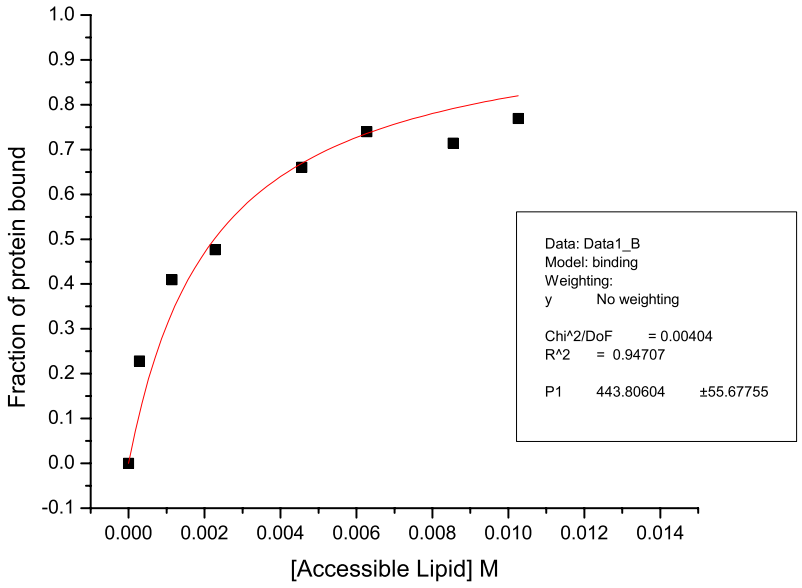

Figure 64. The Ca^{2+} independent binding of the short C2AB construct fitted to the binding equation in 2.2. A K value (P1 in graph) of 444 ± 56 M^{-1} was given by the fit.

This curve was fitted to the equilibrium binding equation (Eqn 2.2) and a binding constant, K, of 444 ± 56 M^{-1} was derived.

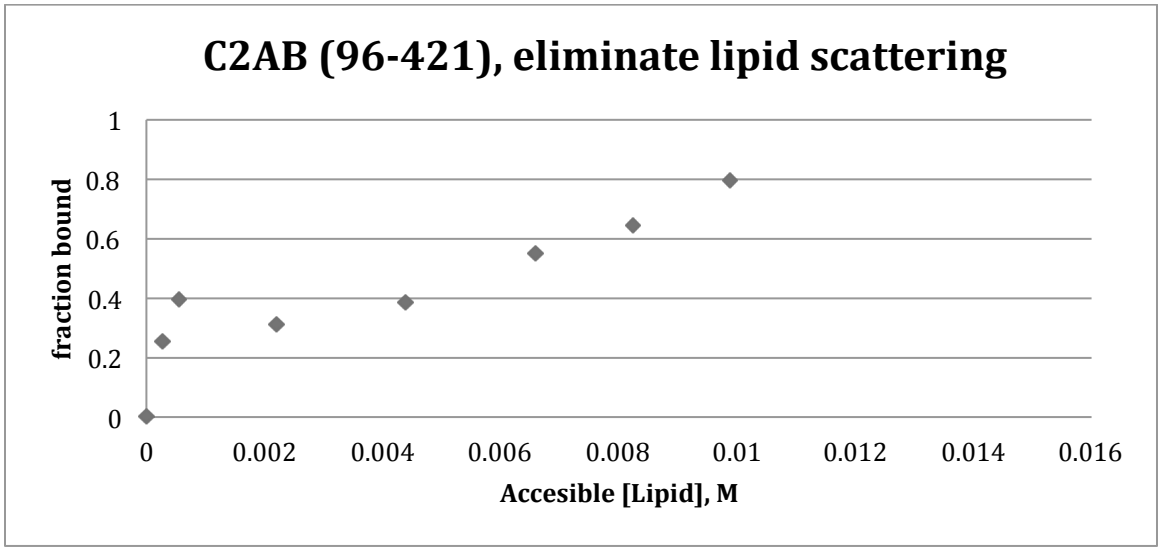

Figure 65. The longer C2AB construct did not seem to show the hyperbolic binding curve

However, repeating the experiment with the new approach to limit light scattering effect on samples did not work for the longer C2AB construct 96-421. It did not exhibit saturation after membrane binding in equilibrium conditions and at concentration that was sufficient for the short construct, 136-421. It also had a curve that was not increasing in a normal manner. Hence, the binding curve could not be fitted to the equilibrium binding equation and the binding affinity for the 96-421 C2AB could not be quantitated.

Discussion

The linker region from 96-136 that is present in the long C2AB construct contains a number of residues that are charged. There are 13 acidic residues (in bold) and 8 basic residues.

[96] KGKEKGGKNA INMKDVKDLG KTMKDQALKD DDAETGLTDG EEKEEP [136]

It seems that this interferes with the membrane binding property of the soluble C2AB domain in its weaker binding mode without Ca^{2+}. Auto-inhibition of the protein domain could be taking place; where a segment of the protein binds to itself and cause the inhibition of its function.

Seven et al reported that there are two different constructs of Syt1 C2AB that can behave differently in its membrane bridging function if one of them is not purified properly[158]. The C2AB fragment (residues 140-421) is highly soluble whereas the longer fragment of C2AB (lnC2AB) containing the N-terminal linker sequence (residues 95-421) tends to oligomerize if it is not completely free of nucleic acid

contamination [158]. Hui et al and Connell et al through cryo-EM showed that the distance separating the syt1 bridged vesicles is ~9nm which suggest Syt1 oligomerizes to facilitate cross-linking of the membrane bilayers[142, 164]. This model is in contrast to a direct-bridging model with the bottom of C2B (where the two highly conserved arginine residues are) also interacts with the membranes [158]. It was shown through NMR data that the longer C2AB fragment is only completely free of nucleic acid contaminants through their rigorous purification protocol of several high salt washes, benzonase treatment and gel-filtration step. The long fragment lnC2AB when purified in this manner bridges bilayer with a separation of ~4nm between vesicles which was consistent with their direct-bridging model[158]. It seems that the long construct of C2AB containing the linker sequence before C2A domain can interfere with the biochemical property of C2AB contributing to its unpredictable membrane binding function.

While it is hard to decipher what is going on exactly and how the acidic linker could be affecting the weak binding mode of C2AB, it could be helpful in answering any experimental anomalies when using this piece of C2AB in the field.

ii) Electrostatic contribution to C2AB membrane binding

From chapter 5, the requirement for a specific coordination between the Ca^{2+} bound synaptotagmin and the negatively charged PS lipid head group was further investigated. The charge density on membrane surface was neutralized with DDAB to understand the electrostatic contribution of C2AB to its membrane binding role.

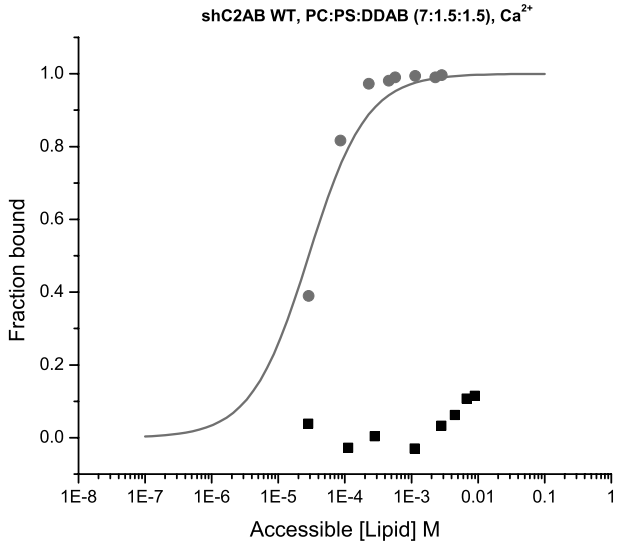

Figure 66.Neutralizing the negative charge on PCPS vesicles by adding equivalent DDAB (positive charged lipid) abolishes membrane binding. Binding of wild-type C2AB is observed with normal PCPS (85:15) vesicles (●) in 1mM Ca^{2+}. Neutralizing the charge on PS by adding DDAB in PCPS vesicles (■) do not exhibit binding of wild-type C2AB in similar buffer conditions.

This was done by utilizing a cationic lipid dimethyldioctadecylammonium bromide (DDAB) to neutralize the negative charge from PS on the membrane.

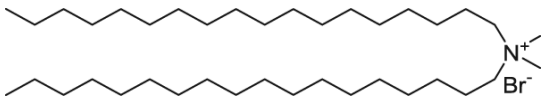

Figure 67. Chemical structure of dimethyldioctadecylammonium bromide (DDAB)

Sucrose loaded LUVs composed of 70 mol% PC, 15 mol% PS and 15 mol% DDAB were made so that the overall net charge on the membrane would be neutral. Unlike the control experiment with PCPS (85:15) vesicles, no binding of wild-type C2AB in the PC:PS:DDAB (70:15:15) vesicles in 1mM Ca^{2+} was observed. Similarly, the binding of just the C2A domain also exhibited similar phenotype in DDAB neutralized vesicles (unpublished data of Weiwei Kuo). Experiments done using an alternative single negatively charged lipid POPG instead of POPS showed binding of C2AB decreased by about half. Binding to vesicles containing just 2% PIP_2, show enhanced binding in both the Ca^{2+} dependent and independent binding mode of C2AB, figures 40 and 41. While comparable or an enhanced binding seem to be possible in different anionic lipids, it is not clear if the C2 domains adopt similar binding orientation with the different anionic lipids.

The effect of substituting Cd^{2+} for Ca^{2+} binding was also investigated to address the requirement of a specific coordination between the PS head group with the protein bound divalent ion[147].

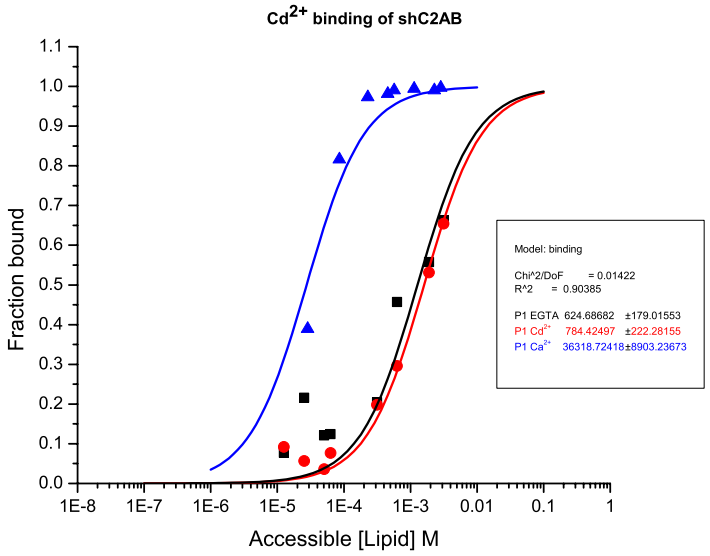

Figure 68. Cadmium does not substitute for Calcium-dependent membrane binding in C2AB

Cd^{2+} was found to be able to substitute for Ca^{2+} in the binding to the C2 domain in PKCα but not facilitate the membrane binding of C2α unlike other divalent metal ions such as Pb^{2+} and Sr^{2+}. The possibility of Syt1 C2AB adopting the same property was investigated. It was found that 1mM Cd^{2+} exhibited similar weak binding of wild-type C2AB in the absence of any divalent cations. Hence this suggested that Cd^{2+} does not substitute for the membrane binding capability of Syt1 in Ca^{2+}. In order to eliminate the weak binding of C2B domain, the experiment was repeated using the shC2A construct. It was found that the presence of Cd^{2+} exhibited a complete loss of membrane binding (unpublished data).

REFERENCES

1. Pang, Z. P. & Sudhof, T. C. (2010). Cell biology of Ca2+-triggered exocytosis. *Curr Opin Cell Biol* **22**, 496-505.

2. Llinás R, S. I., Walton K. (1981). Relationship between presynaptic calcium current and postsynaptic potential in squid giant synapse. *Biophys J* **33**, 323-51.

3. Grupa Robocza Europejskiego Towarzystwa Kardiologicznego ds. stymulacji serca i resynchronizacji we, w., Europejskim Towarzystwem Rytmu, S., Vardas, P. E., Auricchio, A., Blanc, J. J., Daubert, J. C., Drexler, H., Ector, H., Gasparini, M., Linde, C., Morgado, F. B., Oto, A., Sutton, R., Trusz-Gluza, M., Vahanian, A., Camm, J., De Caterina, R., Dean, V., Dickstein, K., Funck-Brentano, C., Filippatos, G., Hellemans, I., Kristensen, S. D., McGregor, K., Sechtem, U., Silber, S., Tendera, M., Widimsky, P., Zamorano, J. L., Priori, S. G., Blomstrom-Lundqvist, C., Brignole, M., Terradellas, J. B., Camm, J., Castellano, P., Cleland, J., Farre, J., Fromer, M., Le Heuzey, J. Y., Lip, G. Y., Merino, J. L., Montenero, A. S., Ritter, P., Schlij, M. J., Stellbrink, C. & European Cardiac, S. (2007). [Guidelines in cardiac pacing and resynchronization therapy]. *Kardiol Pol* **65**, 1449-87; discussion 1488-9.

4. Brose, N. (2014). All roads lead to neuroscience: the 2013 Nobel Prize in Physiology or Medicine. *Neuron* **81**, 723-7.

5. Ray, K. (2014). From fission to fusion: A perspective on the research that won the Nobel Prize in Physiology or Medicine, 2013. *Journal of Biosciences* **39**, 3-11.

6. Rothman, J. E. (1994). Mechanisms of intracellular protein transport. *Nature* **372**, 55-63.

7. Acuna, C., Guo, Q., Burre, J., Sharma, M., Sun, J. & Sudhof, T. C. (2014). Microsecond dissection of neurotransmitter release: SNARE-complex assembly dictates speed and Ca(2)(+) sensitivity. *Neuron* **82**, 1088-100.

8. Fatt, P. & Katz, B. (1951). An analysis of the end-plate potential recorded with an intracellular electrode. *J Physiol* **115**, 320-70.

9. Katz, B. (1950). Action potentials from a sensory nerve ending. *J Physiol* **111**, 248-60.

10. Katz, B. & Miledi, R. (1967). Ionic requirements of synaptic transmitter release. *Nature* **215**, 651.

11. Carr, C. M. & Munson, M. (2007). Tag team action at the synapse. *EMBO Rep* **8**, 834-8.

12. Chapman, E. R. (2002). Synaptotagmin: a Ca(2+) sensor that triggers exocytosis? *Nat Rev Mol Cell Biol* **3**, 498-508.

13. Novick, P., Field, C. & Schekman, R. (1980). Identification of 23 complementation groups required for post-translational events in the yeast secretory pathway. *Cell* **21**, 205-15.

14. Dianna Murray, A. A., Barry Honig, and Stuart McLaughlin. (2002). The role of electrostatic and nonpolar interactions in the association of peripheral proteins with membranes. In *Current Topics in Membranes* Vol. 52, pp. 277-300.

15. Martens, S. & McMahon, H. T. (2008). Mechanisms of membrane fusion: disparate players and common principles. *Nat Rev Mol Cell Biol* **9**, 543-56.

16. Cohen, F. S. & Melikyan, G. B. (2004). The energetics of membrane fusion from binding, through hemifusion, pore formation, and pore enlargement. *J Membr Biol* **199**, 1-14.

17. Li, F., Pincet, F., Perez, E., Eng, W. S., Melia, T. J., Rothman, J. E. & Tareste, D. (2007). Energetics and dynamics of SNAREpin folding across lipid bilayers. *Nat Struct Mol Biol* **14**, 890-6.

18. Martens, S., Kozlov, M. M. & McMahon, H. T. (2007). How synaptotagmin promotes membrane fusion. *Science* **316**, 1205-8.

19. Schekman, R. & Novick, P. (2004). 23 genes, 23 years later. *Cell* **116**, S13-5, 1 p following S19.

20. Brunger, A. T. (2005). Structure and function of SNARE and SNARE-interacting proteins. *Q Rev Biophys* **38**, 1-47.

21. Huber, K. M., Roder, J. C. & Bear, M. F. (2001). Chemical induction of mGluR5- and protein synthesis--dependent long-term depression in hippocampal area CA1. *J Neurophysiol* **86**, 321-5.

22. Li, C., Ullrich, B., Zhang, J. Z., Anderson, R. G., Brose, N. & Sudhof, T. C. (1995). Ca(2+)-dependent and -independent activities of neural and non-neural synaptotagmins. *Nature* **375**, 594-9.

23. Chapman, E. R. (2008). How does synaptotagmin trigger neurotransmitter release? *Annu Rev Biochem* **77**, 615-41.

24. Sollner, T., Whiteheart, S. W., Brunner, M., Erdjument-Bromage, H., Geromanos, S., Tempst, P. & Rothman, J. E. (1993). SNAP receptors implicated in vesicle targeting and fusion. *Nature* **362**, 318-24.

25. Schiavo, G., Benfenati, F., Poulain, B., Rossetto, O., Polverino de Laureto, P., DasGupta, B. R. & Montecucco, C. (1992). Tetanus and botulinum-B neurotoxins block neurotransmitter release by proteolytic cleavage of synaptobrevin. *Nature* **359**, 832-5.

26. Sudhof, T. C. & Rothman, J. E. (2009). Membrane fusion: grappling with SNARE and SM proteins. *Science* **323**, 474-7.

27. Daniel, S., Noda, M., Straub, S. G. & Sharp, G. W. (1999). Identification of the docked granule pool responsible for the first phase of glucose-stimulated insulin secretion. *Diabetes* **48**, 1686-90.

28. Michael, D. J., Ritzel, R. A., Haataja, L. & Chow, R. H. (2006). Pancreatic beta-cells secrete insulin in fast- and slow-release forms. *Diabetes* **55**, 600-7.

29. Jahn, R. & Fasshauer, D. (2012). Molecular machines governing exocytosis of synaptic vesicles. *Nature* **490**, 201-7.

30. McMahon, H. T. & Sudhof, T. C. (1995). Synaptic core complex of synaptobrevin, syntaxin, and SNAP25 forms high affinity alpha-SNAP binding site. *J Biol Chem* **270**, 2213-7.

31. Washbourne, P., Thompson, P. M., Carta, M., Costa, E. T., Mathews, J. R., Lopez-Bendito, G., Molnar, Z., Becher, M. W., Valenzuela, C. F., Partridge, L. D. & Wilson, M. C. (2002). Genetic ablation of the t-SNARE SNAP-25 distinguishes mechanisms of neuroexocytosis. *Nat Neurosci* **5**, 19-26.

32. Sutton, R. B., Fasshauer, D., Jahn, R. & Brunger, A. T. (1998). Crystal structure of a SNARE complex involved in synaptic exocytosis at 2.4 A resolution. *Nature* **395**, 347-53.

33. Antonin, W., Fasshauer, D., Becker, S., Jahn, R. & Schneider, T. R. (2002). Crystal structure of the endosomal SNARE complex reveals common structural principles of all SNAREs. *Nat Struct Biol* **9**, 107-11.

34. Jahn, R. & Scheller, R. H. (2006). SNAREs--engines for membrane fusion. *Nat Rev Mol Cell Biol* **7**, 631-43.

35. Gao, Y., Zorman, S., Gundersen, G., Xi, Z., Ma, L., Sirinakis, G., Rothman, J. E. & Zhang, Y. (2012). Single reconstituted neuronal SNARE complexes zipper in three distinct stages. *Science* **337**, 1340-3.

36. Chen, Y. A. & Scheller, R. H. (2001). SNARE-mediated membrane fusion. *Nat Rev Mol Cell Biol* **2**, 98-106.

37. van den Bogaart, G. & Jahn, R. (2011). Counting the SNAREs needed for membrane fusion. *J Mol Cell Biol* **3**, 204-5.

38. Mohrmann, R., de Wit, H., Verhage, M., Neher, E. & Sorensen, J. B. (2010). Fast vesicle fusion in living cells requires at least three SNARE complexes. *Science* **330**, 502-5.

39. Montecucco, C., Schiavo, G. & Pantano, S. (2005). SNARE complexes and neuroexocytosis: how many, how close? *Trends Biochem Sci* **30**, 367-72.

40. Kesavan, J., Borisovska, M. & Bruns, D. (2007). v-SNARE actions during Ca(2+)-triggered exocytosis. *Cell* **131**, 351-63.

41. Williams, D., Vicogne, J., Zaitseva, I., McLaughlin, S. & Pessin, J. E. (2009). Evidence that electrostatic interactions between vesicle-associated membrane protein 2 and acidic phospholipids may modulate the fusion of transport vesicles with the plasma membrane. *Mol Biol Cell* **20**, 4910-9.

42. Lam, A. D., Tryoen-Toth, P., Tsai, B., Vitale, N. & Stuenkel, E. L. (2008). SNARE-catalyzed fusion events are regulated by Syntaxin1A-lipid interactions. *Mol Biol Cell* **19**, 485-97.

43. Cai, H., Reinisch, K. & Ferro-Novick, S. (2007). Coats, tethers, Rabs, and SNAREs work together to mediate the intracellular destination of a transport vesicle. *Dev Cell* **12**, 671-82.

44. Karatekin, E., Tran, V. S., Huet, S., Fanget, I., Cribier, S. & Henry, J. P. (2008). A 20-nm step toward the cell membrane preceding exocytosis may correspond to docking of tethered granules. *Biophys J* **94**, 2891-905.

45. Burgoyne, R. D. (2007). Neuronal calcium sensor proteins: generating diversity in neuronal Ca2+ signalling. *Nat Rev Neurosci* **8**, 182-93.

46. Martens, S. (2010). Role of C2 domain proteins during synaptic vesicle exocytosis. *Biochem Soc Trans* **38**, 213-6.

47. Matthew, W. D., Tsavaler, L. & Reichardt, L. F. (1981). Identification of a synaptic vesicle-specific membrane protein with a wide distribution in neuronal and neurosecretory tissue. *J Cell Biol* **91**, 257-69.

48. Perin, M. S., Johnston, P. A., Ozcelik, T., Jahn, R., Francke, U. & Sudhof, T. C. (1991). Structural and functional conservation of synaptotagmin (p65) in Drosophila and humans. *J Biol Chem* **266**, 615-22.

49. Kaeser, P. S. & Regehr, W. G. (2014). Molecular mechanisms for synchronous, asynchronous, and spontaneous neurotransmitter release. *Annu Rev Physiol* **76**, 333-63.

50. Herrick, D. Z., Kuo, W., Huang, H., Schwieters, C. D., Ellena, J. F. & Cafiso, D. S. (2009). Solution and membrane-bound conformations of the tandem C2A and C2B domains of synaptotagmin 1: Evidence for bilayer bridging. *J Mol Biol* **390**, 913-23.

51. Sutton, R. B., Davletov, B. A., Berghuis, A. M., Sudhof, T. C. & Sprang, S. R. (1995). Structure of the first C2 domain of synaptotagmin I: a novel Ca2+/phospholipid-binding fold. *Cell* **80**, 929-38.

52. Zhang, X., Rizo, J. & Sudhof, T. C. (1998). Mechanism of phospholipid binding by the C2A-domain of synaptotagmin I. *Biochemistry* **37**, 12395-403.

53. Ubach, J., Lao, Y., Fernandez, I., Arac, D., Sudhof, T. C. & Rizo, J. (2001). The C2B domain of synaptotagmin I is a Ca2+-binding module. *Biochemistry* **40**, 5854-60.

54. Fernandez-Chacon, R., Konigstorfer, A., Gerber, S. H., Garcia, J., Matos, M. F., Stevens, C. F., Brose, N., Rizo, J., Rosenmund, C. & Sudhof, T. C. (2001). Synaptotagmin I functions as a calcium regulator of release probability. *Nature* **410**, 41-9.

55. Pang, Z. P., Cao, P., Xu, W. & Sudhof, T. C. (2010). Calmodulin controls synaptic strength via presynaptic activation of calmodulin kinase II. *J Neurosci* **30**, 4132-42.

56. Geppert, M., Goda, Y., Hammer, R. E., Li, C., Rosahl, T. W., Stevens, C. F. & Sudhof, T. C. (1994). Synaptotagmin I: a major Ca2+ sensor for transmitter release at a central synapse. *Cell* **79**, 717-27.

57. Mackler, J. M., Drummond, J. A., Loewen, C. A., Robinson, I. M. & Reist, N. E. (2002). The C(2)B Ca(2+)-binding motif of synaptotagmin is required for synaptic transmission in vivo. *Nature* **418**, 340-4.

58. Marz, K. E. & Hanson, P. I. (2002). Sealed with a twist: complexin and the synaptic SNARE complex. *Trends Neurosci* **25**, 381-3.

59. McMahon, H. T., Missler, M., Li, C. & Sudhof, T. C. (1995). Complexins: cytosolic proteins that regulate SNAP receptor function. *Cell* **83**, 111-9.

60. Bracher, A., Kadlec, J., Betz, H. & Weissenhorn, W. (2002). X-ray structure of a neuronal complexin-SNARE complex from squid. *J Biol Chem* **277**, 26517-23.

61. Yang, X., Kaeser-Woo, Y. J., Pang, Z. P., Xu, W. & Sudhof, T. C. (2010). Complexin clamps asynchronous release by blocking a secondary Ca(2+) sensor via its accessory alpha helix. *Neuron* **68**, 907-20.

62. Li, F., Pincet, F., Perez, E., Giraudo, C. G., Tareste, D. & Rothman, J. E. (2011). Complexin activates and clamps SNAREpins by a common mechanism involving an intermediate energetic state. *Nat Struct Mol Biol* **18**, 941-6.

63. Giraudo, C. G., Garcia-Diaz, A., Eng, W. S., Chen, Y., Hendrickson, W. A., Melia, T. J. & Rothman, J. E. (2009). Alternative zippering as an on-off switch for SNARE-mediated fusion. *Science* **323**, 512-6.

64. Schoch, S., Deak, F., Konigstorfer, A., Mozhayeva, M., Sara, Y., Sudhof, T. C. & Kavalali, E. T. (2001). SNARE function analyzed in synaptobrevin/VAMP knockout mice. *Science* **294**, 1117-22.

65. Basu, J., Shen, N., Dulubova, I., Lu, J., Guan, R., Guryev, O., Grishin, N. V., Rosenmund, C. & Rizo, J. (2005). A minimal domain responsible for Munc13 activity. *Nat Struct Mol Biol* **12**, 1017-8.

66. Shin, O. H., Lu, J., Rhee, J. S., Tomchick, D. R., Pang, Z. P., Wojcik, S. M., Camacho-Perez, M., Brose, N., Machius, M., Rizo, J., Rosenmund, C. & Sudhof, T. C. (2010). Munc13 C2B domain is an activity-dependent Ca2+ regulator of synaptic exocytosis. *Nat Struct Mol Biol* **17**, 280-8.

67. Ma, C., Su, L., Seven, A. B., Xu, Y. & Rizo, J. (2013). Reconstitution of the vital functions of Munc18 and Munc13 in neurotransmitter release. *Science* **339**, 421-5.

68. Tucker, W. C., Weber, T. & Chapman, E. R. (2004). Reconstitution of Ca2+-regulated membrane fusion by synaptotagmin and SNAREs. *Science* **304**, 435-8.

69. Zhou, A., Brewer, K. D. & Rizo, J. (2013). Analysis of SNARE complex/synaptotagmin-1 interactions by one-dimensional NMR spectroscopy. *Biochemistry* **52**, 3446-56.

70. van den Bogaart, G., Meyenberg, K., Diederichsen, U. & Jahn, R. (2012). Phosphatidylinositol 4,5-bisphosphate increases Ca2+ affinity of synaptotagmin-1 by 40-fold. *J Biol Chem* **287**, 16447-53.

71. Choi, U. B., Strop, P., Vrljic, M., Chu, S., Brunger, A. T. & Weninger, K. R. (2010). Single-molecule FRET-derived model of the synaptotagmin 1-SNARE fusion complex. *Nat Struct Mol Biol* **17**, 318-24.

72. Dai, H., Shen, N., Arac, D. & Rizo, J. (2007). A quaternary SNARE-synaptotagmin-Ca2+-phospholipid complex in neurotransmitter release. *J Mol Biol* **367**, 848-63.

73. Huang, H. & Cafiso, D. S. (2008). Conformation and membrane position of the region linking the two C2 domains in synaptotagmin 1 by site-directed spin labeling. *Biochemistry* **47**, 12380-8.

74. Lai, A. L., Huang, H., Herrick, D. Z., Epp, N. & Cafiso, D. S. (2011). Synaptotagmin 1 and SNAREs form a complex that is structurally heterogeneous. *J Mol Biol* **405**, 696-706.

75. Takamori, S., Holt, M., Stenius, K., Lemke, E. A., Gronborg, M., Riedel, D., Urlaub, H., Schenck, S., Brugger, B., Ringler, P., Muller, S. A., Rammner, B., Grater, F., Hub, J. S., De Groot, B. L., Mieskes, G., Moriyama, Y., Klingauf, J., Grubmuller, H., Heuser, J., Wieland, F. & Jahn, R. (2006). Molecular anatomy of a trafficking organelle. *Cell* **127**, 831-46.

76. Kuo, W., Herrick, D. Z. & Cafiso, D. S. (2011). Phosphatidylinositol 4,5-bisphosphate alters synaptotagmin 1 membrane docking and drives opposing bilayers closer together. *Biochemistry* **50**, 2633-41.

77. Morales, K. A. & Igumenova, T. I. (2012). Synergistic effect of Pb(2+) and phosphatidylinositol 4,5-bisphosphate on C2 domain-membrane interactions. *Biochemistry* **51**, 3349-60.

78. Radhakrishnan, A., Stein, A., Jahn, R. & Fasshauer, D. (2009). The Ca2+ affinity of synaptotagmin 1 is markedly increased by a specific interaction of its C2B domain with phosphatidylinositol 4,5-bisphosphate. *J Biol Chem* **284**, 25749-60.

79. Schiavo, G., Gu, Q. M., Prestwich, G. D., Sollner, T. H. & Rothman, J. E. (1996). Calcium-dependent switching of the specificity of phosphoinositide binding to synaptotagmin. *Proc Natl Acad Sci U S A* **93**, 13327-32.

80. Martin, T. F. (1998). Phosphoinositide lipids as signaling molecules: common themes for signal transduction, cytoskeletal regulation, and membrane trafficking. *Annu Rev Cell Dev Biol* **14**, 231-64.

81. Berridge, M. J. & Irvine, R. F. (1984). Inositol trisphosphate, a novel second messenger in cellular signal transduction. *Nature* **312**, 315-21.

82. McLaughlin, S., Wang, J., Gambhir, A. & Murray, D. (2002). PIP(2) and proteins: interactions, organization, and information flow. *Annu Rev Biophys Biomol Struct* **31**, 151-75.

83. Fukuda, M., Aruga, J., Niinobe, M., Aimoto, S. & Mikoshiba, K. (1994). Inositol-1,3,4,5-tetrakisphosphate binding to C2B domain of IP4BP/synaptotagmin II. *J Biol Chem* **269**, 29206-11.

84. Lai, C. L., Landgraf, K. E., Voth, G. A. & Falke, J. J. (2010). Membrane docking geometry and target lipid stoichiometry of membrane-bound PKCalpha C2 domain: a combined molecular dynamics and experimental study. *J Mol Biol* **402**, 301-10.

85. Landgraf, K. E., Malmberg, N. J. & Falke, J. J. (2008). Effect of PIP2 binding on the membrane docking geometry of PKC alpha C2 domain: an EPR site-directed spin-labeling and relaxation study. *Biochemistry* **47**, 8301-16.

86. McLaughlin, S. & Aderem, A. (1995). The myristoyl-electrostatic switch: a modulator of reversible protein-membrane interactions. *Trends Biochem Sci* **20**, 272-6.

87. Joung, M. J., Mohan, S. K. & Yu, C. (2012). Molecular level interaction of inositol hexaphosphate with the C2B domain of human synaptotagmin I. *Biochemistry* **51**, 3675-83.

88. Harlan, J. E., Yoon, H. S., Hajduk, P. J. & Fesik, S. W. (1995). Structural characterization of the interaction between a pleckstrin homology domain and phosphatidylinositol 4,5-bisphosphate. *Biochemistry* **34**, 9859-64.

89. Ben-Tal, N., Honig, B., Peitzsch, R. M., Denisov, G. & McLaughlin, S. (1996). Binding of small basic peptides to membranes containing acidic lipids: theoretical models and experimental results. *Biophys J* **71**, 561-75.

90. Xue, M., Ma, C., Craig, T. K., Rosenmund, C. & Rizo, J. (2008). The Janus-faced nature of the C(2)B domain is fundamental for synaptotagmin-1 function. *Nat Struct Mol Biol* **15**, 1160-8.

91. Park, Y., Hernandez, J. M., van den Bogaart, G., Ahmed, S., Holt, M., Riedel, D. & Jahn, R. (2012). Controlling synaptotagmin activity by electrostatic screening. *Nat Struct Mol Biol* **19**, 991-7.

92. Bhowmik, A., Ellena, J. F., Bryant, R. G. & Cafiso, D. S. (2008). Spin-diffusion couples proton relaxation rates for proteins in exchange with a membrane interface. *J Magn Reson* **194**, 283-8.

93. Fernandez, I., Arac, D., Ubach, J., Gerber, S. H., Shin, O., Gao, Y., Anderson, R. G., Sudhof, T. C. & Rizo, J. (2001). Three-dimensional structure of the synaptotagmin 1 C2B-domain: synaptotagmin 1 as a phospholipid binding machine. *Neuron* **32**, 1057-69.

94. McLauglin, C. A. B. a. S. (1998). Ultracentrifigution technique for measuring the binding of peptides and proteins to sucrose-loaded phospholipid vesicles. In *Transmembrane Signaling Protocols*, Vol. 84. Humana Press Inc, Totowa NJ.

95. Ames, B. N. (1966). Assay of inorganic phosphate, total phosphate and phosphatases. . *Methods of Enzymology* **8**, 115-118

.

96. Dawidowski, D. & Cafiso, D. S. (2013). Allosteric control of syntaxin 1a by Munc18-1: characterization of the open and closed conformations of syntaxin. *Biophys J* **104**, 1585-94.

97. Altenbach, C., Greenhalgh, D. A., Khorana, H. G. & Hubbell, W. L. (1994). A collision gradient method to determine the immersion depth of nitroxides in lipid bilayers: application to spin-labeled mutants of bacteriorhodopsin. *Proc Natl Acad Sci U S A* **91**, 1667-71.

98. van der Velden, V. H., Panzer-Grumayer, E. R., Cazzaniga, G., Flohr, T., Sutton, R., Schrauder, A., Basso, G., Schrappe, M., Wijkhuijs, J. M., Konrad, M., Bartram, C. R., Masera, G., Biondi, A. & van Dongen, J. J. (2007). Optimization of PCR-based minimal residual disease diagnostics for childhood acute lymphoblastic leukemia in a multi-center setting. *Leukemia* **21**, 706-13.

99. Georgieva, E. R., Roy, A. S., Grigoryants, V. M., Borbat, P. P., Earle, K. A., Scholes, C. P. & Freed, J. H. (2012). Effect of freezing conditions on distances and their distributions derived from Double Electron Electron Resonance (DEER): a study of doubly-spin-labeled T4 lysozyme. *J Magn Reson* **216**, 69-77.

100. P.E. Knowles, B., Morsh, Rattle. (1976). *Magnetic Resonance of Biomolecules*.

101. Levitt, M. H. (2001). *Spin Dynamics*, John Wiley & Sons, Ltd, England.

102. Pochapsky, T. C. P. a. S. S. (2007). *NMR for Physical and Biological Scientists*, Garland Science, New York.

103. McHaourab, H. S., Lietzow, M. A., Hideg, K. & Hubbell, W. L. (1996). Motion of spin-labeled side chains in T4 lysozyme. Correlation with protein structure and dynamics. *Biochemistry* **35**, 7692-704.

104. Guo, Z., Cascio, D., Hideg, K. & Hubbell, W. L. (2008). Structural determinants of nitroxide motion in spin-labeled proteins: solvent-exposed sites in helix B of T4 lysozyme. *Protein Sci* **17**, 228-39.

105. Wertz, B. (1972). *Electron Spin Resonance: Elementary Theory and Practical Applications*, McGraw-Hill.

106. Beier, C. & Steinhoff, H. J. (2006). A structure-based simulation approach for electron paramagnetic resonance spectra using molecular and stochastic dynamics simulations. *Biophys J* **91**, 2647-64.

107. Columbus, L. & Hubbell, W. L. (2002). A new spin on protein dynamics. *Trends Biochem Sci* **27**, 288-95.

108. Jimenez, R. H., Freed, D. M. & Cafiso, D. S. (2011). Lipid and membrane mimetic environments modulate spin label side chain configuration in the outer membrane protein A. *J Phys Chem B* **115**, 14822-30.

109. Freed, D. M., Khan, A. K., Horanyi, P. S. & Cafiso, D. S. (2011). Molecular origin of electron paramagnetic resonance line shapes on beta-barrel membrane proteins: the local solvation environment modulates spin-label configuration. *Biochemistry* **50**, 8792-803.

110. Kroncke, B. M., Horanyi, P. S. & Columbus, L. (2010). Structural origins of nitroxide side chain dynamics on membrane protein alpha-helical sites. *Biochemistry* **49**, 10045-60.

111. Jeschke, G. (2002). Distance measurements in the nanometer range by pulse EPR. *Chemphyschem* **3**, 927-32.

112. Rabenstein, M. D. & Shin, Y. K. (1995). Determination of the distance between two spin labels attached to a macromolecule. *Proc Natl Acad Sci U S A* **92**, 8239-43.

113. Jeschke, G. & Polyhach, Y. (2007). Distance measurements on spin-labelled biomacromolecules by pulsed electron paramagnetic resonance. *Phys Chem Chem Phys* **9**, 1895-910.

114. Altenbach, C., Kusnetzow, A. K., Ernst, O. P., Hofmann, K. P. & Hubbell, W. L. (2008). High-resolution distance mapping in rhodopsin reveals the pattern of helix movement due to activation. *Proc Natl Acad Sci U S A* **105**, 7439-44.

115. Berliner, M. A. H. a. L. J. (2007). *ESR spectroscopy in membrane biophysics*, Springer, New York.

116. Azarkh, M., Singh, V., Okle, O., Seemann, I. T., Dietrich, D. R., Hartig, J. S. & Drescher, M. (2013). Site-directed spin-labeling of nucleotides and the use of in-cell EPR to determine long-range distances in a biologically relevant environment. *Nat Protoc* **8**, 131-47.

117. Higman, V. A., Leidert, M., Diehl, A., Elkins, J., Soundararajan, M., Oschkinat, H. & Ball, L. J. (2006). NMR assignment of human RGS18. *J Biomol NMR* **36 Suppl 1**, 72.

118. Hoffman, R. E. (2006). Measurement of magnetic susceptibility and calculation of shape factor of NMR samples. *J Magn Reson* **178**, 237-47.

119. Williamson, M. P. (2013). Using chemical shift perturbation to characterise ligand binding. *Prog Nucl Magn Reson Spectrosc* **73**, 1-16.

120. Lukasik, S. M., Cierpicki, T., Borloz, M., Grembecka, J., Everett, A. & Bushweller, J. H. (2006). High resolution structure of the HDGF PWWP domain: a potential DNA binding domain. *Protein Sci* **15**, 314-23.

121. Huang, X., Peng, J. W., Speck, N. A. & Bushweller, J. H. (1999). Solution structure of core binding factor beta and map of the CBF alpha binding site. *Nat Struct Biol* **6**, 624-7.

122. Anthis, N. J., Doucleff, M. & Clore, G. M. (2011). Transient, sparsely populated compact states of apo and calcium-loaded calmodulin probed by paramagnetic relaxation enhancement: interplay of conformational selection and induced fit. *J Am Chem Soc* **133**, 18966-74.

123. Young, S. M., Jr. & Neher, E. (2009). Synaptotagmin has an essential function in synaptic vesicle positioning for synchronous release in addition to its role as a calcium sensor. *Neuron* **63**, 482-96.

124. Gaffaney, J. D., Dunning, F. M., Wang, Z., Hui, E. & Chapman, E. R. (2008). Synaptotagmin C2B domain regulates Ca2+-triggered fusion in vitro: critical residues revealed by scanning alanine mutagenesis. *J Biol Chem* **283**, 31763-75.

125. Frazier, A. A., Wisner, M. A., Malmberg, N. J., Victor, K. G., Fanucci, G. E., Nalefski, E. A., Falke, J. J. & Cafiso, D. S. (2002). Membrane orientation and position of the C2 domain from cPLA2 by site-directed spin labeling. *Biochemistry* **41**, 6282-92.

126. Essen, L. O., Perisic, O., Cheung, R., Katan, M. & Williams, R. L. (1996). Crystal structure of a mammalian phosphoinositide-specific phospholipase C delta. *Nature* **380**, 595-602.

127. Shao, X., Davletov, B. A., Sutton, R. B., Sudhof, T. C. & Rizo, J. (1996). Bipartite Ca2+-binding motif in C2 domains of synaptotagmin and protein kinase C. *Science* **273**, 248-51.

128. Malmberg, N. J., Van Buskirk, D. R. & Falke, J. J. (2003). Membrane-docking loops of the cPLA2 C2 domain: detailed structural analysis of the protein-membrane interface via site-directed spin-labeling. *Biochemistry* **42**, 13227-40.

129. Chae, Y. K., Abildgaard, F., Chapman, E. R. & Markley, J. L. (1998). Lipid binding ridge on loops 2 and 3 of the C2A domain of synaptotagmin I as revealed by NMR spectroscopy. *J Biol Chem* **273**, 25659-63.

130. Wu, Z. & Schulten, K. (2014). Synaptotagmin's Role in Neurotransmitter Release Likely Involves Ca(2+)-induced Conformational Transition. *Biophys J* **107**, 1156-66.

131. Grobler, J. A., Essen, L. O., Williams, R. L. & Hurley, J. H. (1996). C2 domain conformational changes in phospholipase C-delta 1. *Nat Struct Biol* **3**, 788-95.

132. Arkhipov, A., Shan, Y., Das, R., Endres, N. F., Eastwood, M. P., Wemmer, D. E., Kuriyan, J. & Shaw, D. E. (2013). Architecture and membrane interactions of the EGF receptor. *Cell* **152**, 557-69.

133. Masumoto, T., Suzuki, K., Ohmori, I., Michiue, H., Tomizawa, K., Fujimura, A., Nishiki, T. & Matsui, H. (2012). Ca(2+)-independent syntaxin binding to the C(2)B effector region of synaptotagmin. *Mol Cell Neurosci* **49**, 1-8.

134. Shao, X., Li, C., Fernandez, I., Zhang, X., Sudhof, T. C. & Rizo, J. (1997). Synaptotagmin-syntaxin interaction: the C2 domain as a Ca2+-dependent electrostatic switch. *Neuron* **18**, 133-42.

135. Verdaguer, N., Corbalan-Garcia, S., Ochoa, W. F., Fita, I. & Gomez-Fernandez, J. C. (1999). Ca(2+) bridges the C2 membrane-binding domain of protein kinase Calpha directly to phosphatidylserine. *EMBO J* **18**, 6329-38.

136. Frazier, A. A., Roller, C. R., Havelka, J. J., Hinderliter, A. & Cafiso, D. S. (2003). Membrane-bound orientation and position of the synaptotagmin I C2A domain by site-directed spin labeling. *Biochemistry* **42**, 96-105.

137. Stein, A., Radhakrishnan, A., Riedel, D., Fasshauer, D. & Jahn, R. (2007). Synaptotagmin activates membrane fusion through a Ca2+-dependent trans interaction with phospholipids. *Nat Struct Mol Biol* **14**, 904-11.

138. Murray, D. & Honig, B. (2002). Electrostatic control of the membrane targeting of C2 domains. *Mol Cell* **9**, 145-54.

139. Rizo, J. & Sudhof, T. C. (1998). C2-domains, structure and function of a universal Ca2+-binding domain. *J Biol Chem* **273**, 15879-82.

140. Edwards, A. S. & Newton, A. C. (1997). Regulation of protein kinase C betaII by its C2 domain. *Biochemistry* **36**, 15615-23.

141. Ochoa, W. F., Corbalan-Garcia, S., Eritja, R., Rodriguez-Alfaro, J. A., Gomez-Fernandez, J. C., Fita, I. & Verdaguer, N. (2002). Additional binding sites for anionic phospholipids and calcium ions in the crystal structures of complexes of the C2 domain of protein kinase calpha. *J Mol Biol* **320**, 277-91.

142. Hui, E., Gaffaney, J. D., Wang, Z., Johnson, C. P., Evans, C. S. & Chapman, E. R. (2011). Mechanism and function of synaptotagmin-mediated membrane apposition. *Nat Struct Mol Biol* **18**, 813-21.

143. Bai, J., Tucker, W. C. & Chapman, E. R. (2004). PIP2 increases the speed of response of synaptotagmin and steers its membrane-penetration activity toward the plasma membrane. *Nat Struct Mol Biol* **11**, 36-44.

144. Miledi, R. (1966). Strontium as a substitute for calcium in the process of transmitter release at the neuromuscular junction. *Nature* **212**, 1233-4.

145. Goda, Y. & Stevens, C. F. (1994). Two components of transmitter release at a central synapse. *Proc Natl Acad Sci U S A* **91**, 12942-6.

146. Shin, O. H., Rhee, J. S., Tang, J., Sugita, S., Rosenmund, C. & Sudhof, T. C. (2003). Sr2+ binding to the Ca2+ binding site of the synaptotagmin 1 C2B domain triggers fast exocytosis without stimulating SNARE interactions. *Neuron* **37**, 99-108.

147. Morales, K. A., Yang, Y., Long, Z., Li, P., Taylor, A. B., Hart, P. J. & Igumenova, T. I. (2013). Cd2+ as a Ca2+ surrogate in protein-membrane interactions: isostructural but not isofunctional. *J Am Chem Soc* **135**, 12980-3.

148. Park, Y., Vennekate, W., Yavuz, H., Preobraschenski, J., Hernandez, J. M., Riedel, D., Walla, P. J. & Jahn, R. (2014). alpha-SNAP Interferes with the Zippering of the SNARE Protein Membrane Fusion Machinery. *J Biol Chem* **289**, 16326-35.

149. Gribble, F. M., Loussouarn, G., Tucker, S. J., Zhao, C., Nichols, C. G. & Ashcroft, F. M. (2000). A novel method for measurement of submembrane ATP concentration. *J Biol Chem* **275**, 30046-9.

150. Kuo, W., Herrick, D. Z., Ellena, J. F. & Cafiso, D. S. (2009). The calcium-dependent and calcium-independent membrane binding of synaptotagmin 1: two modes of C2B binding. *J Mol Biol* **387**, 284-94.

151. Golebiewska, U., Gambhir, A., Hangyas-Mihalyne, G., Zaitseva, I., Radler, J. & McLaughlin, S. (2006). Membrane-bound basic peptides sequester multivalent (PIP2), but not monovalent (PS), acidic lipids. *Biophys J* **91**, 588-99.

152. Gambhir, A., Hangyas-Mihalyne, G., Zaitseva, I., Cafiso, D. S., Wang, J., Murray, D., Pentyala, S. N., Smith, S. O. & McLaughlin, S. (2004). Electrostatic sequestration of PIP2 on phospholipid membranes by basic/aromatic regions of proteins. *Biophys J* **86**, 2188-207.

153. James, D. J., Khodthong, C., Kowalchyk, J. A. & Martin, T. F. (2008). Phosphatidylinositol 4,5-bisphosphate regulates SNARE-dependent membrane fusion. *J Cell Biol* **182**, 355-66.

154. Vennekate, W., Schroder, S., Lin, C. C., van den Bogaart, G., Grunwald, M., Jahn, R. & Walla, P. J. (2012). Cis- and trans-membrane interactions of synaptotagmin-1. *Proc Natl Acad Sci U S A* **109**, 11037-42.

155. Criddle, D. N., Gerasimenko, J. V., Baumgartner, H. K., Jaffar, M., Voronina, S., Sutton, R., Petersen, O. H. & Gerasimenko, O. V. (2007). Calcium signalling and pancreatic cell death: apoptosis or necrosis? *Cell Death Differ* **14**, 1285-94.

156. Honigmann, A., van den Bogaart, G., Iraheta, E., Risselada, H. J., Milovanovic, D., Mueller, V., Mullar, S., Diederichsen, U., Fasshauer, D., Grubmuller, H., Hell, S. W., Eggeling, C., Kuhnel, K. & Jahn, R. (2013). Phosphatidylinositol 4,5-bisphosphate clusters act as molecular beacons for vesicle recruitment. *Nat Struct Mol Biol* **20**, 679-86.

157. Sakaba, T., Stein, A., Jahn, R. & Neher, E. (2005). Distinct kinetic changes in neurotransmitter release after SNARE protein cleavage. *Science* **309**, 491-4.

158. Seven, A. B., Brewer, K. D., Shi, L., Jiang, Q. X. & Rizo, J. (2013). Prevalent mechanism of membrane bridging by synaptotagmin-1. *Proc Natl Acad Sci U S A* **110**, E3243-52.

159. Montaville, P., Coudevylle, N., Radhakrishnan, A., Leonov, A., Zweckstetter, M. & Becker, S. (2008). The PIP2 binding mode of the C2 domains of rabphilin-3A. *Protein Sci* **17**, 1025-34.

160. Malmberg, N. J. & Falke, J. J. (2005). Use of EPR power saturation to analyze the membrane-docking geometries of peripheral proteins: applications to C2 domains. *Annu Rev Biophys Biomol Struct* **34**, 71-90.

161. Rufener, E., Frazier, A. A., Wieser, C. M., Hinderliter, A. & Cafiso, D. S. (2005). Membrane-bound orientation and position of the synaptotagmin C2B domain determined by site-directed spin labeling. *Biochemistry* **44**, 18-28.

162. Lai, A. L., Tamm, L. K., Ellena, J. F. & Cafiso, D. S. (2011). Synaptotagmin 1 modulates lipid acyl chain order in lipid bilayers by demixing phosphatidylserine. *J Biol Chem* **286**, 25291-300.

163. Lee, J. & Lentz, B. R. (1998). Secretory and viral fusion may share mechanistic events with fusion between curved lipid bilayers. *Proc Natl Acad Sci U S A* **95**, 9274-9.

164. Connell, E., Giniatullina, A., Lai-Kee-Him, J., Tavare, R., Ferrari, E., Roseman, A., Cojoc, D., Brisson, A. R. & Davletov, B. (2008). Cross-linking of phospholipid membranes is a conserved property of calcium-sensitive synaptotagmins. *J Mol Biol* **380**, 42-50.